

**THE PRODUCTION OF BIO-JET FUEL FROM PALM FATTY ACID  
DISTILLATE OVER COBALT AND NICKEL SUPPORTED HZSM-12  
CATALYSTS**

Ariya Eka Alel

A Thesis Submitted in Partial Fulfilment of the Requirements  
for the Degree of Master of Science  
The Petroleum and Petrochemical College, Chulalongkorn University  
in Academic Partnership with  
The University of Michigan, The University of Oklahoma,  
Case Western Reserve University, and Institute Français du Pétrole

บทคัดย่อและแฟ้มข้อมูลฉบับเต็มของวิทยานิพนธ์ตั้งแต่ปีการศึกษา 2554 ที่ให้บริการในคลังปัญญาจุฬาฯ (CUIR)  
เป็นแฟ้มข้อมูลของนิสิตเจ้าของวิทยานิพนธ์ที่ส่งผ่านทางบัณฑิตวิทยาลัย

The abstract and full text of theses from the academic year 2011 in Chulalongkorn University Intellectual Repository (CUIR)  
are the thesis authors' files submitted through the Graduate School.

**Thesis Title:** The Production of Bio-jet Fuel from Palm Fatty Acid Distillate over Cobalt and Nickel Supported HZSM-12 Catalysts.  
**By:** Ariya Eka Alel  
**Program:** Petroleum and Energy Technology  
**Thesis Advisor:** Assoc. Prof. Siriporn Jongpatiwut

---

Accepted by The Petroleum and Petrochemical College, Chulalongkorn University, in partial fulfilment of the requirements for the Degree of Master of Science.

..... College Dean  
(Prof. Suwabun Chirachanchai)

**Thesis Committee:**

.....  
(Assoc. Prof. Siriporn Jongpatiwut)

.....  
(Prof. Boonyarach Kitiyanan)

.....  
(Dr. Tanate Danuthai)

## ABSTRACT

6073008063: Petroleum and Energy Technology Program

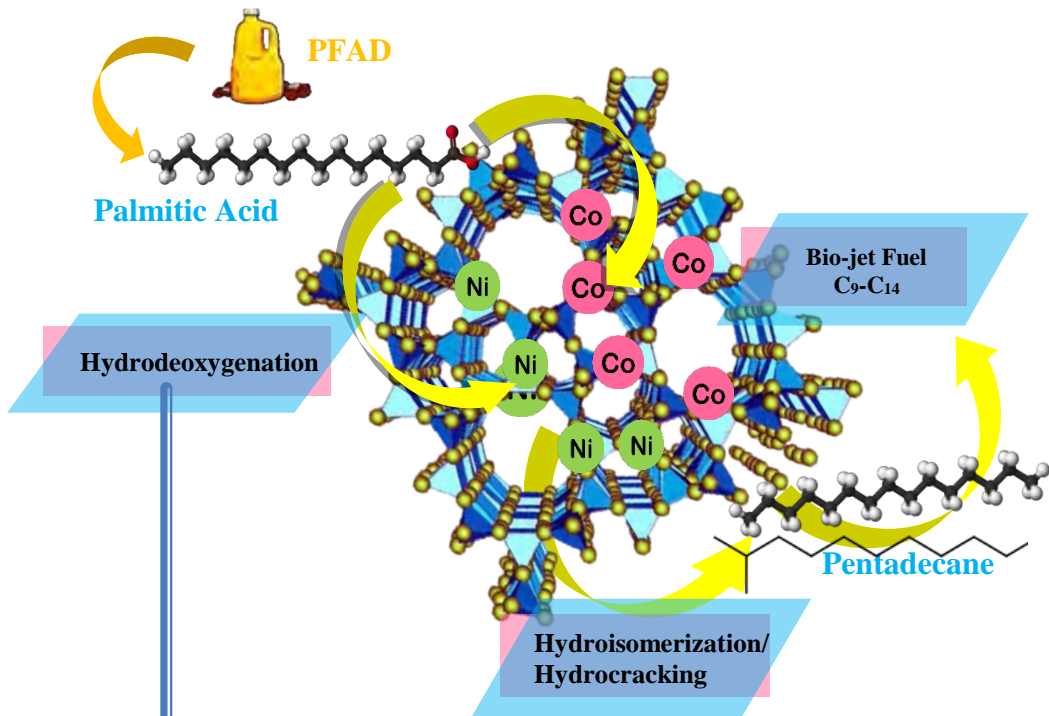
Ariya Eka Alel: The Production of Bio-jet Fuel from Palm Fatty Acid Distillate over Cobalt and Nickel Supported HZSM-12 Catalysts.

Thesis Advisor: Assoc.Prof. Siriporn Jongpatiwut, 101 pp.

Keywords: PFAD, HZSM-12, Cobalt, Nickel, Bio-jet Fuel

Aviation sector becomes one of the largest-developing public transportation nowadays, the number of air passengers always increases year by year. However, this number are proportionally related to the enhance of jet-fuel worldwide demand. The conventional jet-fuel are commonly known as a carbon dioxide emission source and the world has more concern to this pollutant due to its contribution to the climate change. The usage of renewable materials to produce jet fuel is more glanced. One of the renewable sources can be used to generate green jet fuel is palm fatty acid distillate (PFAD) which is a by-product of palm oil production. This bio-jet fuel is converted via hydrogenation and isomerization reaction by using HZSM-12 catalyst which is a one dimensional zeolite structure. Cobalt (Co), nickel (Ni), and bimetallic Co-Ni were used to increase the catalyst activity. The catalysts prepared by various methods i.e. incipient wetness impregnation, ion exchange, and melt infiltration. The best metal used in this study to produce high selectivity of bio-jet fuel is cobalt with selectivity about 44.6% followed by bimetallic Co-Ni (32.8%) and Nickel (30.3%) under identical condition. Based on the experiment, Co/HZSM-12 prepared via melt infiltration showed the highest selectivity of bio-jet fuel which was 55.5% followed by incipient wetness impregnation 51.6% and ion exchange 50.5%. The optimum condition gained for this reaction was 350 °C, 20 bar and LHSV of 1.5 h<sup>-1</sup>. In addition, Co/HZSM-12 exhibited higher selectivity to bio-jet fuel (51.6%) than Co/HZSM-22 (31.1%) under identical condition and preparation.

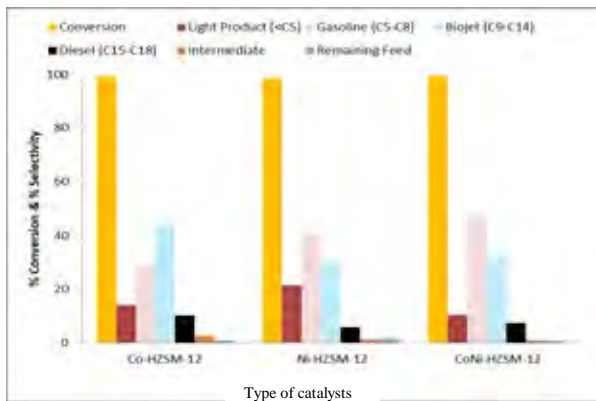
## GRAPHICAL ABSRACT



- Temperature: 350, 375, and 400 (°C)
- Pressure: 10, 20, and 30 (bar)
- Metal Types: Cobalt, Nickel, and CoNi
- Metal Preparation Methods: IWI, IE, MI
- Cobalt Loading: 2.5, 5, and 7.5 (% wt)
- LHSV: 1.5, 2, and 2.5 (h<sup>-1</sup>)

**The Optimum Condition:** 350 °C, 20 bar, LHSV of 1.5 h<sup>-1</sup> and H<sub>2</sub> feed molar ratio of 10 over 5% Co/HZSM-12

Co/HZSM-12 produce high selectivity of bio-jet fuel and *iso*-alkane because cobalt is good in isomerization reaction due to its strong acidity.



## ACKNOWLEDGEMENTS

The author is grateful for the scholarship and funding of the thesis work provided by the Petroleum and Petrochemical College and the ASEAN Scholarship. The funding really helps me to finish my master degree program on time. I also would like my sincere gratitude to thank my advisor Assoc.Prof. Siriporn Jongpatiwut who always helps, supervises and guides me to do my project since the beginning of my work until I finished this thesis book.

I also would like to thank my thesis committees, Prof. Boonyarach Kitiyanan and Dr. Tanate Danuthai for their suggestions which are certainly important and helpful for completion of this thesis.

Moreover, thank you very much to my beloved parents who always sending me much love and support in any condition so I can strongly stand in this college until I gained my master title. A thousand thanks to Mr. Vido Septa Hidayat, thanks for helping in any difficulties I got. Moreover, I want to say my deep appreciation to my Indonesian friends which always willing to spend much time with me even until mid night to finish my work.

The author would also like to say thank you to my lab friends in room 614 and all the lecturers or staff in PPC that help me a lot especially to Mr. Prasit as the international affair representative who responsible to take care of me and other foreign students.

## TABLE OF CONTENTS

	<b>PAGE</b>
Title Page	i
Abstract (in English)	iii
Graphical Abstract	iv
Acknowledgements	v
Table of Contents	vi
List of Tables	x
List of Figures	xi
<b>I      INTRODUCTION</b>	<b>1</b>
<b>II     LITERATURE REVIEW</b>	<b>3</b>
2.1 Bio-Jet Fuel	3
2.2 Bio-Jet Fuel Feedstock	5
2.2.1 Vegetable Oil	6
2.2.2 Fatty Acid	10
2.3 Palm Fatty Acid Distillate	11
2.4 Reaction Kinetics of Bio-jet Fuel Production	16
2.4.1 Hydrodeoxygenation	17
2.4.2 Hydrocracking	20
2.4.3 Hydroisomerization	21
2.4.4 Hydrogenation and Dehydrogenation	25
2.4.5 Hydrogenolysis	25
2.5 Bio-Jet Fuel Catalyst	26
2.5.1 Zeolite Catalyst	26
2.5.2 Zeolite ZSM-12 and ZSM-22	30
2.5.3 Supported Metal Catalyst Type	33

2.6 Catalyst Preparation Method of Bio-Jet Fuel	36
<b>III EXPERIMENTAL</b>	38
3.1 Materials and Equipment	38
3.1.1 Materials	38
3.1.2 Equipment	39
3.2 Experimental Procedure	40
3.2.1 Catalyst Preparations	40
3.2.2 Cobalt, Nickel and Bimetallic Cobalt-Nickel Loading on HZSM-12 and HZSM-22	41
3.3 Catalyst Characterization	41
3.3.1 X-ray Diffraction (XRD)	41
3.3.2 Brunauer-Emmett-Teller (BET)	41
3.3.3 Temperature Programmed Reduction (TPR)	42
3.3.4 Temperature Programmed Desorption (TPD) of Ammonia	42
3.3.5 Temperature Programmed Oxidation (TPO)	43
3.3.6 Transmission Electron Microscopy (TEM)	43
3.4 Catalytic Activity Testing	43
3.4 Product Analysis	46
3.4.1 Liquid Product Analysis	46
3.4.2 Gas Product Analysis	47
<b>IV RESULTS AND DISCUSSION</b>	49
4.1 Characterization of Fresh Catalysts	49
4.1.1 X-ray Diffraction (XRD)	49
4.1.2 X-ray Fluorescence (XRF)	51
4.1.3 Transmission Electron Microscope (TEM)	52
4.1.4 Brunauer-Emmett-Teller (BET)	54
4.1.5 Temperature Programmed Reduction (TPR)	55

4.1.6	Temperature Programmed Desorption of Ammonia (TPD-NH <sub>3</sub> )	56
4.2	Gas Chromatography	57
4.2.1	Feed Analysis	57
4.2.2	Standard Analysis	58
4.3	Catalytic Activity Testing	62
4.3.1	Effect of Reaction Temperature	62
4.3.2	Effect of Different Metal Loading (Co, Ni, and Co-Ni)	64
4.3.3	Effect of Reaction Pressure	67
4.3.4	Effect of Metal (Co) Loading	68
4.3.5	Effect of Metal Preparation Methods	70
4.3.6	Effect of LHSVs	73
4.3.7	Effect of Supported Catalysts (Co/HZSM-12 and Co/HZSM-22)	75
4.4	Proposed Reaction Pathway	77
4.5	Characterization of Spent Catalysts	79
4.5.1	Temperature Programmed Oxidation (TPO)	79
<b>V</b>	<b>CONCLUSIONS AND RECOMMENDATIONS</b>	<b>80</b>
	<b>REFERENCE</b>	<b>81</b>
	<b>APPENDICES</b>	
	APPENDIX A1 Overall Mass Balance of Deoxygenation- Hydroprocessing at Different in Temperature (350, 375 and 400 °C)	87
	APPENDIX A2 Overall Mass Balance of Deoxygenation- Hydroprocessing at Different in Kind of Metal (Co, Ni and Co-Ni)	88
	APPENDIX A3 Overall Mass Balance of Deoxygenation- Hydroprocessing at Different in Reducing Time (2, 3, and 4 h)	90



APPENDIX A4 Overall Mass Balance of Deoxygenation- Hydroprocessing at Different in Pressure (10, 20, and 30 bar)	92
APPENDIX A5 Overall Mass Balance of Deoxygenation- Hydroprocessing at Different in Metal Loading (2.5, 5, and 5 %)	91
APPENDIX A6 Overall Mass Balance of Deoxygenation- Hydroprocessing at Different in Preparation Methods (IWI, IE, and MI)	93
APPENDIX A7 Overall Mass Balance of Deoxygenation- Hydroprocessing at Different in LHSV (1.5, 2, and 2.5 h <sup>-1</sup> )	94
APPENDIX A8 Overall Mass Balance of Deoxygenation- hydroprocessing at different in Zeolite (Co/HZSM-12 and Co/HZSM-22)	96
<b>CURRICULUM VITAE</b>	101

## LIST OF TABLES

TABLE		PAGE
2.1	Major fuel properties of Jet A, Jet-A1, Jet-Bio, and bio-jet fuels	5
2.2	Feed stocks considered for bio jet fuel	6
2.3	Chemical structure of common fatty acids	8
2.4	Comparison of several bio oil feedstock from vegetable	9
2.5	Typical composition (%wt) of PFAD	12
2.6	Fatty acid composition of PFAD	13
2.7	General characteristics of palm fatty acid distillate	14
3.1	Description of system in flow diagram of the continuous flow fixed-bed reactor.	44
3.2	The reaction conditions for hydroprocessing of palm fatty acid distillate in continuous flow fixed-bed reactor.	45
3.3	The chromatographic temperature program for liquid product analysis.	46
3.4	The chromatographic temperature program for gas-phase product analysis	47
4.1	Chemical composition of the synthesized Co, Ni, Co-Ni/HZSM-12, Co/HZSM-12 by incipient wetness impregnation (IWI), ion exchange (IE), and melt infiltration (MI).	51
4.2	Physical properties of the catalysts loaded by Co, Ni, Co-Ni/HZSM-12, Co/HZSM-12 by incipient wetness impregnation (IWI), ion exchange (IE), and melt infiltration (MI).	55
4.3	PFAD composition	58
4.4	Percent Coke of Co, Ni, Co-Ni/HZSM-12, Co/HZSM-12 and	77

Co/HZSM-22.

## LIST OF FIGURES

<b>FIGURE</b>	<b>PAGE</b>
2.1 CO <sub>2</sub> Emission Trends from International Aviation from 2005 to 2050.	4
2.2 Chemical structure of triglycerides.	8
2.3 Palm fatty acid distillate from refining process of crude palm oil.	13
2.4 Palm oil producers by country 2016.	15
2.5 Global vegetable oil production 2011.	15
2.6 The four catalytic pathways proposed for deoxygenation of palmitic acid on 40NiPZ.	17
2.7 Various deoxygenation reaction schemes with other possible reactions including thermodynamic data.	19
2.8 The schematic of hydrocracking reaction.	20
2.9 Mechanism of <i>n</i> -paraffins/ <i>n</i> -alkanes hydroisomerization over bifunctional catalysts.	22
2.10 Effect of reaction temperature on <i>iso</i> -to-normal paraffin ratio in products obtained from hydrocracking of <i>n</i> -decane over strongly acidic catalyst.	23
2.11 Schematic of hydrogenolysis reaction.	26
2.12 Development of zeolite structures (from aluminosilicates to secondary building blocks to zeolite structures) showing zeolite X & Y; zeolite ZSM-5 or silicalite-1; zeolite ZSM-12	

	and zeolite Theta-1 or ZSM-22.	28
2.13	Zeolite structures showing; A: 8-ring, 10-ring and 12-ring members and; B: other types of zeolite structures.	29
2.14	The NMR-refined crystal structure of silica-ZSM-12 (framework type code MTW) with Si sites labelled and unit cell indicated.	32
2.15	Framework of TON zeolite or ZSM-22	32
3.1	Flow diagram of reactor system..	44
4.1	XRD pattern of synthesized parent ZSM-12; ZSM-12; Co, Ni, Co-Ni HZSM-12; HZSM-12 by incipient wetness impregnation, ion exchange, and melt infiltration.	50
4.2	TEM image of HZSM-12	52
4.3	TEM image of Co/HZSM-12 via incipient wetness impregnation.	53
4.4	TEM image of Ni/HZSM-12 via incipient wetness impregnation.	53
4.5	TEM image of Co-Ni/HZSM-12 via incipient wetness impregnation.	53
4.6	TEM image of Co/HZSM-12 via ion exchange (a) and melt infiltration (b).	54
4.7	TPR profile of Co and Ni.	56
4.8	TPD-NH <sub>3</sub> profile of Co, Ni and Co-Ni	57
4.9	The chromatogram of various components in PFAD range analyzed by GC/FID.	58
4.10	Chromatograms of standard oxygenated compounds	59
4.11	Chromatogram of standard <i>n</i> - alkanes	59
4.12	The conversion and selectivity of products over 5 wt.% Co/HZSM-12 catalyst at different temperatures ( Reaction condition: 30 bar, H <sub>2</sub> /feed molar ratio of 10, LHSV 1.5 h <sup>-1</sup> and TOS at 8 h)	61

- 4.13 The product distribution over 5 wt.% Co/HZSM-12 catalyst at different temperatures ( Reaction condition: 30 bar, H<sub>2</sub>/feed molar ratio of 10, LHSV 1.5 h<sup>-1</sup> and TOS at 8 h) 62
- 4.14 The conversion and selectivity of products over 5 wt.% HZSM-12 catalyst at different metal loading Co, Ni, and Co-Ni ( Reaction condition: 350 °C, 30 bar, H<sub>2</sub>/feed molar ratio of 10, LHSV 1.5 h<sup>-1</sup> and TOS at 8 h) 63
- 4.15 The product distribution over 5 wt.% HZSM-12 catalyst at different metal loading Co, Ni, and Co-Ni ( Reaction condition: 350 °C, 30 bar, H<sub>2</sub>/feed molar ratio of 10, LHSV 1.5 h<sup>-1</sup> and TOS at 8 h) 64
- 4.16 The iso-product/n-product distribution over 5 wt.% HZSM-12 catalyst at different metal loading Co, Ni, and Co-Ni (Reaction condition: 350 °C, 30 bar, H<sub>2</sub>/feed molar ratio of 10, LHSV 1.5 h<sup>-1</sup> and TOS at 8 h) 64
- 4.17 The conversion and selectivity of products over 5 wt.% Co/HZSM-12 catalyst at different reaction pressure (Reaction condition: 350 °C, H<sub>2</sub>/feed molar ratio of 10, LHSV 1.5 h<sup>-1</sup> and TOS at 8 h) 65
- 4.18 The product distribution over 5 wt.% Co/HZSM-12 catalyst at different reaction pressure ( Reaction condition: 350 °C, 20 bar, H<sub>2</sub>/feed molar ratio of 10, LHSV 1.5 h<sup>-1</sup> and TOS at 8 h). 66
- 4.19 The conversion and selectivity of products over 5 wt.% Co/HZSM-12 catalyst at different amount metal (Co) loading (Reaction condition: 350 °C, 20 bar, H<sub>2</sub>/feed molar ratio of 10, LHSV 1.5 h<sup>-1</sup> and TOS at 8 h) 67
- 4.20 The product distribution over 5 wt.% Co/HZSM-12 catalyst at different amount metal (Co) loading (Reaction condition: 350 °C, 20 bar, H<sub>2</sub>/feed molar ratio of 10, LHSV 1.5 h<sup>-1</sup> and

	TOS at 8 h)	67
4.21	The conversion and selectivity of products over 5 wt.% Co/HZSM-12 catalyst at different metal preparation methods (Reaction condition: 350 °C, 20 bar, H <sub>2</sub> /feed molar ratio of 10, LHSV 1.5 h <sup>-1</sup> and TOS at 8 h).	69
4.22	The product distribution over 5 wt.% Co/HZSM-12 catalyst at different different metal preparation methods (a) incipient wetness impregnation (b) ion exchange (c) melt infiltration (Reaction condition: 350 °C, 20 bar, H <sub>2</sub> /feed molar ratio of 10, LHSV 1.5 h <sup>-1</sup> and TOS at 8 h).	70
4.23	Calcined Co/HZSM-12 metal preparations	70
4.24	The conversion and selectivity of products over 5 wt.% Co/HZSM-12 catalyst at different LHSV (Reaction condition: 350 °C, 20 bar, H <sub>2</sub> /feed molar ratio of 10, and TOS at 8 h).	71
4.25	The product distribution over 5 wt.% Co/HZSM-12 catalyst at different different LHSV (Reaction condition: 350 °C, 20 bar, H <sub>2</sub> /feed molar ratio of 10, and TOS at 8 h).	72
4.26	Liquid products obtained over (a) 5 wt.% Co/HZSM-12 and (b) 5 wt.% Co/HZSM-22 catalysts by melt infiltration method (Reaction condition: 350 °C, 20 bar, LHSV 1.5 h <sup>-1</sup> , H <sub>2</sub> /feed molar ratio of 10).	73
4.27	The conversion and selectivity of products that obtain over (a) 5 wt.% Co/HZSM-12 and (b) 5 wt.% Co/HZSM-22 catalysts by melt infiltration method. (Reaction condition: 350 °C, 20 bar, H <sub>2</sub> /feed molar ratio of 10, and TOS at 8 h).	74
4.28	The conversion and selectivity of products over 5 wt.% Co/HZSM-12 and 5 wt.% Co/HZSM-22 (Reaction condition: 350 °C, 20 bar, H <sub>2</sub> /feed molar ratio of 10, and TOS at 8 h)	74

4.29	Proposed reaction pathway of bio-jet fuel from palmitic acid.	76
4.30	TPO profile of Co/HZSM-12 and Co/HZSM-22	77





## CHAPTER I

### INTRODUCTION

In this industrial era, the enhancement of fossil energy demand including its impact to the environment becomes the greatest challenges which have forced the world to find and consume the newest sustainable energy that is environmentally friendly (Yaya *et al.*, 2018). Climate change is the current issue that is caused by utilizing a big number of non-renewable fossil fuel which produce large CO<sub>2</sub> emissions that has been stealing worldwide attention by becoming one of the Sustainable Development Goals main agenda (Fabiana *et al.*, 2018). Aviation is one of the strongest-developing public transportation sectors. Universal aircraft operations may consume approximately 1.5 billion barrels of Jet A-1 fuel, delivering around 705 million tons (Mt) of CO<sub>2</sub> in 2013 and it is expected to increase by up to 5% annually then it could reach more than six times in 2050 if the consumption rate grow in the same number (Paul *et al.*, 2018). Moreover, changing of fossil jet fuel to be green renewable jet fuel becomes the significant choice to gain the environmental policy and world economic stability.

Bio-jet fuels are commonly produced from vegetable oil that contains oxygenated compounds fatty acid (C<sub>8</sub>-C<sub>18</sub>) and their derivatives such as stearic acid (C<sub>18</sub>) and palmitic acid (C<sub>16</sub>). There are some sources of vegetable oil that have been using as a feedstock of bio jet fuels production, *i.e.* coconut (Zoltan *et al.*, 2016), *Jatropha* (Il-Ho *et al.*, 2018), *Camelina* (Edmund *et al.*, 2016) and Palm (Vorranutch *et al.*, 2018). However, the usage of vegetable oil for fuel is always being controversial and critical issue because it would increase inadvertently the price of edible vegetable oil and build unhealthy competition between fuel and food. Hence, fatty acid or palm fatty acid distillate (PFAD) as a by-product of palm refining process become the good choice to be a bio-jet fuels feedstock related to the number of palm oil production in the world. PFAD particularly contains high free fatty acids approximately 85% (FFA, 85 wt. %), triglycerides for about 10 wt. % and another compounds like sterols, vitamin E and squalene.

There are some reactions occurred during bio jet production process by deoxygenation methods, they are reported as follow: hydrodeoxygenation (HDO), hydrodecarbonylation (HDC), and decarboxylation (DCX) (Yaya *et al.*, 2018). Hence, using deoxygenation method for bio jet fuel treatment purpose to remove some oxygenated compound, carboxylic and carbonyl group contained in fatty acid molecules. Afterward, it is also followed by hydroprocessing that includes hydrogenation, hydrocracking and hydroisomerization. Zeolite support have been extensively explored in many industrial sectors including catalyst for isomerization and cracking of long chain alkanes involves the range of jet fuel (C9-C14) over their acid sites. Lately, bi-functional metal or zeolite catalysts have been expanded to improvement of bio-oil (Ding *et al.*, 2016). The Co/HZSM-12 catalysts could be considered for bio-jet fuel production. Introducing Co into acid-support zeolite may possess excellent hydrogenation function. Furthermore, it is also exhibit great efficiency and stability. The Ni/HZSM-12 catalyst as the recent study was utilized to compare with metal Co to inspect the effect of pore size and morphology that suitable for bio-jet fuel production (Yaya *et al.*, 2018).

In this study, the production of bio-jet fuels from PFAD was investigated in a continuous flow fixed-bed reactor. The Co/HZSM-12 and Ni/HZSM-12 catalysts were prepared by two methods that is incipient wetness impregnation method and melt infiltration method to investigate the conversion, selectivity, and stability during the catalytic activity testing. The fresh catalysts were characterized by XRD, XRF, TEM, BET, TPR and TPD. In addition, the spent catalysts were characterized by TPO. Moreover, the effect of temperature, pressure, % metal loading and space velocity are also optimized to satisfy the yield of bio-jet fuels.

## **CHAPTER II**

### **LITERATURE REVIEW**

#### **2.1 Bio-jet Fuel**

In 2015 the United Nations has released and validated the sustainable development goals (SDGs) which expect to be achieved in 2030 or people know as Agenda 2030. The SDGs has 17 goals involving all aspects of sustainability and all sector of society (Blanc *et al.*, 2017). One of the principles Agenda 2030 is climate action which is related with greenhouse gasses (GHG) emission and climate change. In current years, there has been a significant enhancement in the amount of pollutants in the air, mainly greenhouse gasses which is responsible for global warming. The result of this unquestionable phenomenon has attracted the world to pay attention since many years, such as accelerating of the polar ice caps liquify, increasing the earth temperature, and animal species extinction. (Grabmeier, 2012).

CO<sub>2</sub> is the most common gas among the GHG and become the main climate change agent due to the combustion of fossil fuel particularly from transport sector. Moreover, in the sector of transportation the energy combustion stream grows to more than 25% of the entire CO<sub>2</sub> emission in the world, and the aviation sector contribute CO<sub>2</sub> emission arround 2% (Yang *et al.*, 2018).

Some studies have inquired the expansion of air transportation related to global CO<sub>2</sub> emissions, the reduction of certain number CO<sub>2</sub> emissions are required more work to revise the recently trends. In addition, the increasing of fossil jet fuel technology and progress in efficiency improvements will proportionally related to the increasing of jet fuel consumption followed by the emission of CO<sub>2</sub>. As seen in Figure 2.1 data from International Civil Aviation Organization (ICAO) withing years increase the emission of the CO<sub>2</sub> from air transportation increase (Thran, D and J, Ponitka., 2016).

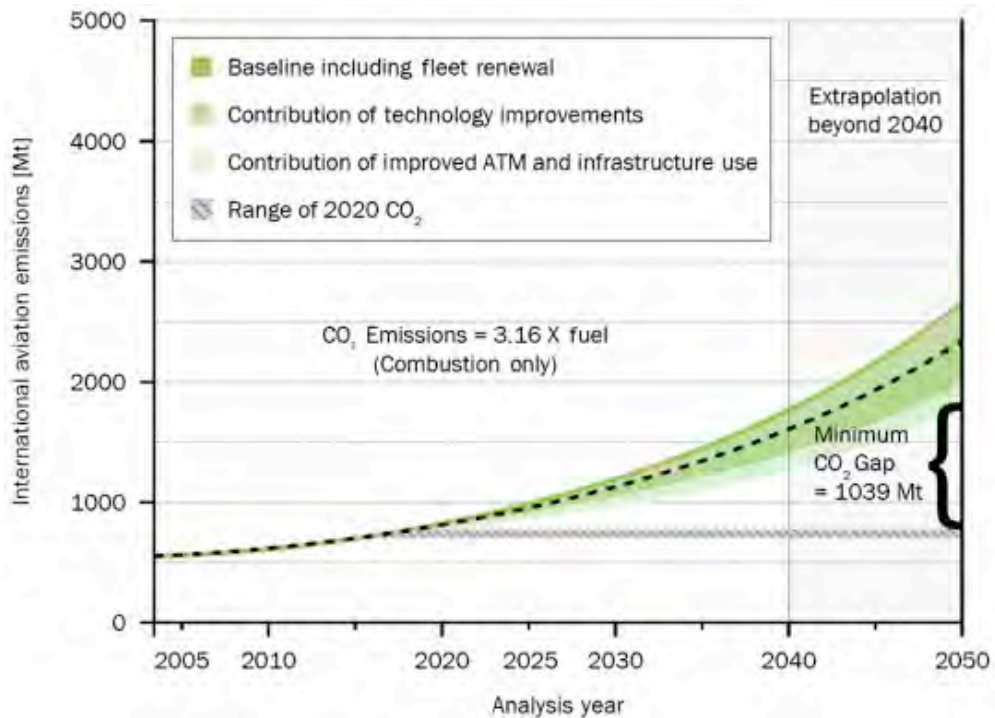


**Figure 2.1** Plot of emission of CO<sub>2</sub> within increasing number of years.

Jet fuel are mainly produced from petroleum refining process that used for activate and power the airplane by utilizing gas turbine power unit. Jet turbine fuel have not been completely substituted by bio green jet fuel cause some reasons. The jet turbine fuel mainly consists of approximately 70% paraffin (straight and branched) and around 30% cyclic hydrocarbon involving aromatic hydrocarbon and cycloalkanes, it is composed a carbon number in range C<sub>9</sub>-C<sub>15</sub>. In the other hand, bio jet fuel, also clarified that the fossil jet fuel and synthetic paraffinic kerosene (SPK) has the similar composition (Yang *et al.*, 2018).

Nowadays, jet fuels have been the most important classes in aviation industry. It is considerably as the main fuel in air transportation especially in civil aviation. The type of jet fuel that commonly utilized in civil aircraft are Jet-A and Jet-A-1, while for the military sector, the regular fuel that is used is JP-8 which has the similar

composition to Jet-A fuel. For the properties of each jet fuel, it can be searched in (Table 2.1) (Yu *et al.*, 2018).

**Table 2.1.** Major fuel properties of Jet A, Jet-A1, Jet-Bio, and Bio-jet fuel (Han *et al.*,2018)

Properties	Fuels			
	Jet A	Jet A-1	Jet-Bio	Bio-jet fuel
H/C ratio	1.96	2.01	1.98	
Molecular weight (g/mol)	142 ± 20	143 ± 4 140.8	172 ± 5 159	210
Aromatic content (%)	25.0	25.0	9.4	
DCN (Ignition delay)	47.1 ± 0.3 (4.37 ms)	46.6 ± 0.6 (4.42 ms)	62 ± 0.6 (3.24 ms)	
Density (kg/m <sup>3</sup> at 15 °C)	775–840	793.8	786	767
Flash point (°C)	38 min	38 min	52	66
Freezing Point (°C)	−40 max	−47 max	−58	−49
Net heat of combustion (MJ/kg)	42.8 min	42.8 min	43.44	
TSI (Smoke point)	17.2 (25 mm)	17.3 (25.14 mm)	10.1 (45.88 mm)	

## 2.2 Bio-jet Fuel Feedstock

Since about 2007, and particularly since 2011, aircrafts, commercial jet aircraft producers, and jet engine manufacturers, have been involved in testing bio jet fuels and evaluating which kind of sustainable jet fuel to explore, and try to observe how to habituate to the lawmaking procedures or IATA rules that are due to come

into effect within a very short time period. In the other condition the economic margins of all aircrafts are very strict. The expense of fuel (up to 34% of expense in the end 2013) is a main donator to their operating expense. So they must to search a resource of sustainable and green fuel for blending which permits them to satisfy with adjustment and strong commitments on CO<sub>2</sub>-eq emissions reduction, but it is should be still in a predetermined limit of Jet A-1 fuel expense that has been projected. And every airline will not be easier to pay more that their rival will be paying (Elhaj *et al.*, 2016).

There are three categories for the feedstocks that have already been utilized in producing aviation fuel that shown in Table 2.2.

**Tabel 2.2** Feedstocks considered for bio jet fuel (Oslo and Avinor., 2012)

<b>Feedstock</b>	<b>Type</b>	<b>Origin</b>
Vegetable oils	Palm oil	Malaysia, Indonesia
	Rapeseed oil	Europe, Canada
	Soybean oil	Brazil, USA, Argentina
Sugar	Sugarcane	Brazil
	Sugar beet	EU
Grains	Corn	USA, Argentina
	Wheat	USA, Canada, Australia

### 2.2.1 Vegetable Oil

Considering high content of triglycerides causes vegetable oil as the strong and ideal candidates for producing renewable bio jet fuels and biodiesel due to the rich content of triglycerides. Figure 2.2 exhibited that vegetable oils may have essentially 90 to 98% of triglycerides, where a glycerol group which contain three fatty acid chain inclosed to it. Different lengths of carbon chain of fatty acid which contained in triglyceride molecules and in double bonds number become interesting as bio-jet fuel feedstocks. Furthermore, the vegetable oil including general fatty acid are made up of stearic, palmitic, oleic, linoleic and linolenic (Wang, 2012). Each

fatty acid has different composition in vegetable oils which affect the quality of bio oil (Sajjadi *et al.*, 2016). That fatty acid group including their structures are shown in Table 2.3. Moreover, beside fatty acid chains, vegetable oils also have mono- and di-glycerides as the remainder approximately 2-10 % of whole contents. Vegetable oils consist of two types, mono- and di-glyceride, which are free fatty acid (commonly 1 to 5%), phospholipid, phosphatides, carotenes, tocopherol, sulfur compounds, and some amount of water (Wang, 2012).

There are two sources of bio-jet fuel feedstock from vegetable oils that are edible oils and non-edible oils. Edible oils are well known as the first generation feedstock of bio fuel, they are primarily come from cereal and oilseed food crops, such as soybean (*glycine max L.*) oils, sugarcane (*Saccharum officinarum L.*), corn (*Zea mays L.*), rapeseed (*Brassica napus L.*), etc. Vegetable oils gained from edible plants are not recommended due to the conflict between oils and food. The example of non-edible oils sources for bio-jet fuel production are jatropha oil, algae oil, animal fats, an etc. For the comparison of several bio oil feedstock from vegetable oil including their type (edible or non-edible oils) can be seen on Table 2.3 (Antonio *et al.*, 2017).

Vegetable oils are commonly gained by mechanical, solvent aided or enzymatic extraction processes. The solvent aided extraction method has been categorized as higher efficiencies technique in fast reaction (Antonio *et al.*, 2017). The better result on the products properties gained are achieved by special hydrocracking of triglycerides as compared to the transesterification. In the other hand, the clean burning great content in alternatives raw materials for producing of bio jet fuel as the green energy is growing more significant which is parallel to the increasing demand of bio jet fuel feedstock quantity. However, the renewable jet fuels have to corresponding with the actual conventional fossil fuels in order to does not make problems in fuel distribution systems (Eller *et al.*, 2016).

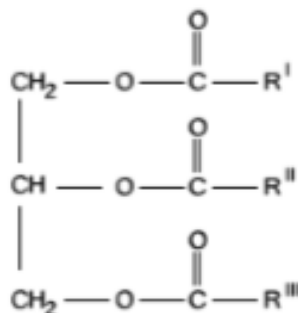


**Figure 2.3** Triglyceride chemical structure (Wang, 2012).

**Table 2.4** List of common fatty acids and its structure (Wang, 2012).

Fatty acid	Systematic name	Structure	Formula
Lauric	Dodecanoic	12:0	C <sub>12</sub> H <sub>24</sub> O <sub>2</sub>
Myristic	Tetradecanoic	14:0	C <sub>14</sub> H <sub>28</sub> O <sub>2</sub>
Palmitic	Hexadecanoic	16:0	C <sub>16</sub> H <sub>32</sub> O <sub>2</sub>
Stearic	Octadecanoic	18:0	C <sub>18</sub> H <sub>36</sub> O <sub>2</sub>
Arachidic	Eicosanoic	20:0	C <sub>20</sub> H <sub>40</sub> O <sub>2</sub>
Behenic	Docosanoic	22:0	C <sub>22</sub> H <sub>44</sub> O <sub>2</sub>
Lignoceric	Tetracosanoic	24:0	C <sub>24</sub> H <sub>48</sub> O <sub>2</sub>
Oleic	Cis-9-Octadecenoic	18:1	C <sub>18</sub> H <sub>34</sub> O <sub>2</sub>
Linoleic	Cis-9,cis-12-Octadecadienoic	18:2	C <sub>18</sub> H <sub>32</sub> O <sub>2</sub>
Linolenic	Cis-9,cis-12,cis-15-Octadecatrienoic	18:3	C <sub>18</sub> H <sub>30</sub> O <sub>2</sub>
Erucic	Cis-13-Docosenoic	22:1	C <sub>22</sub> H <sub>42</sub> O <sub>2</sub>



**Table 2.5** Various feedstock for bio-oil production from Vegetable (Mayasari *et al.*, 2014)

Vegetable Oil	Oil Content(%)	Cetane index (CI)	Food/Non Food
Palm Oil	23-25	65	Food
Jatropha	27-40	57.1	Non Food
Coconut oil	63-65	70	Food
Soybean oil	17.5	45-47	Food
Rapeseed oil	38-43	52	Non Food
Reutalis	40-50	53.9	Non Food
Trisperma			
Sunflower oil	38-43	49	Non Food

There are so many prior studied and researched about converting vegetable oil to bio jet fuel as renewable energy. Eller *et al.*, 2016 observed the reaction mechanism in production of bio-jet fuel derived from natural triglycerides which is coconut oil started by the particular hydrocracking with less amount of chemical usage and energy consumption, produce lower pollutant of dengerous material and has suitable economic references. Sulfided NiMo/Al<sub>2</sub>O<sub>3</sub> catalyst were used in this study under different reaction condition.

Cheng *et al.* (2014) used a batch reactor system to convert the soybean oil to produce high quality of bio-jet fuel which have high number of *iso* alkane products and low aromatic hydrocarbon compound via hydrocracking reaction using two kind of zeolites catalysts which are HY zeolite and zeolite HZSM-5 supporting Ni (8 wt.%) and Mo (12 wt.%) under conditions of 330-410 °C, 10-50 bar hydrogen pressure for 8 h. Zeolite HY has more result as compared to zeolita HZSM-2 in term of jet range selectivity (40.3% and 13.5%) and for aromatic hydrocarbon selectivity (23.8% and 58.9%, respectively). The jet-fuel production from oil by using zeolite HY in this study required more energy as compared to zeolite HZSM-12. This is

might be correlated to the smaller pore diameter of HZSM-12 (0.54 nm) than zeolite HY (0.74 nm), so alkanes could not be diffuse before the shorter carbon chain such as aromatic hydrocarbon has been successfully formed by the cracking of heavy products which also have higher selectivity to light hydrocarbons.

De Sousa *et al.* (2016) used Pd supported on carbon to quantitatively convert the palm kernel oil by hydrodeoxygenation in fixed bed reactor under mild conditions (300 °C, 5 bar hydrogen pressure, 5 h of reaction) to produce approximately 82% jet-fuel selectivity in total hydrocarbon products.

### 2.2.2 Fatty Acid

Animal fats have been used as the feedstock of fatty acid and all its derivatives to produce bio-oil, while vegetable oil has recently been recognized as a possible source for renewable hydrocarbon production (Miao *et al.*, 2018). Both fatty acids and vegetable oil have the identical structure which are the presence of methyl group at the end of the carbon chain of the molecule (labeled omega,  $\omega$ ) and a carboxyl group at the other end. Each carbon atom is designated with different symbols such as  $\alpha$  carbon is named for carbon atom next to the carboxyl group and the  $\beta$  carbon is used to show the subsequent one. Fatty acid generally consists of two types, they are saturated fatty acids which have no branch of hydrocarbon and unsaturated fatty acids which contain monounsaturated and polyunsaturated hydrocarbon. Saturated fatty acids generally have 12-22 carbon atoms. There are some examples of saturated fatty acids such as palmitic acid, stearic acid and lauric acid. Monounsaturated means it has one carbon-carbon double bond such as oleic acid, while polyunsaturated fatty acids have more than one carbon-carbon double bond such as linoleic and EPA (Rustan and Christian., 2005).

Itthibenchapong and friends (Itthibenchapong *et al.*, 2017) investigated the usage of Ni-MoS<sub>2</sub>/ $\gamma$ -Al<sub>2</sub>O<sub>3</sub> catalyst in generating a high quality of bio-jet fuel by using the alternative source which is palm kernel oil via deoxygenation reaction. Liquid processing methods were dominated in this process by using thiourea sulfurization catalyst, they found that C<sub>12</sub> is the dominant product from the palm kernel oil conversion over those catalysts. The optimum results for

this study is under condition of 330°C, H<sub>2</sub> pressure of 50 bar, LHSV of 1 h<sup>-1</sup>, and H<sub>2</sub>/oil ratio of 1000N (cm<sup>3</sup>cm<sup>-3</sup>). The product yield is approximately 92% which came from schematic reaction of HDO with product yield rises ~60% with 58% selectivity to C<sub>10</sub>-C<sub>12</sub> for the jet fuel.

The other studied used catalyst HZSM-12 and HZSM-22 to produce high selectivity of bio-jet fuel by using renewable non-edible oil materials as the feedstock. The non-edible oil which jatropha oil was converted to be desired hydrocarbon chain via deoxygenation reaction of stearic acid and jatropha fatty acid from jatropha oil by hydrolysis process without added hydrogen. The purposed of this study was to show the performance of the catalysts by adding W particles on it. The reaction resulted that by adding W particles on the support, deoxygenation increase around 86% which exhibited two times higher than without adding W. The most products obtained in this study was the saturated hydrocarbon (C<sub>17</sub> and C<sub>15</sub>) (Choi *et al.*, 2018).

Moreover, Cao *et al* (2018) studied about the performance of Co/HZSM-22 catalysts on the conversion of palmitic acid (common composition in palm oil) which conducted in hydrodeoxygenation and hydroisomerization reaction. The reaction condition of this study was 260°C, 2 MPa for 4 hours in batch reactor. There are three methods of metal preparation used in this study namely incipient wetness impregnation, wetness impregnation, and melt infiltration. The result obtained that bi-functional catalyst Co/HZSM-22 exhibited a potent catalyst activity in producing bio-jet fuel with high conversion and great stability.

### **2.3 Palm Fatty Acid Distillate**

CPO industry was proceeding the fresh fruit palm oil to produce two main products which are RBD olein and RBD olein. However, this process also has by product that is palm fatty acid distillate (PFAD), this PFAD will be removed during the process of CPO production. Palm fruit oil contains a lot of free fatty acid which was analyzed by determined the amount of fat after the enzymes degradation. Rainforest Foundation Norway has been reported that palm fatty acid distillate

(PFAD) has small market than the main product of CPO industry. PFAD has rich composition of free fatty acid eventhough it was only a by-product amd it can be converted for 100%. Figure 2.3 explain the flow diagram of palm fatty acid production from the cride oil refining process. Currently, PFAD utilized as feedstock for many kind of products such as animal feed, the oleochemical industry, laundry soap, and energy combustion/process heat. (Regnskogfondet.,2017).

The light brown semi-solid is the appearance of palm fatty acid distillate (PFAD) in lower temperature. It can be melted to a brown liquid by increasing the temperature more than 80 °C. There are some free fatty acid contained in PFADs particularly palmitic acid and oleic acid, they are 43.0 – 49.1% and 34.7 – 37.2% respectively then followed by linoleic and stearic etc. The types of free fatty acids in Palm Fatty Acid Distillate including their composition can be seen on table 2.5. The rest components are triglycerides, partial triglycerides and unsaponifiable matters. PFADs contain approximately 81% of free fatty acids, 14.4% of glycerides, 0.5% vitamin E, 0.8% squalence, 0.5% sterols, and 2.2% others, it can be seen on table 2.6. The application of palm fatty acid distillates except which have been mentioned above includes food emulsifier, assited the rubber processing and pharmaceutical products , and in flavours and fragrances industries. (Ping *et al.*, 2009).

**Tabel 2.6**PFAD composition (%wt) ( Top, 2010)

<b>Composition</b>	<b>Weight Percentage</b>
Free fatty acids	81.7
Glycerides	14.4
Vitamin E	0.5
Squalence	0.8
Sterols	0.5
Others	2.2

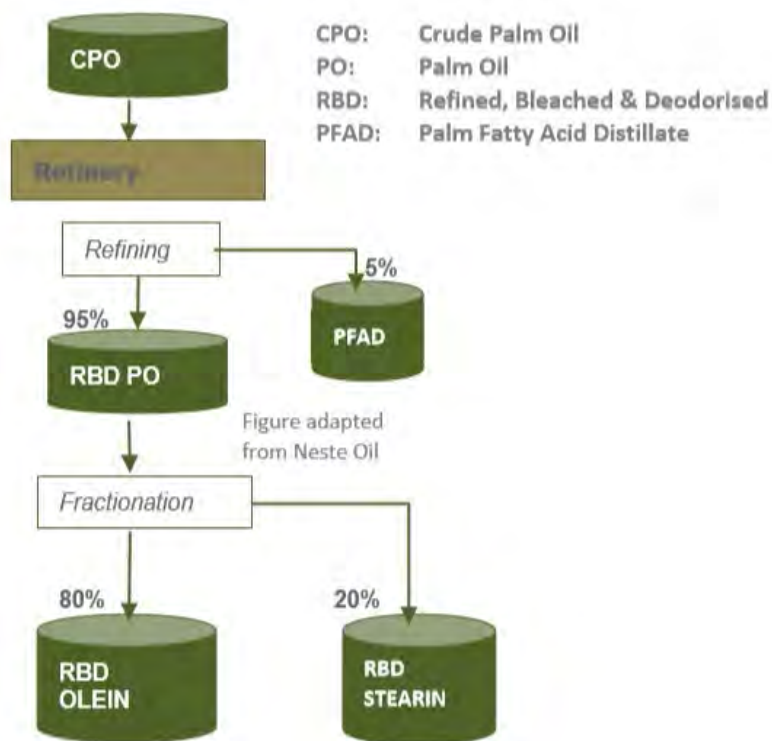


**Figure 2.3** The flow diagram of crude palm oil refining process to produce palm fatty acid distillate (Regnskogfondet.,2017).

**Table 2.7** The composition of fatty acid in PFAD (Ping *et al.*, 2009)

Composition	Weight Percentage
C8:0 capric	0 – 0.3
C10:0 caprylic	0 – 0.2
C12:0 lauric	0.1 – 2.4
C14:0 myristic	0.9 – 1.6
C16:0 palmitic	43.0 – 49.1
C16:1 palmitoleic	0.1 – 0.3
C18:0 stearic	4.0 – 4.5
C18:1 oleic	34.7 – 37.2
C18:2 linoleic	8.5 – 9.7
C18:3	0.3 – 0.5
C20:0 arachidic	0.0 – 0.4
Others	0 – 0.2

**Table 2.8** Palm fatty acid distillate characteristics.

	Tay (2007)		Bonny & Mochtar 2009	
	Range	Mean	Range	Mean
Titre (°C)	46-48.3	46.7	46-28.3	46.7
Iodine value (I <sub>2</sub> /100g)	46.3-57.6	54.8	46.3-57.6	54.8
Free fatty acid (%) (as palmitic acid)	72.7-92.6	86.4	80-90	NA
Moisture content	0.03-0.24	0.104	0.03-0.24	0.104
Unsaponifiable matter (%)	1.0-2.5	1.61	1.1-2.3	1.56
Saponification value (mg KOH/g sample)	200.3-215.4	209.5	200.3-249.4	210.0
Mass per volume (kg l <sup>-1</sup> )	0.8640-0.888	0.8725	0.864-0.888	0.8725

As the feedstock of PFADs, nowadays palm oil is a significant and multipurpose raw material for any industry, food and non-food, even palm oil latterly become the second most used and traded oil in the world. Around 17 primary oils and fats are produced from palm oil and it is predicted to be the world greatest oil produced. Figure 2.5 informed the % number of vegetable oil consumed all over the world in 2011, it can be seen that palm oil still become number one oil production in the world, eventhough it recently taking second place after soybean oil. South East Asia become the leader of palm oil production in the world, Indonesia and malaysia are the largest producers among the countries. They produces roughly 85% of the whole world production and followed by Thailand 4% and Colombia 2% (Figure 2.4)

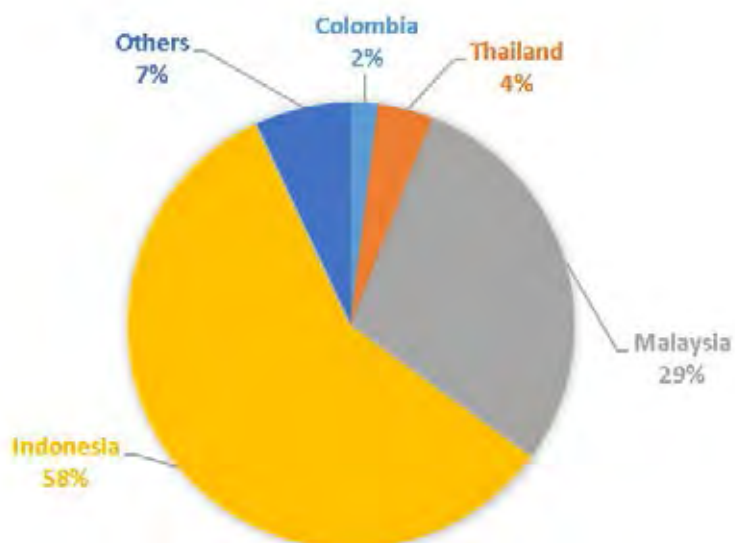


**Figure 2.4** The distribution of palm oil in some countries (Varqa, 2017).

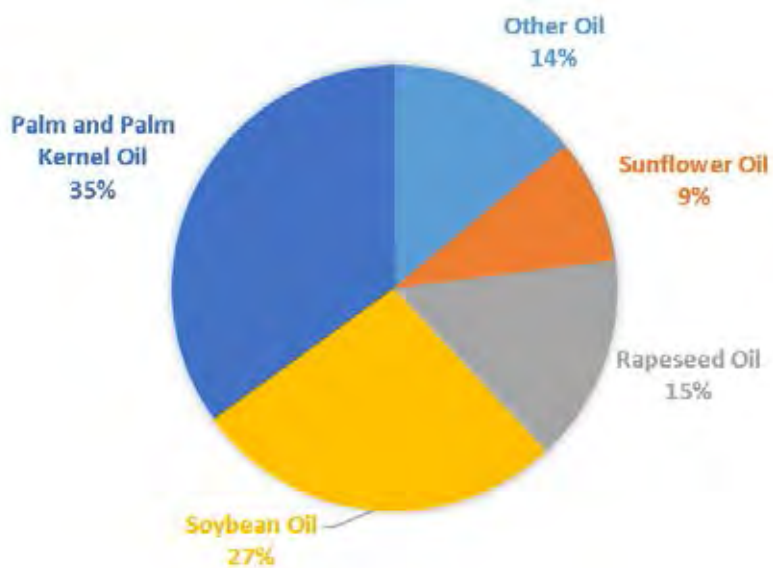


**Figure 2.5** The production of vegetable oil in the year 2011 (Koushki *et al.*, 2015).

## 2.4 Reaction Kinetics of Bio-jet Fuel Production

UOP's green jet fuel process technology (Ecofining™ SPK process) composes of two main steps. They are deoxygenations step and isomerization /cracking (hydrocracking) step. Both of deoxygenation and hydrocracking are based on hydroprocessing technology which is commonly used in modern refineries like nowadays to produce transportation fuel. However, there are a lot of process technologies that are available at commercial or pre-commercial scale to convert bio material like vegetable oil into renewable jet fuel. And there are many researches which still try to develop other process technologies to produce bio jet fuel from bio-based.

Hydrodeoxygenation, hydroisomerization/hydrocracking, and hydrogenation are the major reactions which are utilized to produce biojet fuel in this study. The previous similar study gained by Liu *et al* (2015). They investigated the effect of monometallic nickel on some support catalysts in converting palmitic acid through deoxygenation reaction in a fixed-bed reactor. The support catalysts used in this study were HZSM-22, Ni<sub>x</sub>P/HZSM-22, Ni<sub>2</sub>P/HZSM-22, the unsupported Ni<sub>x</sub>P and the unsupported Ni<sub>12</sub>P<sub>5</sub> catalysts. The decarbonylation and decarboxylation mechanisms of palmitic acid over those catalysts were analyzed by using DRIFT in situ spectroscopy. The rational deoxygenation pathways over 40NiPZ are shown in Figure 2.6.

Intermediate products such as C<sub>14</sub>H<sub>29</sub>-CH<sub>2</sub>-CHO (a) were generated by following two steps which are the dissociation of H<sub>2</sub> on Ni<sub>x</sub>P (Ni<sub>12</sub>P<sub>5</sub> and Ni<sub>2</sub>P) and forming H<sub>2</sub>O by the combination of H with OH (in palmitic acid). The conversion of palmitic acid into pentadecane could be immediately occurred through decarboxylation reaction simultaneously (b). Finally, the Bronsted acid and Lewis acid sites on HZSM-22 directly interact with palmitic acid to promote isomerization and cracking reaction respectively. H molecule in HZSM-22 and the C-C bonds in palmitic acid will be integrated with OH molecules in palmitic acid. They are deactivated by the carbonium ion reaction. Those reactions will be formed the H<sub>2</sub>O and ketones. Moreover, ketones resulted in this step can be converted into hydrocarbon by decarbonylation in step a (c). Simultaneously, aromatic hydrocarbons (or short chain



hydrocarbons) and  $C_cH_d-COOH$  can be generated from palmitic acid via cracking and isomerization. Finally,  $C_cH_d-COOH$  could be advance converted into hydrocarbons via decarbonylation and decarboxylation reaction as mentioned in Figure 2.6(d).

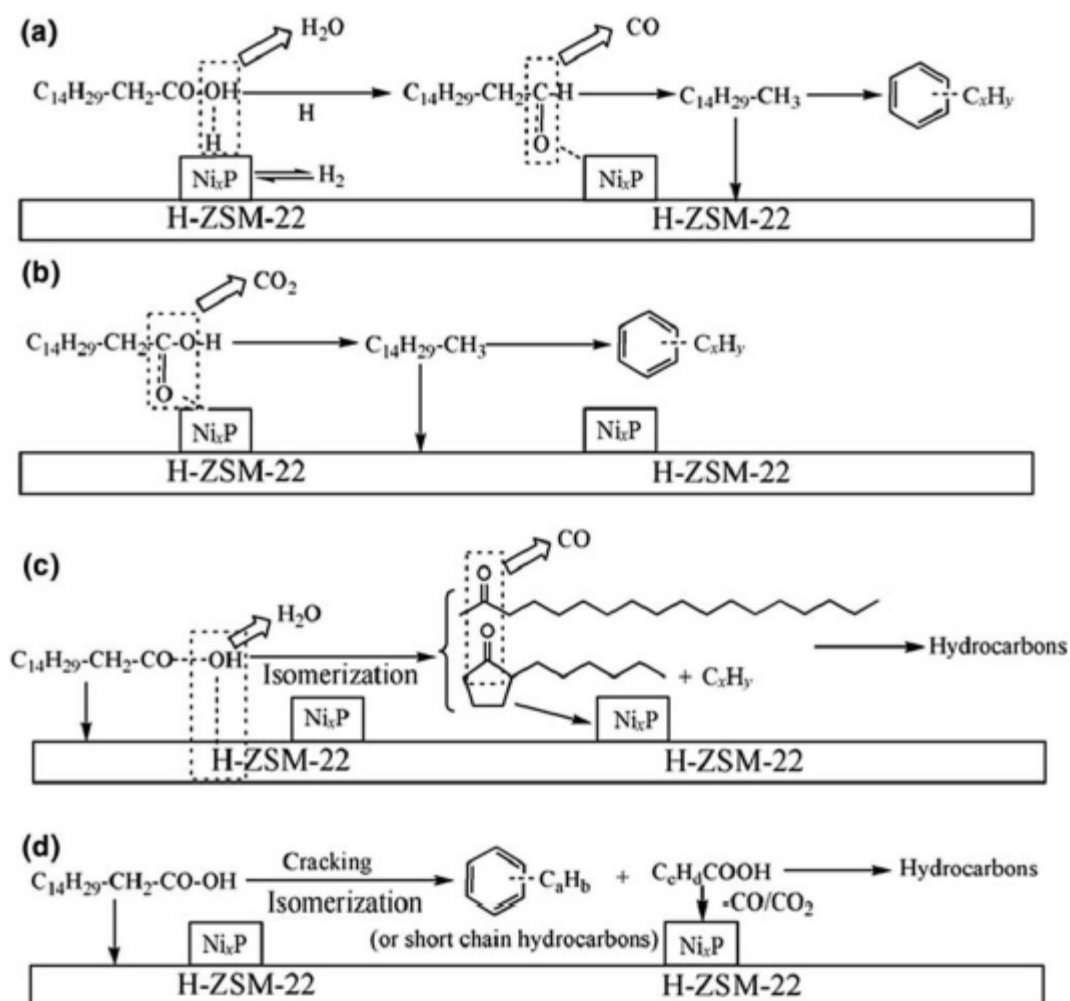


**Figure 2.6** The various catalytic schematics can be applied in palmitic acid conversion via deoxygenation on 40NiPZ. (a) Decarbonylation, (b) Decarboxylation, (c) Initial isomerization and (d) Initial isomerization and cracking (Liu *et al.*, 2015).

#### 2.4.1 Hydrodeoxygenation

The usage of fatty acid and vegetable oils in upgrading of bio-oil presence the high oxygen content, low time stability and have a low heating value.

The improvement is needed to take off the oxygen content in the system and to produce high quality crude oil. Catalysis is known as the most efficient among the oxygen removal techniques. In upgrading bio-oil to industrial level usually has two main routes: high pressure hydrodeoxygenation (HDO), the focus of this study, and catalytic fast pyrolysis with zeolites.

Hydrodeoxygenation (HDO) is used to take out and extract the oxygen from bio-oil at high pressure operation, this process also used hydrogen as the carrier gas to give the high-grade oil product. Furthermore, Hydrodeoxygenation is a chemical process which consolidated the change of the unsaturated fatty acids into saturated fatty acids and removing oxygenated compounds from the fatty acid structure. The objectives of this process are to reduce the O/C ratio and to increase H/C ratio at the same time. This process occurs over a heterogeneous catalyst at moderate or high temperature and higher hydrogen pressure. During hydrodeoxygenation process, the main by-product is water which may decrease the catalyst activity (Pattanaik and Misra, 2017).

There are many catalysts used in hydrodeoxygenation process. The most popular catalysts of this process are sulfide cobalt-molybdenum and nickel-molybdenum bimetallic catalysts support on alumina. However, the application of sulfide metal catalysts provide hydrocarbon products by some sulfur contamination which are toxic to environment. Furthermore, the cost of noble metals is very high so they are less favorable as hydrodeoxygenation catalysts. Therefore, it becomes important to improve non-sulfided transition metal catalysts for fatty acids conversion via hydrodeoxygenation to produce hydrocarbon fuels with free sulfur (Pattanaik and Misra, 2017).

There are three main reaction pathways: decarbonylation, decarboxylation which is the most desired route (no water product), and direct hydrodeoxygenation (HDO) for deoxygenation process to produce straight chain hydrocarbons and other possible reactions occurring in the process like the water-gas-shift reaction and hydrogenation as shown in Figure 2.7.

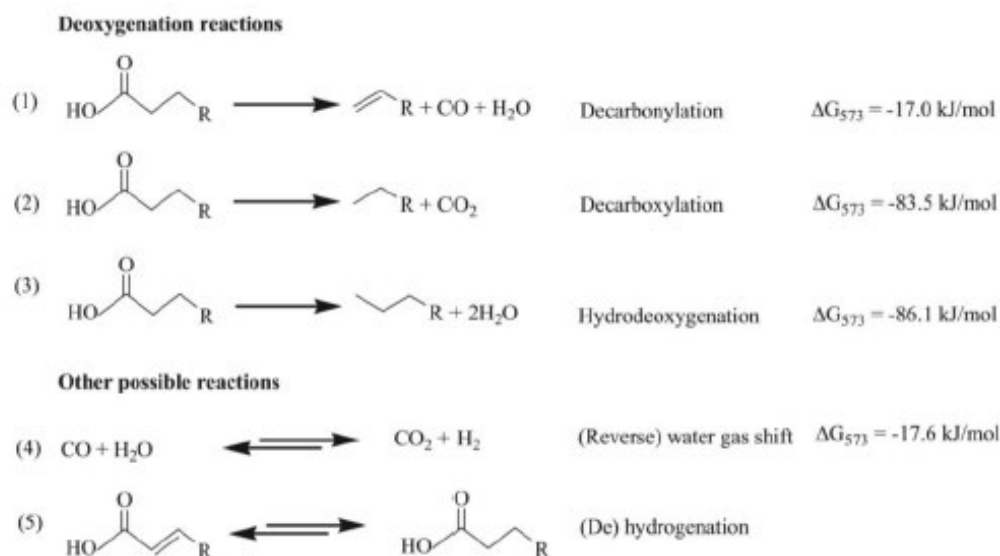


**Figure 2.7** The types of deoxygenation reaction mechanism with other possible reactions and the thermodynamic data ( $\Delta G_{573}$  in kJ/mol at 0.1 MPa) (Pattanaik and Misra, 2017).

Decarbonylation (DCN) pathway which consumed  $\text{H}_2$  for forming aldehyde as an intermediate and producing  $\text{H}_2\text{O}$  and  $\text{CO}$  (carbon monoxide) by C–O bond cleavage and C–C bond rupture, respectively. Decarboxylation (DCX) pathway, occur by elimination  $-\text{COOH}$  as  $\text{CO}_2$  which consumed no  $\text{H}_2$  and favor increasing reaction temperature, oxygen in fatty acid is removed in the form of  $\text{CO}_2$  (carbon dioxide) by the direct attack at C–C bond. Hydrodeoxygenation (HDO) pathway which consumed large quantity of  $\text{H}_2$  and consequence produced  $\text{H}_2\text{O}$ , separation of oxygen in fatty acid takes place via C=O bond hydrogenation, C–O bond rupture and further C–C bond cleavage by aldehyde and alcohol as intermediates. (Hermida *et al.*, 2015; Pattanaik, 2017)

The reaction factor such as the hydrodeoxygenation process, optimization of reaction temperature and hydrogen pressure, species of catalyst and catalyst loading designed to avoid side reactions as most as possible and have higher selectivity towards to meet specific products.

Snåre *et al.* (2006) investigated the activity of noble metal such as Pd, Pt, Ru, Ir, Os, and Rh then the non-noble metal which is Ni as the active components

on some support catalysts such as Al<sub>2</sub>O<sub>3</sub>, SiO<sub>2</sub>, and activated carbon in deoxygenation of stearic acid through semi-batch reactor by using dodecane as solvent. From the result, Pd on the mesoporous carbon shown the most powerful and efficient catalysts in term of producing more *n*-heptadecane by deoxygenation reaction of stearic acid. It gave almost complete conversion with the high selectivity of C17 products. Furthermore, Os < Ru < Ir < Rh < Ni < Pt < Pd is the order sequence of corresponded metals on the same support catalysts which explain the activity of deoxygenation of stearic acid.

#### 2.4.2 Hydrocracking

Hydrocracking reaction is an essential catalytic chemical mechanism which commonly used in petroleum refining industry for producing of valuable lower-boiling products such as gasoline, kerosene, jet fuel, and diesel oil in the presence of hydrogen and a catalyst from the middle and heavy distillates and residuals that have a high-boiling range. The process runs through reaction condition at elevated temperatures (260–425 °C) and pressures (35–200 bar) by flowing the hydrogen-rich atmosphere that leads to higher gas production and lower liquid yield. Figure 2.8 represents a hydrocracking reaction:



**Figure 2.8** The schematic of hydrocracking reaction.

In the hydrocracker system, two particular chemical reactions were included they are catalytic cracking of long chain hydrocarbon into the shorter chain unsaturated hydrocarbons and the fresh chain saturated hydrocarbon with hydrogen (Eia, 2013). In fact, there are many steps of hydrocracking over catalyst. For example, the hydrocracking of *n*-paraffins over a bifunctional catalyst goes through the following steps:

1. *n*-paraffins adsorption on the metal sites
2. *n*-olefins formation by dehydrogenation

3. Metal sites desorption and diffusion to acid sites
4. Conversion of olefin by skeletal isomerization and/or cracking through carbenium ion intermediates on the acid sites.
5. Desorption of formed olefins from acid sites and diffusion to metal sites
6. Hydrogenation of these olefins (*n*- and *iso*-) in metal sites
7. Desorption of resulting paraffins

Li *et al.* (2016) studied developing zeolite catalysts to produce jet bio-fuel from palm oil by hydrocracking. They used five different Ni-loaded zeolites as catalysts are Ni/SAPO-34, Ni/MCM-41, Ni/HY, Ni/SAPO-11 and Ni/Hbeta under conditions of 370-410 °C, 30 bar and 8 h. They indicate that Ni/SAPO-34 is an excellent catalyst for giving the highest alkane/arene selectivity ratio and Ni/HY gave the highest biojet fuel yield. The reason of these results are structure selectivity of catalysts and acid intensity by Ni/SAPO-34 catalyst has LTA structure and weak acid intensity so zeolite SAPO-34 gave the highest alkane/arene selectivity ratio. For Ni/HY catalyst has FAU structure and high acid density so it gave high arene activity.

#### 2.4.3 Hydroisomerization

In modern petroleum refining industry and technology the hydroisomerization is used as conventional method for converting of *n*-paraffins to more branch isoparaffins in hydrocarbon mixture over bifunctional catalysts which containing both the metal and acid sites. Moreover, hydroisomerization is an industrial process which now more suitable in application to petroleum refining process for the transformation of linear paraffins into their corresponding isomers than selective hydrocracking or dewaxing at usually high hydrogen pressure (at least 20 bar), even though in recent studies the reaction can be achieved at 1 atm. Thus, hydroisomerization also has been used to produce high octane gasoline and low-pour-point diesel as well as for enhancement viscosity of waxy materials such as slack waxes (Bauer *et al.*, 2014). As shown in Figure 2.9 it obviously explained that there are two main parameters influenced the performance of catalyst over bifunctional catalysts. First, the stability between metal site function and the bronsted acid site and

second, the diffusivity of intermediate alkane in the microporous area of acid support catalyst (Wang *et al.*, 2019).

The general process or mechanism of normal alkane hydroisomerization over bi-functional catalysts also clearly mentioned in Figure 2.9. First of all after the hydrogenation process on the metal site, *n*-alkane will be transformed to corresponding alkane intermediate. Then, it diffuses into the channel of micropore in acid site supports and is protonated and isomerized on Brønsted acid site. There are two reaction mechanisms included in isomerization processes over Brønsted acid site which are “pore mouth” and the “key lock”. The “pore mouth” is used to explain the formation mechanism of mono branched alkane with the branched position near the end of the carbon chain which figure out the deep penetration of molecules in microporous channel. In contrast, mono branched alkane with central branched position will be produced when only some part of molecules penetrate into the channel of micropores which produced by “key lock” mechanism. After those isomerization mechanism, the *i*-alkane intermediates are hydrogenated on metal sites in order to transform to relating *i*-alkane intermediate (Brouwer, 2018)

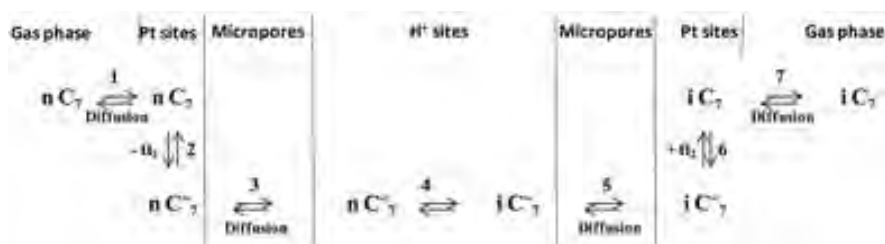


**Figure 2.9** Hydroisomerization pathway of *n*-paraffins/*n*-alkanes by using bifunctional catalysts (e.g. zeolites loaded with metals) (Wang *et al.*, 2015).

Because of the non-compatible cold flow characteristics of the normal alkane products generated from vegetable oil over hydrodeoxygenation reaction it can only be blended in low ratios with jet fuels. Therefore, the *n*-paraffins must be converted or upgraded into the corresponding *iso*-paraffins by the process of hydroisomerization to appropriately improve these properties. However, a further

hydrocracking is needed if the length of normal paraffin chain exceeds  $n\text{-C}_{15}$  before doing the hydroisomerization of jet fuel production.

The hydrogenation-to-acidity ratio is significantly effect on the hydrocracking of paraffin. The *iso*-to-normal ratio in product paraffin increased with decreasing reaction temperature because the cracking rate of *iso*-paraffins increases faster than that of *n*-paraffins at higher temperature. This is illustrated by the hydrocracking of *n*-decane in Figure 2.10. The *iso*-to-normal ratio also increases when the catalyst contains a weak hydrogenation component and strong acid component. The higher *iso*-to-normal ratio is attributed to a higher rate of isomerization of olefinic intermediates at the strong acidic sites (Scherzer and Gruia, 1996).

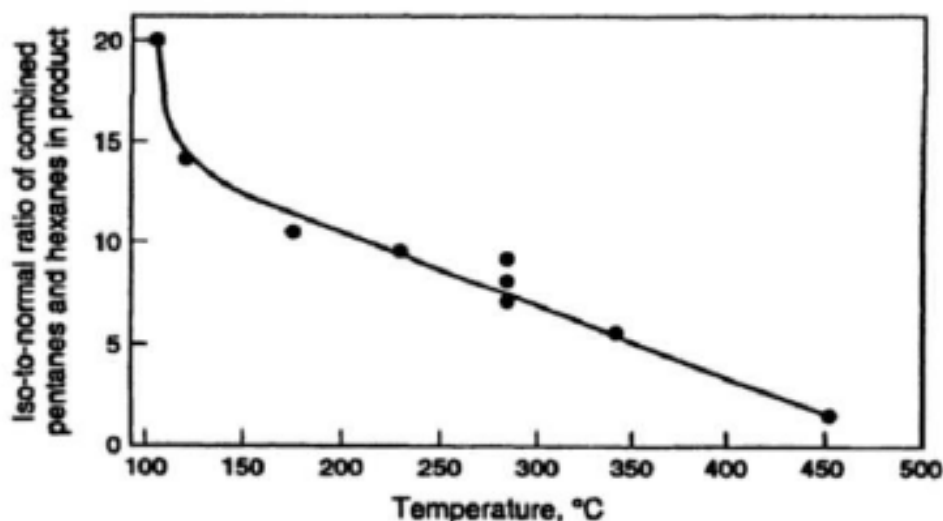


**Figure 2.10** Effect of reaction temperature on *iso*-to-normal paraffin ratio in products obtained from hydrocracking of *n*-decane over strongly acidic catalyst (Scherzer and Gruia, 1996).

Commonly alumina, zirconia, and sulfides are some oxide types that is used in acidic supports which apply to reaction of bi-functional catalysts to promote the hydroisomerization reaction. Another type of zeolites that have been used as acidic support are MOR, BEA, ZSM-5, MAZ, OFF, USY, ZSM-22, MCM-22 and zeolite-like solid acids such as SAPO-11, AlPO-5, SAPO-41. They generally perform with the metal sites such as Pt, Ni, Pd, Co, Mo, Ir, Ru, Rh and Re. There are two

processes through consecutive branching reactions over zeolites proceed (i.e., isomerization of *n*-paraffins), while cracking reactions occur in parallel with isomerization (Santos *et al.*, 2011).

In 2013, Lee *et al.* has been studied the production of high quality bio-jet fuel from FT-wax through *n*-dodecane hydroisomerization over Pt/Y zeolites. They tried to vary the acid characteristics of the zeolite to find the optimum selectivity of bio jet fuel from the model reactant. They also compared different range of acid by differentiating the ratio SiO<sub>2</sub> to Al<sub>2</sub>O<sub>3</sub> on each acid support such as NaY (SiO<sub>2</sub>/Al<sub>2</sub>O<sub>3</sub> = 5.1), HY (SiO<sub>2</sub>/Al<sub>2</sub>O<sub>3</sub> = 80) and HY (SiO<sub>2</sub>/Al<sub>2</sub>O<sub>3</sub> = 200). According to the result, the higher ratio of SiO<sub>2</sub>/Al<sub>2</sub>O<sub>3</sub> the selectivity of the *iso*-products declined and the conversion of *n*-dodecane also decreased. In addition, HY with the ratio SiO<sub>2</sub>/Al<sub>2</sub>O<sub>3</sub> of 80 represented the highest hydroisomerization reaction activity. This paper also studied the effect of various temperatures in the range of 280–360 °C under a constant pressure of 40 bar, and they found that the selectivity of *n*-dodecane decreased with the temperatures increased, while the conversion of products increased. However, the increasing of pressure in the system resulted the lower isomerization activity and efficiency, it might be due to the adsorption of *n*-dodecane on active surface was blocked by the hydrogen molecule when competing with *n*-dodecane in high pressure. They also developed the catalyst activity by loading the various amount of metal on the support in the range of 0.1–1.0%. However, they did not find any significant difference in term of *iso*-dodecane selectivity by vary the amount of metal, while the acid site strength has more effect.

In 2016, Ju *et al* synthesized bi-functional Pt/ZSM-12 catalysts to produce high multi-branched and mono-branched isomers from *n*-C<sub>15</sub> paraffin to find the high specification of jet-fuel. Based on their study, Pt/HZSM-12 catalysts did the reaction effectively and it were the appropriate catalysts to produce high yield of jet fuel. The aim of this research is to convert lipid to aviation fuel by following desired mechanism. Firstly, the lipid oil was selected from algae or oil-bearing crops which has a lot of fatty acid contains especially C<sub>16</sub>. Second, the hydrolysis of all lipid in order to be converted into fatty acid. Third, generated C<sub>15</sub> with rich *n*-paraffin content from fatty acid over decarboxylate, and finally *n*-paraffin further converted to be



multi-branched C<sub>15</sub> molecules via hydroisomerization reaction, while the obtained products can be used as jet fuel blend. The reaction pathways were conducted under reaction condition of temperature in a range of 200-340 °C, 30 bar hydrogen pressure and 2.5 h<sup>-1</sup> of *n*-pentadecane WHSV. For further study, they also compared the different support catalysts loaded by Pt particles which are Pt/ZSM-22 and Pt/USY. They reported that Pt/ZSM-22 resulted the higher ratio of multi/mono-isomers with the reaching value of 2.0. It can be concluded that Pt/ZSM-12 catalyst was the suitable catalyst for hydroisomerization reaction in conversion of lipid oil to bio-jet fuel.

#### 2.4.4 Hydrogenation and Dehydrogenation

Chemical reaction between molecular hydrogen (H<sub>2</sub>) and another compound or element is known as hydrogenation reaction. Generally, hydrogenation is applicable in reducing process by using catalysts such as platinum, palladium and nickel or saturating organic compound process by reducing double and triple bonds in hydrocarbons. Catalysts are required for any reaction condition, while non-catalytic hydrogenation only appropriate at very high temperatures.

In 1897 Sabatier found that the presence a trace of nickel as a catalyst eased the addition of hydrogen to the molecules of carbon compounds.

The reaction condition such as temperature, hydrogen pressure, kind of solvent, and the type of catalyst used become crucial to determine the optimum and the best performance of the hydrogenation reaction by using catalyst. The appropriate hydrogenation catalyst can lead to the deactivation or the promotion by some substances which indicated as the inhibitor, poisons, or the promoters. For the examples, in one case the impurities from the substrate can be hydrogenated or the product can be a factor which lead to hydrogenation, normally on the next stage of the reaction.

The other purpose of dehydrogenation of hydrocarbons is to breakdown of two carbon-hydrogen bonds by simultaneous formation of a hydrogen molecule and a molecule which contains a double carbon-carbon bond, and it normally generates the desired product. The hydrocarbon with double bond chain has

high reactive point that allows the use of hydrocarbon intermediates molecules which suitable for the production of typical petrochemical products such as polymers.

#### 2.4.5 Hydrogenolysis

Hydrogenolysis is a chemical reaction which use hydrogen for cleavage or lysis (breakdown) the carbon–carbon or carbon–heteroatom single bond. There are many kind of heteroatom, normally consist of oxygen, nitrogen or sulfur. In addition, hydrogenolysis process is used in catalytic reaction by using hydrogen gas. Moreover, a related reaction is hydrogenation, where hydrogen is added to the molecule, without cleaving bonds. (Connor *et al.*, 1932). The hydrogenolysis reaction is shown in Figure 2.11:



**Figure 2.11** Schematic of hydrogenolysis reaction.

### **2.5 Bio-jet Fuel Catalyst**

According to preparation method, catalysts are divided to two type: bulk/support catalyst and impregnated catalyst. Support/solid acid and bases catalyst is more favourable for hydro-conversion of vegetable oils due to its several advantages such as solid acids are safer and easier to control than the liquid catalyst which are corrosive and require expensive material, they are also an easy separation and recycling material). There are some comprehensive type of catalyst adopted to convert vegetable oils to sustainable bio-fuel, they are zeolite or molecular sieve catalyst, metal oxide catalyst both basic and acid side ( such as calcium oxide and magnesium oxide), and others (activated coal/inert catalyst) (Chiaramonti *et al.*, 2016).

### 2.5.1 Zeolite Catalyst

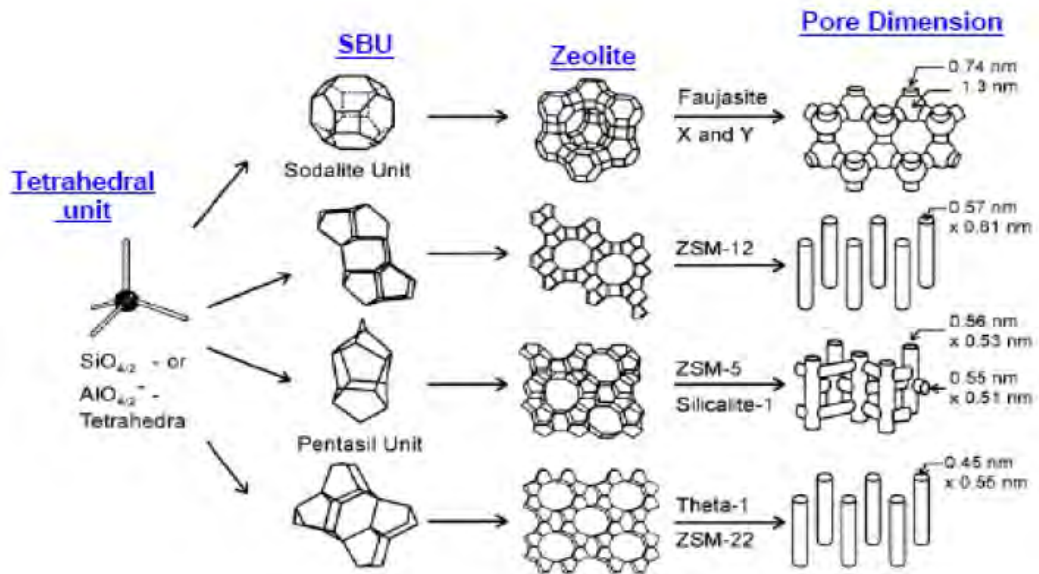
Molecular sieve, known as zeolite are crystalline aluminosilicates which consist of complex molecule. Zeolite catalysts have different ratio of silica to alumina and it look like three-dimensional porous structure that exhibit a potent catalytic activity for biofuel production. There are some zeolite catalyst which mostly used in catalytic cracking of vegetable oil to produce biofuel due to their cracking ability for heavy oil fraction: ZSM-5, Ni/ZSM-5, Zeolite HY, Ru/ZSM-5, Pt/ZSM-12, SAPO-11, HZSM-5, Ni-HZSM-5, MCM-14, beta zeolit, and etc.

The very low freezing point of commercial aircraft fuel which is more than zero degree (jet A is  $-40^{\circ}\text{C}$  and jet A-1 is  $-47^{\circ}\text{C}$ ) become the strong reason to use acidic zeolite-supported metal catalyst for vegetable oil hydrodeoxygenation of jet fuel. Zeolite known as multipurpose catalysts due to its pore size distribution, chemical composition and ion-exchange abilities. Special thing in zeolite is it has both acidic and basic characteristic. Zeolite become the most common catalysts that used in industrial field because they are cheap and environmentally friendly. Moreover, they also have high porosity and absorb surface area which help them to do ion-exchange.

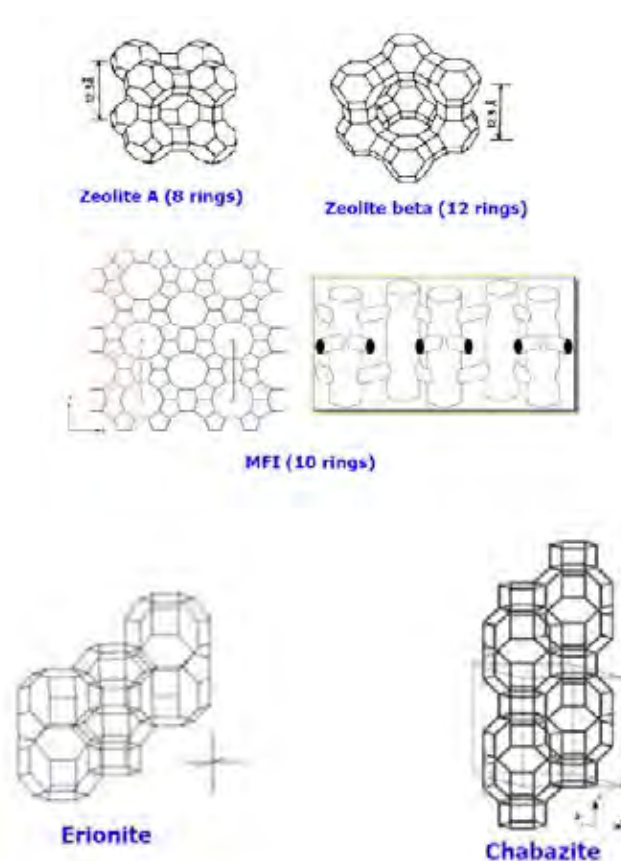
The general formula of zeolite catalyst is  $M_{x/n}[(\text{AlO}_2)_x(\text{SiO}_2)_y] \cdot z\text{H}_2\text{O}$ , where M is an extra-framework cation that balance the anionic charge of the framework. There are three types of zeolite catalyst according to their volume of pore and interconnected between the SBUs and the oxygen bridges. First is called small-pore zeolite which has diameter for about  $2.8 - 4 \text{ \AA}$  with contain 6-8 rings member (e.g sodalite and zeolite A), next is medium-pore zeolite with diameter between  $5$  to  $6 \text{ \AA}$  and contain 10-membered rings (e.g ZSM-type catalyst), and the last is named large-pore zeolite with containing 12-membered rings which has diameter more than  $7 \text{ \AA}$  (zeolite X and Y, and faujasite-type). (Shahinuzzaman, 2017)

Figure 2.12 shows the type of zeolite catalyst depending on volume of pore and interconnected between the SBUs and the oxygen bridges. It can be observed that the oxygen bridges interconnected the pentasil chains (SBUs of ZSM-5) to form corrugated sheet with 10-numbered of ring holes. Moreover, between each vertex there are vertices where each 10-ring hole has Al or Si with an O bonded. The

connection of each corrugated sheet by the oxygen bridge is used to form a structure with straight 10-ring channels which connected parallelly with the corrugations and sinusoidal 10-ring channel perpendicular to the sheet. Figure 2.13 is the examples of other categories of zeolite catalyst (Daramola *et al*, 2012).



**Figure 2.12** Zeolite structures growth from aluminosilicates to secondary building blocks to zeolite structures and the pore dimension (Daramola *et al*, 2012)



**Figure 2.13** Zeolite structures showing; A: 8-ring, 10-ring and 12-ring members and; B: other types of zeolite structures (Daramola *et al*, 2012)

Among heterogeneous catalysts, due to its properties zeolite Y type is become one of the important catalyst because it has great active which useful for catalytic fluid cracking. Zeolite Y has a spherical cages structure with diameter about 1.3 nm which are connected with four neighbouring cages (0.74 nm diameter) tetrahedrally, that is why the zeolite Y has the relatively unfold pore system. Zeolite ZSM-12 consists of 12-membered rings with 0.57–0.61 nm in pore dimension while ZSM-5 which has 10-membered ring pores, they also considered as the important heterogeneous catalysts in intersecting system (Shahinuzzaman, 2017).

Chiaramontie *et al*, 2016 reported that H-ZSM-5 is the most common catalyst which is used in conversion of vegetable oil. It was operated in the range

350-440°C at 0.1 g g<sup>-1</sup> of CTO (Catalyst to Oil ratio). A large amount of diesel range hydrocarbon (not quantified in mass) were obtained with high mass fraction liquid yield (up to 90-93%). The parameter of this research include density and viscosity, it were close to diesel fuel properties. However, the micropore of H-ZSM 5 is unable to be entered by the molecule of biomass due to its size and thereby its oxidation ability reduced. To enhance the efficiency of HZSM-5 catalyst, Weng *et al*, 2015 tried to use microporous and mesoporous mixed catalyst to increase the yield of bio jet fue drived from biomass (sorbitol) such as Ni-SBA-15, Ni-HZSM-5, and Ni-HZSM-5/SBA-15 which obtained efficiency 12.3%, 22.4%, and 40.4% respectively.

### 2.5.2 Zeolite ZSM-12 and ZSM-22

ZSM-12 zeolite (MTW) firstly publicated in 1974 by Ronsinski *et al*. The morphology of ZSM-12 catalyst is one dimensional pore system, it is a type MTW molecular sieve according to the zeolite database and it has 12-membered rings (MR). Due to its good properties on the shape selectivity to the cracking of long hydrocarbon chain, ZSM-12 type becomes one of the most important catalyst in bio-fuel production from renewable sources and it also exhibited slower coke deposition because it has good resistance to the carbonaceous deposit so, this catalyst can life longer. because it has quite larger pore size than MFI and ZSM-5 zeolite which is about 0.56 to 0.61 nm. Furthermore, one-dimensional pore zeolite can be morphology control in significant to enhance catalytic behavior and mass transfer ( Gopal and smirniotis, 2002).

ZSM-22 well known as TON type based on zeolite database. ZSM-22 has the same channel dimesional as ZSM-12 catalyst that is 1-dimensional with pore opening of 6 rings. This othorhombic cell zeolite classified as mesopore zeolite because it only has pore diameter about 5.71 (Zeolite database, 2019). ZSM-22 catalyst also use as hydroconversion of alkane with impragnated platinum as metal support ( Choudhury *et al*, 2012)

Normally, medium pore one dimensional zeolites have a liking pore mouth/key-lock mechanism which are declared to control the degree of branching. Therefore, medium pore one dimensional zeolites such as ZSM-22, ZSM-23, ZSM-

48 and ZSM-12 have been used as acidic support (Deldari,2015). The Brønsted acidity level of them is suitable for regenerating isomer selectivity and the yield with minimum cracking. Aftermath, the hydroisomerization and hydrocracking reactions occur continuously in the system, with the sequence of products being mono-branched isomers, di-branched isomers and then cracked products (Mehla *et al.*, 2013).

In crystallization of zeolite, the organic template is one of the most expensive materials. Some template from tetraalkylammonium cations such as tetraethylammonium (TEA<sup>+</sup>), methyltriethylammonium (MTEA<sup>+</sup>) and benzyltrimethylammonium (BTMA<sup>+</sup>) is the most common organic template that can be used in HZSM-12 synthesis which are added during the crystallization in the form of hydroxides, chlorides and bromides (Ronsinski *et al.*, 1974; Rubin, 1986 and Chu and Kuehl, 1984). Among the others template the using of MTEABr in ZSM-12 synthesis may be cost more than using TEOH or TEABr template, they are considered as the cheaper one (Gopal and Smirniotis, 29 2001). TEABr template is the cheapest one for crystallization of MTW. However, In 2003, Yoo *et al.* declared that the reported that TEABr template gave more narrow synthesis as compared to TEOH template.

Gopal and Smirniotis (2003) studied about the production of light naphtha by isomerization reaction and the simultaneous benzene saturation over Pt/ZSM-12 catalyst. They found that Pt supported ZSM-12 yielded the higher selectivity to the desired product as compared to Zeolite Y and  $\beta$ . They also found that Pt/ZSM-12 has lower coke deposition. Moreover, Pt/Pd-ZSM-12 catalyst has been reported had good result in hydroisomerization of  $n$ -C<sub>8</sub>/C<sub>7</sub>/C<sub>6</sub> and it also exhibited multi-branched isomers (Deldari *et al.*, 2005). The function of zeolite framework, acidity and its textural properties affect to the hydroisomerization of long chain hydrocarbons especially the external surface area of the catalyst. It was become the main contributor in the reaction pathways and pore-mouth in determining the product selectivity. (Martensa *et al.*, 2001). According to the result, it was become very important to select the zeolite morphology and did the right analysis in term of the external surface area of the catalyst to choose the better properties of the catalyst in producing high selectivity of the desired products. Therefore, it becomes crucial to

analyze the influence of the crystal size and zeolite morphology on hydroisomerization of long chain *n*-paraffins to produce high selectivity of *iso*-paraffin products. (Mehla *et al.*, 2013).

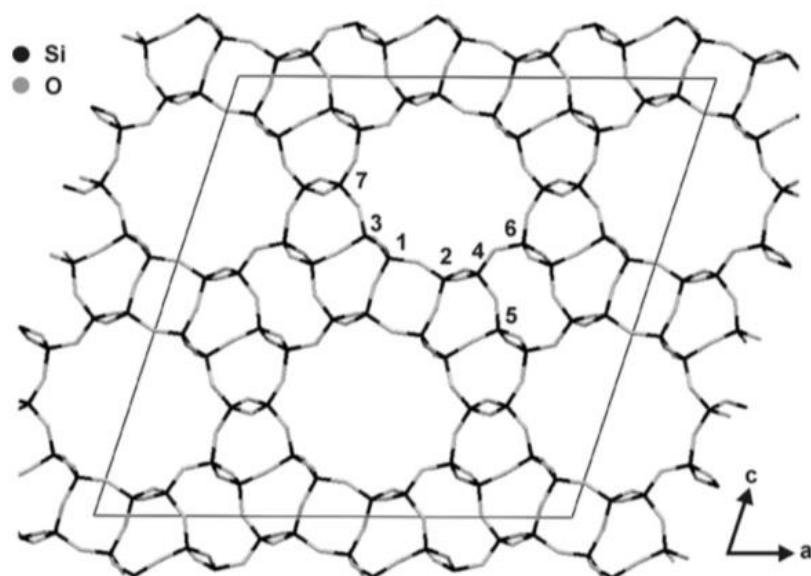


**Figure 2.14** The NMR-refined crystal structure of silica-ZSM-12 (framework type code MTW) with Si sites labeled and unit cell indicated (Brouwer., 2008).

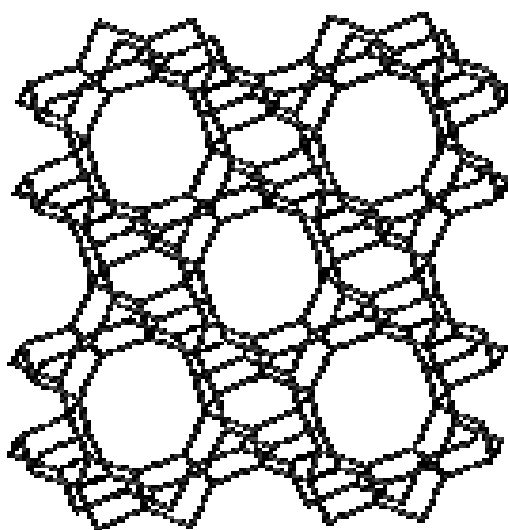


**Figure 2.15** Framework of TON zeolite or ZSM-22.



### 2.5.3 Supported Metal Catalyst Type

Most of industrial field basically used zeolites as hydroisomerization catalysts, which contain the acid site to present the hydrogenating-dehydrogenating function, various noble metals such as Pt, Pd, Rh, Ir, Ru, Re and Ni have been studied to find the optimum result, it associated mostly with mordenite or CaY.. Compared to another noble metal-zeolite catalysts, Pt or Pd loaded Y, mordenite, and beta exhibited the high activity and selectivity to hydroisomerization of *n*-alkanes. Bifunctional catalysts have shown the high selectivity and efficiency of alkane hydroisomerization which lead to hydrogenating/dehydrogenating and isomerization function of those bifunctional catalysts.. (De Lucas *et al.*, 2006).

Among the catalysts, bifunctional catalysts has been tested that it has high performance in term of alkane hydroisomerization with both hydrogenating/dehydrogenating and isomerization function. Eventhough, the noble metal are very active but they are not favourable to use because of its high cost and the rarity of noble metal catalysts that is not suitable for industrial used. Furthermore, the poisons and impurities in the feedstock such as sulfur, heavy metals and oxygenated compounds can effect a significant deactivation of noble metal catalysts due to their sensitivity to catalyst poisons and impurities.

Nickel is a very active metal in hydrogenation catalysis. It is also a cheap element thus allowing its use as a bulk metal (e.g. as Raney nickel) as well as in the form of highly loaded supported catalysts. This also gives rise to some sulfur resistance, just because much sulfur is needed to fully poison highly loaded catalysts. On the other hand, the carcinogenic toxicity of nickel compounds is a big concern in the preparation and disposal of catalysts. Most researchers have been investigated that nickel oxide when supported on kieselguhr shows the potent catalyst activity than the an unsupported one. However, the reduction temperature required for the supported oxide was higher than the an unsupported oxide (350–500 °C), while cobalt is reported to possess excellent hydrogenation function, thus it is intentionally selected as metal centers (Cao *et al.*, 2018)

The activity of Al-MCM-41 was studied to convert guaiacol, a typical lignin derived via vapor-phase hydrodeoxygenation (HDO). The zeolite was loaded

by some amount of Ni and Co particle under reaction condition of 400 °C and atmospheric pressure. This study reported that Ni is suitable for ring opening activity whereas Co more favorable in deoxygenation activity. The main products of this methyl transfer over bifunctional catalyst reaction are not only benzene and phenol but also some amount of toluene, cresol and other methylated C<sub>7-12</sub> products presented. Beside favored HDO route to remove oxygen, the Co/Al-MCM-41 also lead the transalkylation to discourage the carbon loss via methanization. However, cobalt particle seems to have more coke deposit around the catalyst which accelerated the catalyst deactivation in term of HDO activity than transalkylation (Tran *et al.*, 2016)

Peng *et al.*, (2011) have been studied the conversion of stearic acid and microalgae oil over selective deoxygenation reaction over bifunctional catalyst (Nickel supported catalyst). They used two type of zeolites as the supports which are H-ZSM-5 and H-beta by varying the Si/Al ration, the reaction take place in a batch reactor. According to the result, this study obtained the total conversion of the stearic acid by 10% Ni/HZSM-22 (Si/Al of 45) catalyst. However, this ratio of Si/Al gave lower enough selectivity to C17 and C18 for only about 43% which indicated the severe cracking to those alkane products and presence the high acidity of catalyst. On one hand, using the same catalyst but higher ratios Si/Al (120 or 200) performed the lower acidity, further cracking and the selectivity of C17 and C18 products increase gradually to 84% and 93% respectively. In addition, Ni/Beta catalysts with 10 wt.% of Ni content and 75 ratios of Si/Al exhibited the same result as the former catalyst. However, it has a lower selectivity to *iso* alkane which explained the less acid site appear in the supported catalyst that may be result the great *iso*-alkane products. The hydrotreated microalgae oil converted over a 10% Ni/H-Beta catalyst (Si/Al = 180), the main products of this microalgae oil conversion was the saturated fatty acids especially the stearic acid with the selectivity about exceeded 70 wt.% within 1 hr. In higher resident time, saturated fatty acid yield slightly decreased while the alkane yields increased (mainly including C17 and C18 alkanes) by increasing the time.

Among the chemical reactions hydrodeoxygenation (HDO) is considered as one of the most appropriate way to produce biofuels from pyrolysis bio-

oil from lignocellulose which may have similar properties to those derived from petroleum field. Based on this study, there have been different acidity which were exhibited by non-conventional hydrotreating catalysts in the catalytic HDO of anisole by using metallic Ni and Co supported on micro-mesoporous catalysts structure. They also studied about the performance of the catalysts in term of HDO route based on the phase of each metal and the support properties. To achieve the objective of this study, they use three different support which are hierarchical ZSM-5, mesostructured pure silica SBA-15 and mesostructured Al-SBA-15 that has different textural and acidic properties. The stainless steel high pressure batch reactor was used to conduct the reactions at 220°C and with the flow of pure hydrogen 50 bar. There is some interaction occur between the metallic particle (Ni or CO) with the support catalyst which also explained the dispersion of the metal species on the porous support. This phenomenon is certainly caused by the natural effect from the support catalyst and the number of Al particles present on the support. Thus, they also found there is a great correlation between the support acid sites and the metallic active phases, which is good in enhancing the HDO of anisole. According to their study, Ni-based catalysts (Ni/Al-SBA-15 and Ni/HZSM-5) exhibit higher anisole conversion as compared to Co-based materials in term of of the acid site of the support. The highly interaction between the Co particles and the acidic support can be the main reason of resulting the lower activity of the catalyst which prevents the total Co reduction prior to the reaction. Ni/h-ZSM-5 shown good activity in hydrodeoxygenation, hydrodeiromatization and isomerization reactions, which indicated that high quality of bio-fuel can be produce by Ni/h-ZSM-5 due to its good activity in bio-oil processing (Sankaranarayanan *et al.*, 2015).

Moreover, Cao *et al.*, 2018 tried to compare the activity of two metal on the HZSM-22 support they are monometallic cobalt and monometallic nickel. This research was trying to convert palmitic acid feedstock to high quality *iso*-products of bio-jet fuel. The reaction happened under condition at 260 °C for 4 h in the presence of 4 MPa H<sub>2</sub> through the hydrodeoxygenation and hydroisomerization. They also studied the effect of preparation methods to the properties of the catalyst in the way to produce high selectivity of bio-jet fuel. Based on the result, Ni/HZSM-22

prepared by incipient wetness impregnation exhibited the complete conversion of palmitic acid with the selectivity of the main products 0.8% of *n*-C<sub>14</sub>, 17% of iso-C<sub>15</sub>, 26.4% of *n*-C<sub>15</sub>, 24.2% of iso-C<sub>16</sub> and 31.2% of *n*-C<sub>16</sub>. Moreover, Co/HZSM-22 under identical reaction condition (260 °C, 4 h, 4 MPa H<sub>2</sub>) over incipient wetness impregnation method also gave the good performance in term of conversion and the products selectivity and the main products was *n*-C<sub>14</sub>, iso-C<sub>15</sub>, *n*-C<sub>15</sub>, iso-C<sub>16</sub> and *n*-C<sub>16</sub>. However, Co/HZSM-22 has better properties to yield more *iso*-product compare to Ni/HZSM-22 with mole ratios of both iso-alkanes/*n*-alkanes (1.0) and the ratio of two main products C<sub>16</sub>/ C<sub>15</sub> (3.0), while Ni/HZSM-22 gained only 0.7 of iso-alkanes/*n*-alkanes and 1.3 of C<sub>16</sub>/ C<sub>15</sub>. On the one hand, applying cobalt particle on the support will lead the HDO route more than Ni particle which is good to produce more C<sub>16</sub> products that applicable to bio-jet fuel properties over similar HZSM-22 condition and preparation method. Moreover, the presence of metallic Co particles on the H-ZSM-22 support catalyst by impregnation shown lower temperature of weak and higher temperature of strong acid sites than Ni supported H-ZSM-22, especially for strong acid sites, because it has advantage in isomerization reaction to generate more *iso*-products. Therefore, Co/HZSM-22 catalysts become the more appropriate bi-functional catalyst with low Co loading for bio-oil development to produce high quality of jet fuel.

## 2.6 Catalyst Preparation Method of Bio-jet Fuel

Some methods are used to prepare the supported catalyst to get the high performance and activity of the catalyst. The methods also keep upgrade all the time to enhance the activity and stability of the products. The popular way to prepare the catalyst with metal support is incipient wetness impregnation, it is used water as the solvent to dissolve molecular complexes of the metal precursor as the active phase ranging from just the simple salt to the more complexes building of organometallic. The other methods which are significantly used are incipient wetness impregnation and melt infiltration. This two ways can reduce the use of solution in many other methods have such as wet impregnation, ion-exchange, and metal-deposition. Melt

infiltration itself even does not use any solution. So, it can minimize the contaminated water by the zeolite and it become more economic.

Mou *et al.*, 2016 has been studied about the catalyst preparation methods by using melt infiltration and impregnation. According to their result in term of catalyst activity melt infiltration display the higher ethylbenzene dehydrogenation products and also gave less the deactivation time as compared to impregnation catalyst. Another study from De Jong and co-workers also found that melt infiltration method has higher activity which is proved by it Fischer-Tropsch synthesis reaction result. Moreover, melt infiltration method is kind of free solvent method (solid state), the use of this system will use energy efficiently due to the less problem in solvent preparation, production, purification and recycling. However, currently the solid state method for material carrier just deeply studied on supporting single active component. In principle it has further possibility to apply two or more active components on the catalyst as well as with solution-based method such as incipient wetness impregnation or ion exchange, either by as sequential manner or simultaneous.

Cao *et al.*, 2018 reported the result of different preparation methods on the catalysts activity, they used bi-functional Co/HZSM-22 in this study to know the effect of metal sites which prepared by those various methods. The raw materials used in this research was palmitic acid, it will be converted to be high quality of bio-jet fuel via hydrodeoxygenation and hydroisomerization reaction. According to their study, melt infiltration method was reported as the appropriate method in metal distribution on the support, while incipient wetness impregnation was suitable to increase the acid strength of the catalysts eventually in high Co loading. However, both preparation methods were indicated blockage the micropores, but melt infiltration shown totally blockage which can be affected the catalyst activity on the surface. Moreover, Co/HZSM-22 prepared by incipient wetness impregnation gave more C<sub>16</sub> products and *iso*-paraffin selectivity as compared to melt infiltration method, it might be because the high Co loading and the acid site built. In addition, incipient wetness impregnation also exhibited high stability on palmitic acid conversion. The

distribution of some extent of products is affected by the aggregation and leaching of Co particles in recycle run.

## CHAPTER III EXPERIMENTAL

### 3.1 Material and Equipment

#### 3.1.1 Materials

##### *3.1.1.1 Feedstock*

- Palm fatty acid distillate (obtained from OPG Tech Co., Ltd.)

##### *3.1.1.2 Chemical Reagents*

- Colloidal silica LUDOX HS-40 (40 wt.%, Dupont)
- Sodium aluminum oxide (Alfa Aesar, Technical grade)
- Tetraethylammonium hydroxide solution (TEAOH, 40 wt.% in water, Fluka)
- 1,6 diaminohexane (98 wt.%, Sigma-aldrich)
- Pottasium hydroxide (KOH, 98%, Alfa Aesar)
- Aluminium Sulphate (  $\text{Al}_2\text{SO}_4 \cdot 8\text{H}_2\text{O}$ , Alfa Aesar)
- Ammonium Nitrate ( Alfa Aesar)
- Cobalt nitrate hexahydrate ( $\text{CoNO}_3 \cdot 6\text{H}_2\text{O}$ )
- Nickle nitrate hexahydrate ( $\text{NiNO}_3 \cdot 6\text{H}_2\text{O}$ )
- Dichloromethane ( $\text{CH}_2\text{Cl}_2$ )
- Pyridine ( $\text{C}_5\text{H}_5\text{N}$ , 98 % purity, Carlo Erba)
- N,O-bis(trimethylsilyl)-trifluoro acetamide (BSTFA,  $\text{C}_8\text{H}_{18}\text{F}_3\text{NOSi}_2$ , 99 % purity, ACROS) or POMA (99.9 % purity)

##### *3.1.1.3 Standard Chemicals and Others*

- Acetone ( $\text{CH}_3\text{COCH}_3$ , 98 % purity, Labscan)
- Methanol ( $\text{CH}_3\text{OH}$ , 99.9 % purity, Labscan)

- Hexane (C<sub>6</sub>H<sub>14</sub>, 99.9 % purity, Labscan)
- Deionized water

#### 3.1.1.4 Gases

- Hydrogen (99.99 % purity, BIG)
- Nitrogen (99.99 % purity, Linde)
- Helium (99.99 % purity, Linde)
- Air zero (99.99 % purity, Linde)

#### 3.1.2 Equipment

- High pressure packed-bed continuous flow reactor system;
- Mass flow controller (Brooks instrument 5850E)
- Teledyne ISCO syringe pumps 1000D
- Back pressure regulator (SIEMENS)
- 3/4" O.D.x16" long stainless steel reactor
- Three-zone tubular furnace with a temperature controller (Cabolite)
- Gas chromatograph (Agilent GC 7890 equipped with injector, DB-5HT column and FID)
- Chamber Furnace (Cabolite)
- Teflon-lined with stainless-steel autoclave 80 ml capacity.
- X-ray diffractometer (XRD, Rigaku/ Smartlab)
- X-ray fluorescence (XRF)
- Transmission electron microscopy (TEM)
- Surface area analyzer (SAA, Quantachrome/Autosorb-1)
- Temperature programmed reduction (TPR) apparatus
- Temperature programmed desorption (TPD) apparatus
- Temperature programmed oxidation (TPO) apparatus
- Hot & stirrer plate (Cole Parmer)
- Oven



## 3.2 Experimental Procedures

### 3.2.1 Catalyst Preparation

#### *3.2.1.1 Synthesis of ZSM-12 Catalyst*

Zeolite ZSM-12 was synthesized via conventional (static) hydrothermal treatment from hydrogel solution with molar composition  $100\text{SiO}_2:1\text{Al}_2\text{O}_3:1\text{Na}_2\text{O}:25\text{TEAOH}:1500\text{H}_2\text{O}$  according to the study in situ assembly of zeolite nanocrystals into mesoporous aggregate by Yunming Fang *et al.* (2008).

First, the certain amount of TEOAH solution was diluted with dionized water and sodium aluminium oxide for about 10 minutes until the solution mixed well. To that solution, Ludox which mixed with dionized water was added under 250 rpm magnetic stirrer for 24 hours until the hydrogel perform uniformly. The synthesis gel was transferred to the teflon-lined stainless-steel autoclaves and put to the oven for hydrothermal synthesis under autogenous pressure to form the pure crystal of zeolite ZSM-12. The gel was heated under  $160\text{ }^\circ\text{C}$  for 60 h, then it need to be cooled down at room temperature naturally. The powder of ZSM-12 was filtrated by vacuum filtration then washed with dionized water frequently and dried at  $120\text{ }^\circ\text{C}$  overnight. The organic template was removed by calcination at  $550\text{ }^\circ\text{C}$  with heating rate  $10\text{ }^\circ\text{C}/\text{min}$  and dwelling time 5 h.

#### *3.2.1.1 Synthesis of ZSM-22 Catalyst*

Different from ZSM-12 zeolite, the ZSM-22 was synthesize by dynamic method. The gel was obtained according to recipe of Stefan Ernst *et al* with molar composition  $27\text{NH}_2(\text{CH}_2)_6\text{NH}_2 : 13\text{K}_2\text{O} : \text{Al}_2\text{O}_3 : 91\text{SiO}_2 : \text{H}_2\text{O}$ . The solution were divided to be four, and each solution was stirred for 5 min. The final solution give addition mixing for two hours to get the final gel.

The autoclave was filled by then with the resultant gel and it was heated at  $160\text{ }^\circ\text{C}$  for 48 h under dynamic condition. After the hydrothermal treatment the autoclave was quenched in cooled water. The powder was filtered by vacuum filtration and washed thoroughly with dionized water. The final form was dried at

120 °C overnight. The organic template was removed by calcination at 550 °C with heating rate 10 °C/min and dwelling time 5 h.

#### *3.2.1.2 Catalyst Treatment with Ammonium Nitrate*

After the first calcination, the as-synthesized ZSM-12 was treated with 1 Molar of  $\text{NH}_4\text{NO}_3$  solution to form the acid side of the zeolite via ion-exchange for three times at 80 °C, and then washed with distilled water to remove the nitrate ions. The resultant zeolite put to the oven to dry at 120 °C and calcined for 5 h at 550 °C in flowing dry air with a heating rate of 10 °C/min to obtain the acidic form of the zeolite (HZSM-12).

#### 3.2.2 Cobalt, Nickel and bimetallic Cobalt-Nickel Loading on HZSM-12 and HZSM-22

The zeolite was loaded with Co, Ni, and Co-Ni by incipient wetness impregnation, ion-exchange and melt infiltration method. After that, the mixture was gradually dried in an oven at 120 °C to remove excess water for 12 h. Then the dried nickel supported was calcined at 550 °C for 5 h (heating rate of 10 °C/min).

### **3.3 Catalyst Characterization**

#### 3.3.1 X-ray Diffractometer (XRD) of fresh catalysts

X-ray diffraction was utilized to investigate the information about crystalline phase of synthesized catalyst by a Rigaku X-ray diffractometer, RINT-2200 with Cu tube for generating  $\text{CuK}\alpha$  radiation (1.5406 Å) and operating condition of 40 kV. The sample was measured in the  $2\theta$  range of 5–50° with a scanning rate of 5 °/s.

#### 3.3.2 Brunauer-Emmett-Teller (BET) of fresh catalysts

To measure the surface area of the fresh and spent catalyst was used the surface area analyzer (Quantachrome/Autosorb-1) instrument by using the BET methods. Firstly, the fresh or spent catalyst should be outgassed to remove the moisture or humidity and other volatile adsorbents which might be adsorbed on the

catalyst surface at 250 °C under vacuum condition for 10 h prior to the analysis. For the analysis stage, the quantity of the gas adsorbed or desorbed on the surface of the solid catalysts should be determined by purging the N<sub>2</sub> gas at equilibrium vapor pressure by static volumetric method continuously. The analysis station containing the solid sample inside the sample cell was kept at the constant temperature until it reached the equilibrium. The data from volume-pressure will be used to calculate the BET surface area.

### 3.3.3 Temperature Programmed Reduction (TPR) of fresh catalysts

To measure the amount or quantity of the reducing state of the metal species present in the prepared catalyst and to investigate the reduction state of the catalyst as a function of temperature, temperature programmed reduction was used in this study. The catalyst was prepared in a ¼" O.D. quartz tubular reactor with certain weight, normally for each test it was used 0.1 g of catalyst, then the tube with the catalyst was heated (10 °C/min) under a He flow up to 400 °C. To remove the moisture from the catalyst surface, it need to be kept in this condition for 1 h. After that the sample was cooled down at room temperature, indicated the pretreatment was done. For analysis, the sample was streamed by 5% H<sub>2</sub>/Ar gas with 10 °C/min of heating rate. The amount of hydrogen consumed was used to determine the peak and it was detected on-line by an SRI model 110 TCD detector as a function of temperature.

### 3.3.4 Temperature Programmed Desorption (TPD) of Ammonia of fresh catalysts

Temperature programed desorption of ammonia method was used to analyze the acidity of the zeolite catalysts. First, the sample of the catalysts was preapred in a ¼" O.D. quartz tubular reactor for 0.2 gram weight, and the He gas was flowed into the system at 300 °C for 3 hours (10 °C/min) to reduce the catalyst, whereas the purpose of this treatment was to remove the moisture from the catalyst surface. After reduction, under the H<sub>2</sub> flow the sample was cooled down to room temperature and then analysis stage took place by exposing the NH<sub>3</sub> 5% He in to sample with a flow rate of 30 ml/min. After that, the sample was heated to 900 °C

with a heating rate of 10 °C/min. SRI model of 110 TCD detector was used to determine the amount of ammonia consumed as a function of temperature.

### 3.3.5 Temperature Programmed Oxidation (TPO) of spent catalysts

This instrument was used to determine the quantity and characteristic of coke deposition on the burnt catalyst and analyzed the characteristics of the coke during the catalyst reaction testing. First, 0.5 gram of the catalyst which already tested on the system were prepared in a reactor system by flowing of 5% O<sub>2</sub> in He continuously then gradually increased the temperature with a heating rate of 10 °C/min. The sample of the spent catalyst was conducted in a 1/4" quartz fixed-bed reactor which it has already dried at 120 °C overnight before, and it was insulated by two layers of glass wool. The signal of the system need to be stabilized before the analysis run for around 30 min under flowing 2% O<sub>2</sub> gas in He. Then, the system was heated in flowing He gas until it reach the stable temperatures of 800 °C at 10 °C/min of heating rate. The CO<sub>2</sub> produced by the oxidation of the coke species was observed by monitoring mass 44. To get the quantity result or the percent weight amount of the coke, He gas was flow inside the reactor after it reached 800 °C, then doing the Co<sub>2</sub> pulse for few minute to get at least two graph of the pulse peak. The ratio of integrated peak between the Co<sub>2</sub> and O<sub>2</sub> consumed can be noted as the amount of the coke.

### 3.3.6 Transmission Electron Microscopy (TEM) of fresh catalysts

The morphology of prepared catalyst was observed by a transmission electron microscopy (JEM-1400). For TEM analysis, the catalyst was dilute in the appropriate solvent, sonicated, and dry in the copper grid at room temperature.

## **3.4 Catalytic Activity Testing**

The catalyst testing to produce high quality of bio-jet fuel via hydrodeoxygenation, hydrocracking, and hydroisomerization reaction from palm fatty acid distillate (PFAD) were carried through 3/4" O.D., continuous flow fixed-bed reactor under high hydrogen pressure conditions and high temperature. The schematic of the reactor system and the description of flow-diagram are performed in Figure 3.1 and Table 3.1, respectively. Firstly, the reactor unit were prepared by packing 4 ml of solid catalyst in the middle of two pieces glass wool. Then, the H<sub>2</sub> was flown to the system to reduce the catalyst for 3 h under reduction temperature of the catalyst. After that, the feed was prepared and calibrated then the pressure and temperature of the system were adjusted to desired values by flowing the hydrogen gas. The feed which is PFAD was fed to the reactor by teledyne isco syringe pumps 1000D. The flow controller and the back pressure regulator were used to adjust and control the carrier gas flow and the reaction pressure, respectively.

Both liquid product and gas product were collected and analyze every 1 h for 10 h reaction. The gas product was analyzed continuously by using a Shimadzu GC-17A gas chromatograph equipped with a capillary HP-PLOT/Al<sub>2</sub>O<sub>3</sub> "S" deactivated column and FID detector and the quantity of the gas produce was determined by wet test gas meter (Ritter TG 05/2). The liquid product was trapped and collected in a condenser by prepared vial. Finally, the liquid product was analyzed by another gas chromatograph, Agilent 7890 equipped with a DB-5HT column and FID detector.

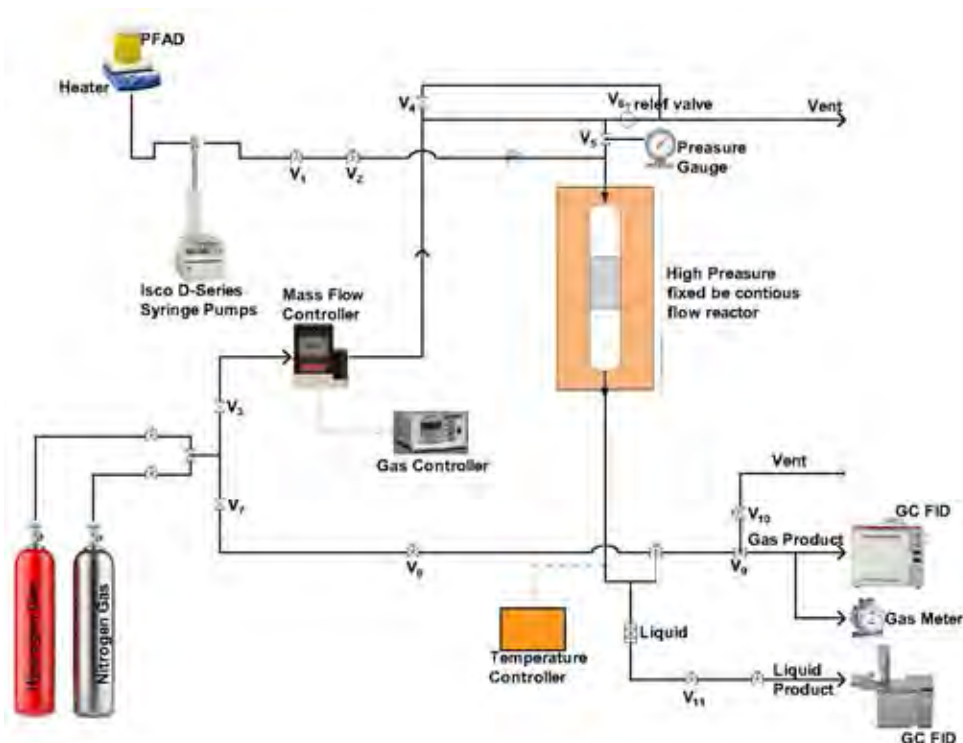


**Figure 3.1** Schematic diagram of reactor system for catalyst testing.

**Table 3.1** Description of system in flow diagram of the continuous flow fixed-bed reactor.

No.	Part	Description
1	V1	On-off valve for feedstock from ISCO syringe pumps
2	V2	Checking valve for avoiding the backward flow of the feedstock
3	V3	Three ways valve for switching between nitrogen gas and hydrogen gas flow
4	V4	Checking valve for avoiding the backward flow of hydrogen or nitrogen gas
5	V5	Needle valve for releasing gas from the system
6	V6	Relief valve for releasing pressure overload in the system
7	V7	Three ways valve for switching the direction of nitrogen gas flow

8	V8	Needle valve for controlling pressure in back pressure regulator
9	V9	Three ways valve for switching between vent gas and gas to GC lines
10	V10	On-off valve for releasing pressure from back pressure regulator
11	V11	Metering valve for gathering the liquid product from condenser
12	R1	Continuous flow fixed-bed reactor where hydroprocessing reaction take place
13	FC	Flow controller to set flow rate for the desired H <sub>2</sub> /feed molar ratio
14	PG	Pressure gauge for indicating pressure in packed bed reactor
15	PC	Back pressure regulator for controlling the pressure in reactor

The hydroprocessing reaction of PFAD is performed at temperature, pressure, liquid hourly space velocity (LHSV), and H<sub>2</sub>/Feed ratio as shown in Table 3.2.

**Table 3.2** The reaction conditions for hydroprocessing of palm fatty acid distillate in continuous flow fixed-bed reactor.

Parameter	Value
Percent Co loading (wt.%)	2.5- 7.5
Reaction Temperature (°C)	350 - 400
Reaction pressure (bar)	10 - 30
LHSV (h-1)	1.5 - 2.5
Volume of Catalyst (ml)	4
H <sub>2</sub> /feed molar ratio	10
Carrier gas	H <sub>2</sub>
Metal Type	Cobalt, Nickel, Cobalt-Nickel
Metal Preapration	Incipient wetness impregnation, ion exchange, melt infiltration

### 3.5 Product Analysis

#### 3.5.1 Liquid Products Analysis

The liquid products were quantified by a gas chromatograph (Agilent 7890) equipped with FID detector. The liquid products from the hydrocracking of PFAD contain non-polar hydrocarbons. The non-polar hydrocarbons were determined by using DB-5 column (non-polar column).

The GC operating condition was summarized as follows:

Injector temperature	: 50 °C
Detector temperature	: 380 °C
Carrier gas	: He
Column type	: Capillary column (DB-5HT: diameter 0.32 mm length 30 m)

The following chromatographic temperature program in Table 3.3 was used for liquid product analysis:

**Table 3.3** The chromatographic temperature program for liquid product analysis.

Step	Temperature (°C)	Rate (°C/min)	Holding time (min)
1	50	-	5
2	169	10	10
3	380	20	10

To calculate the quantity of liquid products and the area of each products represents by the chromatogram peak were used GC/FID (Agilent 7890) and analyzed hourly then the peak were converted to gram unit by Equation 3.1 because the each peak of products detected by FID detector can be varied from area unit to gram unit directly.

$$\text{Weight of product } i \text{ (g)} = \frac{(\text{area of product } i) \times (\text{grams of liquid product})}{\text{total areas of liquid product}} \quad \text{Eq. 3.1}$$



The conversion and products selectivity of each product were calculated by Equations 3.2 and 3.3:

$$\text{Conversion (\%)} = \frac{\text{moles of feed converted} \times 100}{\text{moles of feed input}} \quad \text{Eq. 3.2}$$

$$\text{Selectivity to product } i \text{ (\%)} = \frac{\text{moles of product } i \times 100}{\text{moles of overall products}} \quad \text{Eq. 3.3}$$

### 3.5.2 Gas Products Analysis

The composition of gas product was analyzed hourly by GC/FID (Shimadzu GC-17A). The operating condition of GC was summarized as follows:

Temperature of injection	: 150 °C
Temperature of detector	: 250 °C
Carrier gas type	: He
Column	: capillary HP-PLOT/Al <sub>2</sub> O <sub>3</sub> “S” deactivated column

The following chromatographic temperature program in Table 3.4 was used for gas product analysis:

**Table 3.4** The analysis products of gas-phase in chromatographic temperature program.

Step	Temperature (°C)	Rate (°C/min)	Holding time (min)
1	40	-	3
2	70	15	0
3	170	5	0
4	190	1	1

To calculate the quantity of gas products and the area of each products represents by the chromatogram peak were used GC/FID (Shimadzu GC-17A) and analyzed hourly then the peak were converted to gram unit by comparing with the area of methane from gas standard by mol% (equal to vol%), as shown in Equation 3.4.

$$\text{Weight of product } i \text{ (g)} = \frac{(\text{areas of product } i \text{ per } 1 \text{ ml}) \times (\text{mol of methane per } 1 \text{ ml}) \times (\text{overall gas product } (\frac{\text{ml}}{\text{h}}))}{(\text{mol of carbon atom}) \times (\text{reference area of methane per } 1 \text{ ml}) \times (\text{molecular weight } (\frac{\text{g}}{\text{mol}}))} \quad \text{Eq. 3.4}$$

The calculations of conversion, selectivity and yield of product are defined as shown in Equations 3.5, 3.6 and 3.7, respectively

$$\text{Conversion (\%)} = \frac{(\text{weight of feed input} - \text{weight of feed remaining}) \times 100}{\text{weight of feed input}} \quad \text{Eq. 3.5}$$

$$\text{Selectivity of product } i \text{ (\%)} = \frac{\text{weight of product } i \times 100}{\text{weight of total product}} \quad \text{Eq. 3.6}$$

$$\text{Yield of product } i \text{ (\%)} = (\text{conversion}) \times (\text{selectivity of product } i) \quad \text{Eq. 3.7}$$

## CHAPTER IV

### RESULTS AND DISCUSSION

In this study, the parent HZSM-12 and HZSM-22 catalysts with certain ratio  $\text{SiO}_2/\text{Al}_2\text{O}_3$  was synthesized by conventional and dynamic hydrotreatment respectively which can be confirmed by XRD and XRF result. The Co, Ni, and Co-Ni were loaded to the support by three methods which are incipient wetness impregnation, ion exchange, and melt infiltration. The activity of the catalysts in converting PFAD to bio-jet fuel were also elucidated.

#### 4.1 Characterization of Fresh Catalyst

##### 4.1.1 X-ray Diffraction (XRD)

Figure 4.1 shows the XRD patterns of synthesized ZSM-12, HZSM-12, 5% wt Co/HZSM-12, 5% wt Ni/HZSM-12, and 5% CoNi/HZSM-12. The dominant peaks at  $2\theta = 7.55^\circ$ ,  $8.93^\circ$ , and  $21.0^\circ$  which represent the (101), (201), and (310) planes of ZSM-12 respectively which indicated the good crystallinity of the parent ZSM-12 zeolite. The positions and relative intensities of ZSM-12 zeolite agreed with data from previous studies (Meier *et al.*, 1996; Pedrosa *et al.*, 2006). Moreover, there is no significant different between the planes of ZSM-12 and HZSM-12 catalysts, except the increasing of the peak intensity. It means the dealumination to create acidic form of parent ZSM-12 give only a slightly change on its crystallinity. After that, the support catalysts were loaded with different metal site via impregnation method, Co/HZSM-12 shows the characteristic peaks of CoO species at  $2\theta = 31.26^\circ$  and  $36.24^\circ$  which elucidated the planes (111) of cubic CoO, while the peaks appeared at  $2\theta = 37.24^\circ$  and  $45.64^\circ$  which clarified the (101) and (200) planes are corresponding to NiO species at Ni/HZSM-12 catalyst. Furthermore, two characteristic peaks of CoO and NiO species bimetallic CoNi/HZSM-12 accured at  $2\theta = 31.26^\circ$  (111) and  $45.64^\circ$  (200), respectively. The XRD pattern of cobalt loaded on support HZSM-12 under different methods of preparation were also explained in Figure 4.1.

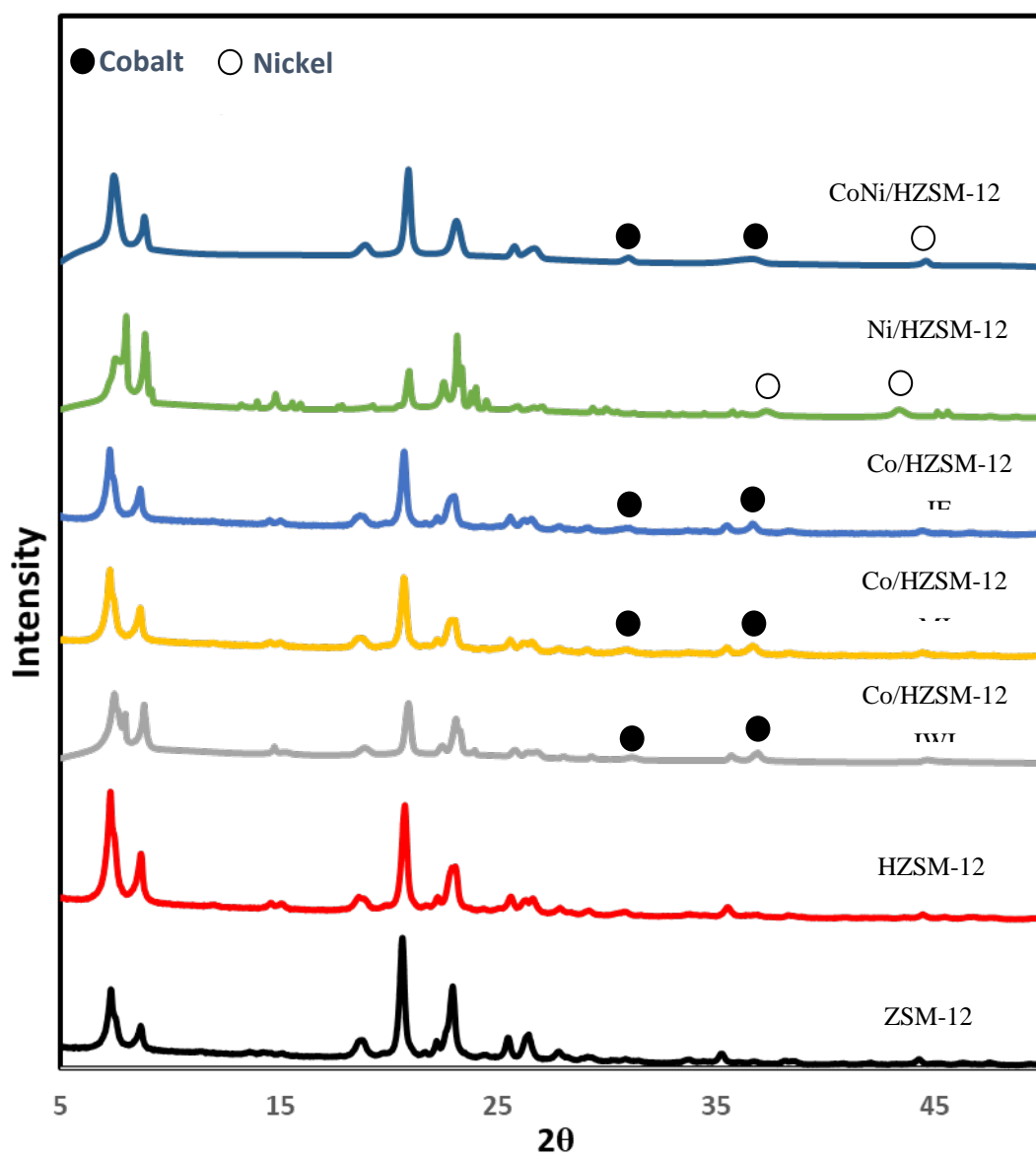


**Figure 4.1** XRD pattern of synthesized parent ZSM-12; ZSM-12; Co, Ni, Co-Ni HZSM-12; HZSM-12 by incipient wetness impregnation, ion exchange, and melt infiltration.

#### 4.1.2 X-ray Fluorescence (XRF)

The XRF characterization technique was used to identify and determine the chemical composition which can be explained by XRF result in Table 4.1. Parent HZSM-12 was synthesized by conventional hydrothermal treatment with the following molar composition of  $1\text{Na}_2\text{O}:100\text{SiO}_2:1\text{Al}_2\text{O}_3:25\text{TEAOH}:1500\text{H}_2\text{O}$ . According to the result the weight percent of each metal on the support were quite different from the theoretical value, some are higher than theoretical and others are lower. It might be due to the effect of metal preparation technique. The metal which prepared by ion exchange had lower XRF value than theoretical compared to other methods. It was expected that the metal lost with the solvent during the preparation, while the other methods only use little amount of solvent.

**Table 4.1** Chemical composition of the synthesized Co,Ni, Co-Ni/HZSM-12, Co/HZSM-12 by incipient wetness impregnation (IWI), ion exchange (IE), and melt infiltration (MI).

Catalysts	% metal (wt. %)	
	Theoretical	XRF
Co/HZSM-12	5	4.61
Ni/HZSM-12	5	5.02
Co-Ni/HZSM-12	Co of 2.5	2.20
	Ni of 2.5	2.37
IWI Co/HZSM-12	5	4.61
IE Co/HZSM-12	5	4.29
MI Co/HZSM-12	5	4.61

### 4.1.3 Transmission Electron Microscope (TEM)

The TEM image is used to determine the crystalline size of the zeolite and also the dispersion of the metal on the support HZSM-12 catalysts. The image of transmission electron microscope are shown in Figures 4.2 - 4.6. Figure 4.2 shown the TEM image of parent HZSM-12, it can be seen that the parent HZSM-12 has a cubic shape crystal, it was suitable to the previous study from da Silva *et al* in 2019 and the size of cubic phase of HZSM-12 is around 55 nm, it was similar to the previous study (Parmer *et al.*, 2014; Sanhoob *et al.*, 2014). In Figure 4.3, the Co/HZSM-12 prepared by incipient wetness impregnation, the dark spot of metal seem to be dispersed well on the support. The TEM images of metallic nickel and bi-metallic nickel on support HZSM-12 which also prepared by IWI method is illustrated in Figures 4.4 and 4.5. Figure 4.6 (a) and (b) shows TEM image of Co loaded on the support via ion exchange and melt infiltration, respectively. It can be seen that cobalt highly dispersed on the support by melt infiltration method as compared to both incipient wetness impregnation and ion exchange. However, cobalt also highly blocked the micropore of zeolite that can be clarified by the big dark spot on the TEM image in Figure 4.6.

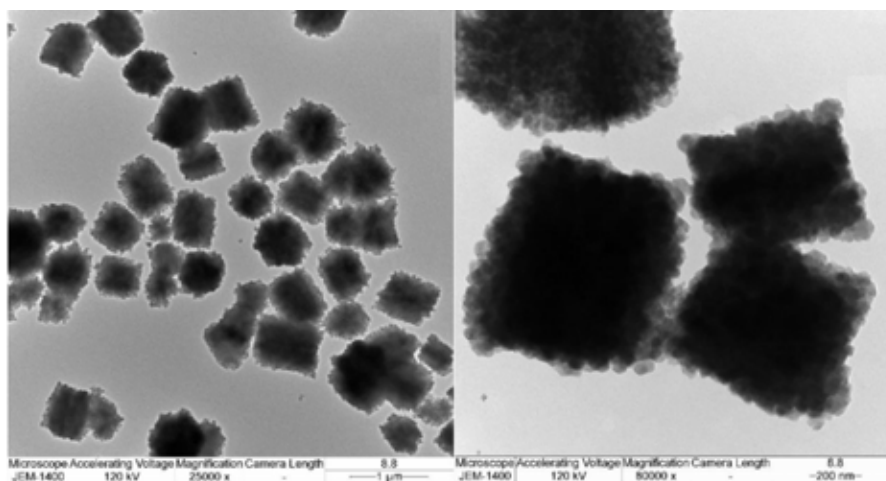


**Figure 4.2** TEM images of parent HZSM-12.

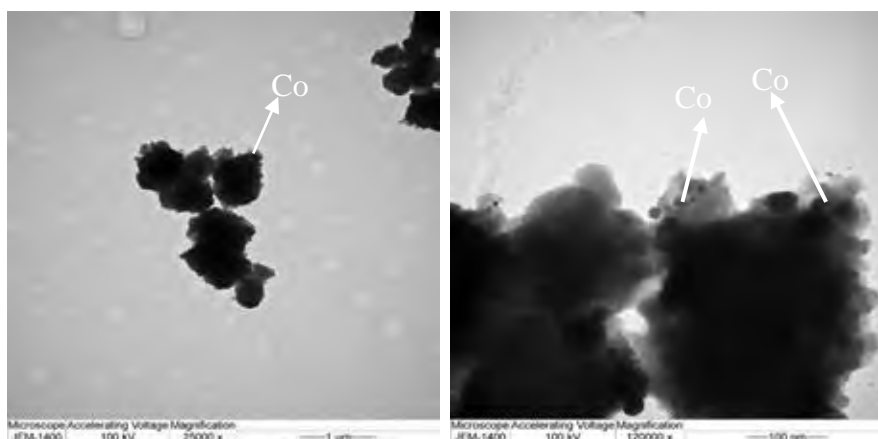


**Figure 4.3** TEM images of Co/HZSM-12 prepared by incipient wetness impregnation.

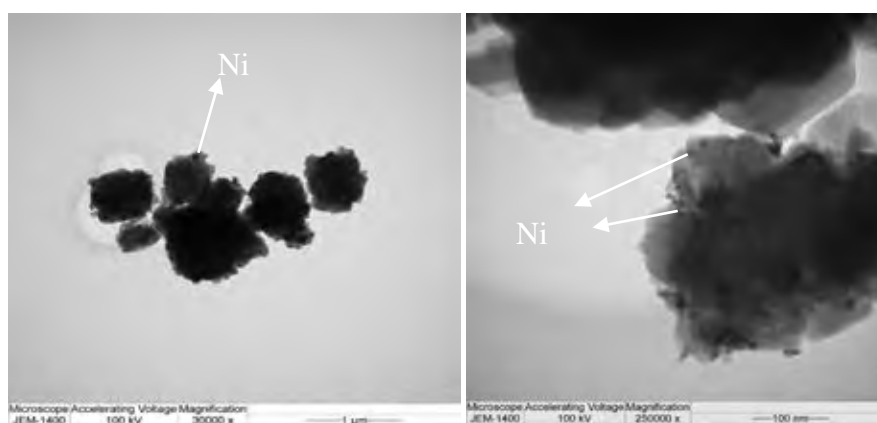


**Figure 4.4** TEM images of Ni/HZSM-12 prepared by incipient wetness impregnation.

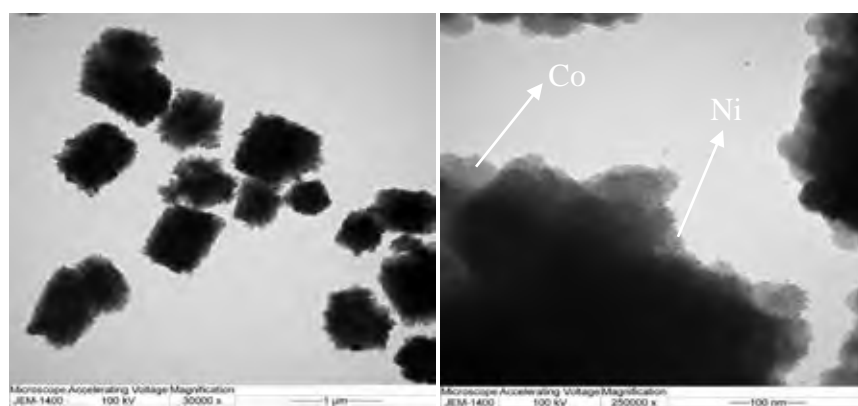


**Figure 4.5** TEM images of Co-Ni/HZSM-12 prepared by incipient wetness impregnation.

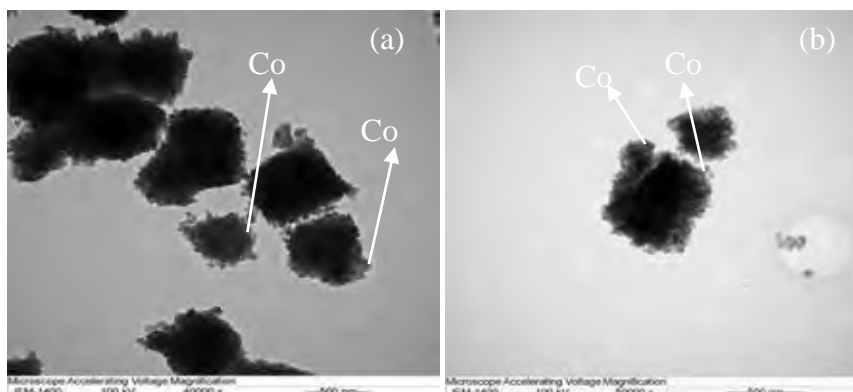


**Figure 4.6** TEM images of Co/HZSM-12 prepared by ion exchange (a) and melt infiltration (b).

#### 4.1.4 Brunauer-Emmett-Teller (BET)

Brunauer-Emmett-Teller (BET) method were used to analyze the surface area and micropore volume of each catalyst. The textural properties of the parent HZSM-12, Co, Ni and Co-Ni HZSM-12 catalysts then the properties of Co/HZSM-12 by incipient wetness impregnation, ion exchange, and melt infiltration are summarized in Table 4.3. The total surface area was calculated by the Brunauer-Emmett-Teller (BET) equation, the external surface area and the micropore volume was obtained by the t-plot method and the total pore volume was obtained by Barrett-Jayner-Halenda (BJH) analysis of the adsorption branch of the isotherm. The BET surface area, external surface area, micropore volume and total pore volume of 5 wt.% Co/HZSM-12 catalyst via incipient wetness impregnation was similar to the parent HZSM-12, indicating that 5 wt.% Co/HZSM-12 catalyst had highly dispersion of nickel particles on zeolite support corresponded to the TEM results. After loading different metal such as Ni and bimetallic Co-Ni, the BET surface area, external surface area, micropore volume and total pore volume of samples were slightly decreased. From Table 4.3 it can be observed that the incipient wetness impregnation gave the same result in terms of BET surface area, external surface area, micropore volume and total pore volume with the parent HZSM-12, while the other two methods decreased a lot. It indicated that cobalt metal highly blocked the micropore.



**Table 4.3** Physical properties of the catalysts loaded by Co, Ni, Co-Ni/HZSM-12, Co/HZSM-12 by incipient wetness impregnation (IWI), ion exchange (IE), and melt infiltration (MI).

<b>Zeolite</b>	<b>S<sub>BET</sub> (m<sup>2</sup>/g)</b>	<b>S<sub>Ext</sub> (m<sup>2</sup>/g)</b>	<b>V<sub>micro</sub> (ml/g)</b>	<b>V<sub>total</sub>(ml/g)</b>
ZSM-12	289	76	0.112	0.213
HZSM-12	287	76	0.106	0.213
5% wt Co/HZSM-12	282	76	0.102	0.202
5% wt Ni/HZSM-12	257	72	0.099	0.226
5% wt CoNi/HZSM-12	251	60	0.101	0.190
IWI Co/HZSM-12	282	76	0.102	0.202
IE Co/HZSM-12	230	74	0.081	0.198
MI Co/HZSM-12	217	60	0.075	0.196

#### 4.1.5 Temperature Programmed Reduction (TPR)

Temperature programmed reduction was utilized to evaluate the reduction temperature of the catalysts. The reduction of particles is depended on the location of the metal on the support and of its interaction with the support, as also with the structure of the oxide formed. Figure 4.6 shows the TPR results of reduced NiO and CuO. Two dominant peak regions were found (Ni/HZSM-12) at approximately 330-550 °C corresponding to the reduction of Ni<sup>2+</sup> from the NiO formed and NiO from the different crystal sizes and at between 550- 620 °C exhibited strong interaction between the metal and support. From TPR graph of Co/HZSM-12 was also found two main peaks at range 330-400 °C which correlated to the reduction of Co<sup>2+</sup> from the CoO formed and CoO from the different crystal sizes (Pedrosa *et al.*, 2006) and another peak at 400 - 550 °C (Co/HZSM-12 line) exhibited strong

interaction between the cobalt and the zeolite (Cao *et al.*, 2017). TPR result of bimetallic Co-Ni/HZSM-12 from Figure 4.6 exhibits the stronger peak at range between 270 – 330 °C indicating the strong interaction between the metal cobalt and nickel. In addition, the peak in the range of 330 – 550 °C correspond to the reduction of the  $\text{Co}^{2+}$  or  $\text{Ni}^{2+}$  from their oxide form.

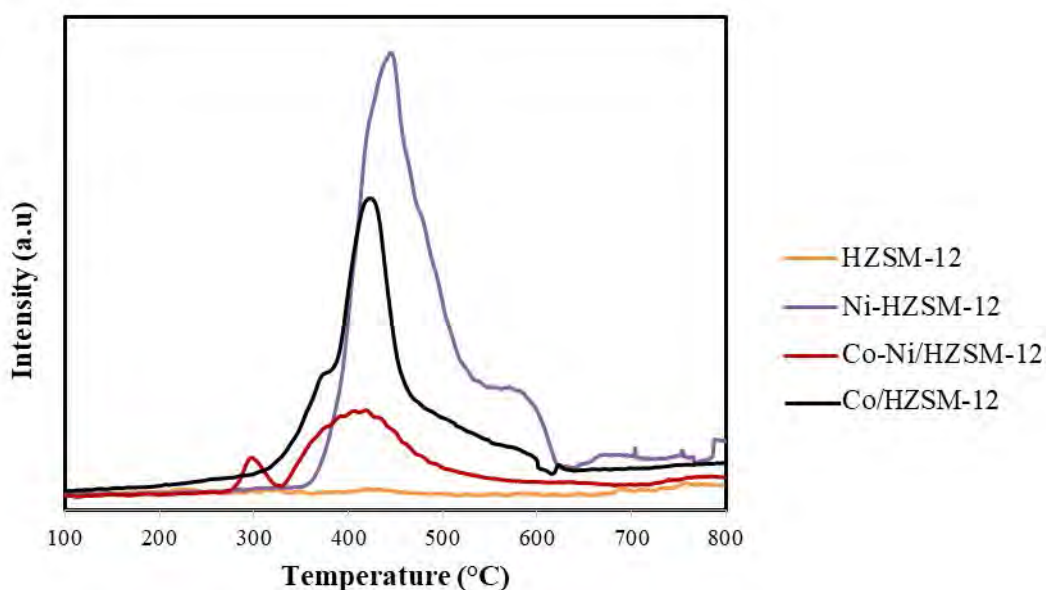


**Figure 4.7** TPR profiles of monometallic Co, Ni, and bimetallic CoNi support HZSM-12 catalyst.

#### 4.1.6 Temperature Programmed Desorption of Ammonia (TPD-NH<sub>3</sub>)

Temperature programmed desorption of ammonia is used to identify the desorption peak of prepared catalyst. The acid sites (strong acid and weak acid) can be evaluated by investigating the TPD-NH<sub>3</sub> peak. Figure 4.8 shows the TPD-NH<sub>3</sub> result of reduced NiO and CuO. Ni/HZSM-12 line presented the two peaks at 400-500 °C indicated as the weak acid site, while the strong acid site refers to the peak at 650-750 °C. Moreover, TPD result for Co/HZSM-12 also exhibited two peaks which are at 450-550 °C and 550-750 °C respectively, it is corresponding to weak and strong acid site. According to this result, it can be concluded that Co/HZSM-12 had higher strong acid site as compared to Ni/HZSM-12. TPD result for Co-Ni/HZSM-12 also exhibited

two peaks at 350-500 °C and 500-550 °C corresponding to weak and strong acid site. Furthermore, the two big peak area found in the result of Co-Ni/HZSM-12 TPD ammonia profile, the first peak which correspond to weak acid site is exist at 300-500 °C and the strong acid site at 500 - 650 °C. Among the metal, Co showed the highest acid site which can be beneficial for bio-jet fuel production.

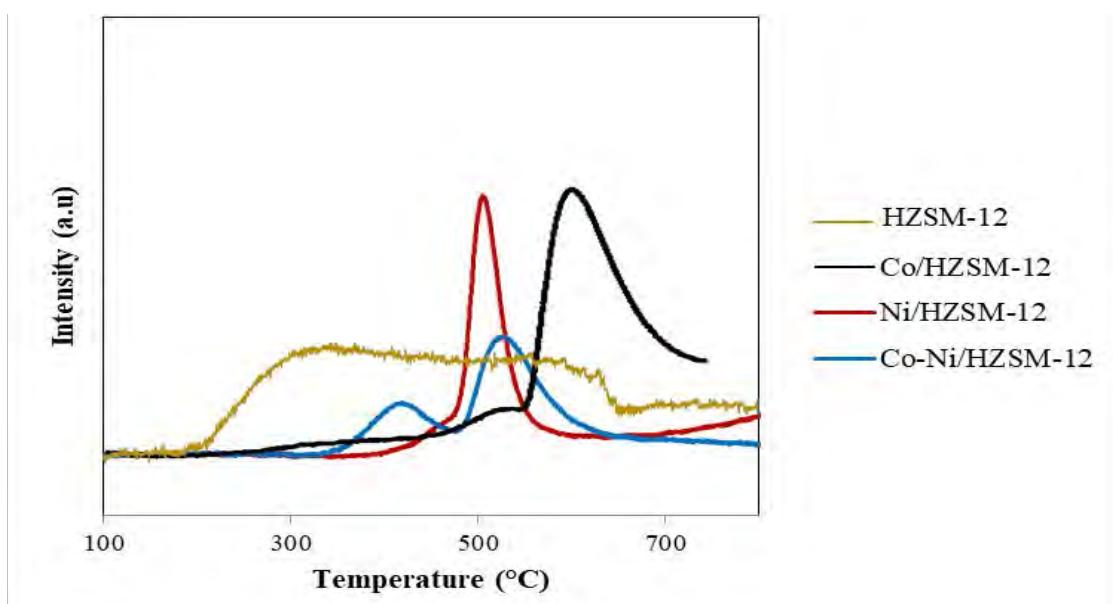


**Figure 4.8** TPD-NH<sub>3</sub> profiles of monometallic Co, Ni, and bimetallic CoNi support HZSM-12 catalyst.

## 4.2 Gas Chromatography of Feed and Standard Analysis

### 4.2.1 Feed Analysis

GC/FID (Agilent 7890A) were used to analyze palm fatty acid distillate (PFAD) feedstock . The chromatogram and composition are exhibited in Figure 4.8 and Table 4.4, respectively. It can be seen from Figure 4.9 that the main peak appeared are hexadecane, octadecane, palmitic acid, oleic acid, stearic acid, mono-glycerides, di-glycerides and tri-glycerides with the retention time of chromatogram at 14.8, 17.0, 19.9, 24.1, 24.9, 29-33, 33-38, and 38-43, respectively. Moreover, Table 4.4 shows the chemical composition in palm fatty acid distillate. It can be concluded

that PFAD mostly contains palmitic acid and oleic acid, while the other trace components are hexadecane, octadecane, stearic acid, mono-, di-, and tri-glycerides.

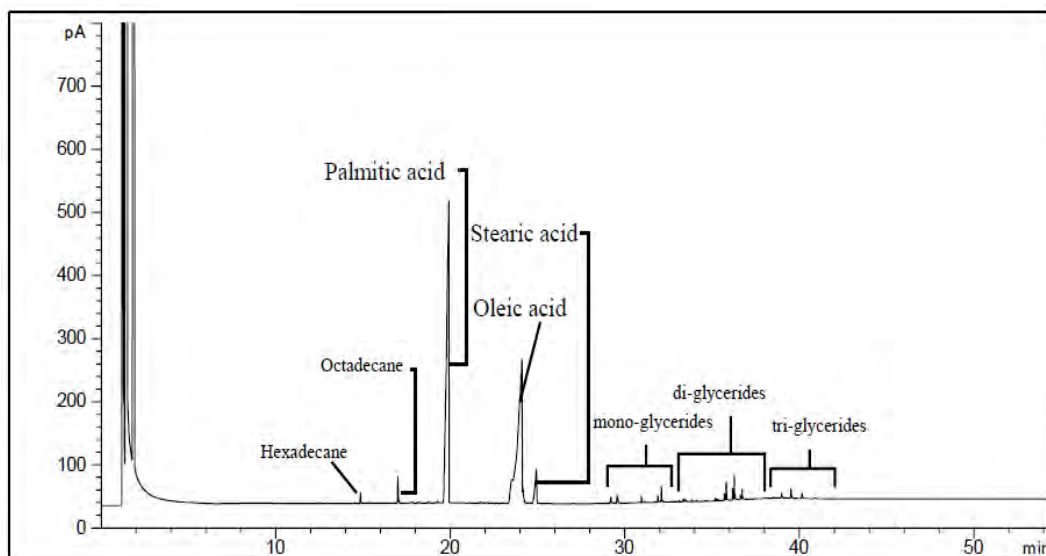


**Figure 4.9** The chromatogram of various components in PFAD range analyzed by GC/FID.

**Table 4.4** Feed (PFAD) composition

Feed components	Amount (wt. %)
Palmitic acid	46.48
Oleic acid	43.41
Stearic acid	4.00
di-glycerides	2.28
Mono-glycerides	1.45
Octadecane	1.14
Tri-glycerides	0.86
Hexadecane	0.38

#### 4.2.2 Standard Analysis

Gas chromatograph equipped with an FID detector from Agilent 7890A was used to detect the component of liquid products from the reaction. Firstly, the chromatograms of liquid standard were analyzed to clarify the composition of feedstock and liquid products. Figure 4.10 and 4.11 show the polarity liquid standard (oxygenated compounds) and non-polarity liquid standard (*n*-alkanes), respectively.

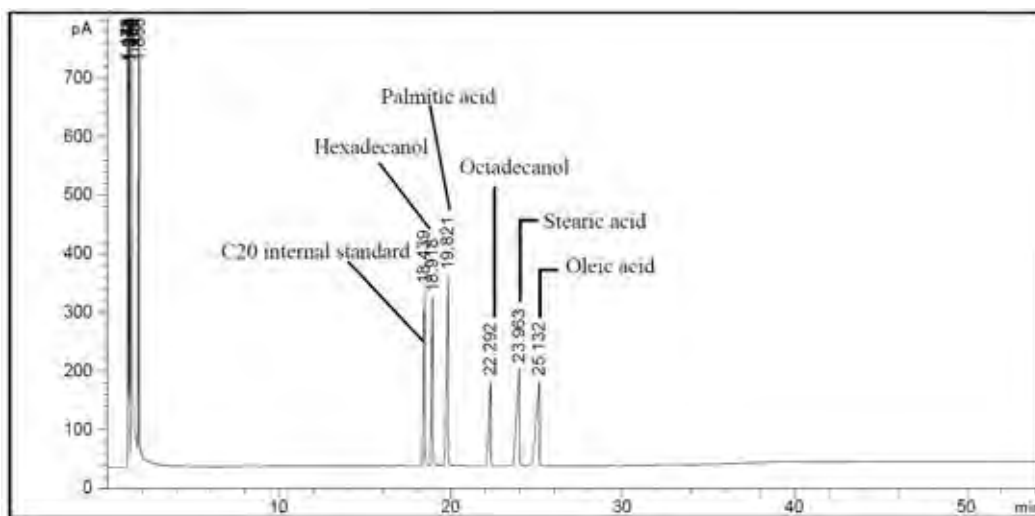


**Figure 4.10** Chromatograms of standars oxyganated compounds.

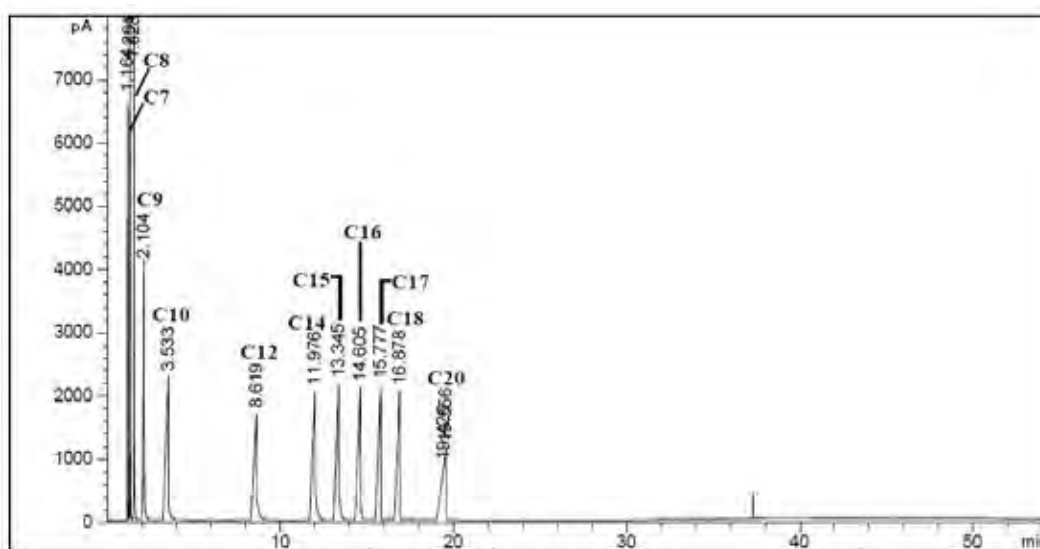


**Figure 4.11** Chromatogram of standard *n*- alkanes

Figure 4.11 exhibits the chromatograms of standard oxygenated compounds in types of fatty acid and alcohol as the remaining feed and intermediate in the result of catalytic activity testing. Furthermore, the chromatogram standard of *n*-alkanes from catalytic activity testing such as heptane (C<sub>7</sub>), octane (C<sub>8</sub>), nonane (C<sub>9</sub>), decane (C<sub>10</sub>), undecane (C<sub>11</sub>), dodecane (C<sub>12</sub>), tetradecane (C<sub>14</sub>), pentadecane (C<sub>15</sub>), hexadecane (C<sub>16</sub>), heptadecane (C<sub>17</sub>), and octadecane (C<sub>18</sub>) were also shown in Figure 4.10.

### 4.3 Catalytic Activity Testing

Palm fatty acid distillate as the feedstock of this research has been converted to bio-jet fuel by equipped fixed-bed flow reactor. The 2.5-5 wt.% of HZSM-12 with various metal loaded (Co, Ni, bimetallic Co-Ni) were tested. This part would also investigated the product selectivity and yield of each reaction condition ( temperature at 350 – 400 °C, pressure of 10-30 bar, liquid hourly space velocity (LHSV) of 1.5 – 2.5 h<sup>-1</sup>, and H<sub>2</sub>/feed molar ratio of 10) and the effect of metal preparation methods which are incipient wetness impregnation, ion exchange, and melt infiltration.

#### 4.3.1 Effect of Reaction Temperature

The effect of reaction temperature to the selectivity and the yield of product were studied by conducting the reaction condition at 30 bar, LHSV of 1,5 h<sup>-1</sup> and H<sub>2</sub>/feed molar ratio of 10. The catalyst used was 5 wt.% of Co/HZSM-12. The testing temperature was varied from 350 to 400 °C. Figure 4.12 performed the result of product composition in converting PFAD to bio-jet fuel. It demonstrated that the temperature range between 350- 400 °C has nearly complete conversion. In addition, the conversion of gasoline and light product increased with increasing temperature. This indicated that hydrocracking of the heavier product to lighter are prefer at high temperature. Moreover, Arrhenius Equation ( $k = Ae^{-E/RT}$ ) explains that the increasing of cracking yield correlated to the catalytic activity and the reaction rate. This indicate that the hydrocracking of heavy product to lighter product was prefer at high reaction temperature. However, selectivity of bio-jet fuel are decreased with increasing

temperature due to the significant cracking of heavy product to the light product and gasoline. Moreover, the highest selectivity of bio-jet fuel with hydrocarbon range C<sub>9</sub>-C<sub>14</sub> over 5 wt.% Co/HZSM-12 is 350 °C. Therefore, the reaction temperature at 350 °C has been chosen as the optimal reaction temperature for further study the effect of different metal loading (Co, Ni, and Co-Ni) because of its good performance in bio-jet fuel selectivity and low selectivity to light product, gasoline, and diesel production.

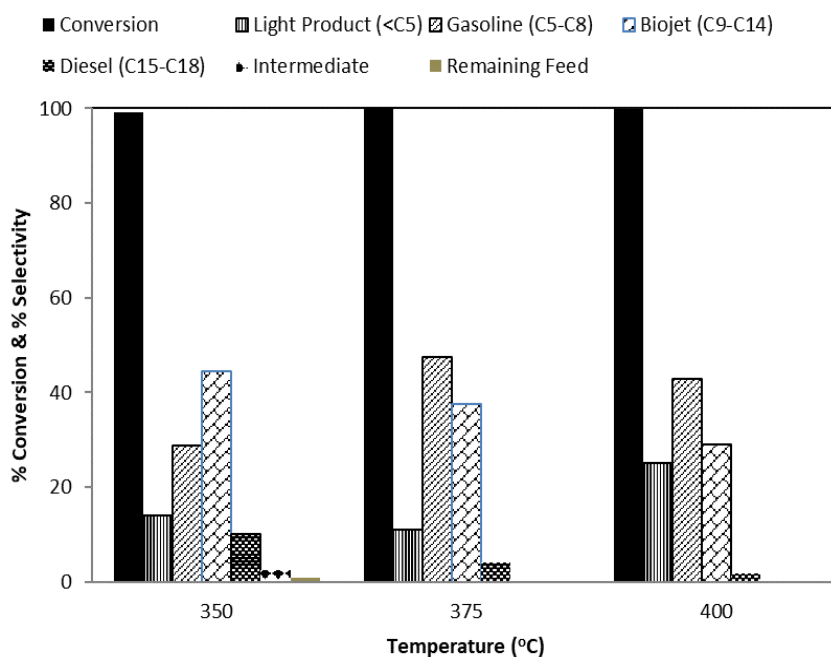


**Figure 4.12** The conversion and selectivity of products over 5 wt.% Co/HZSM-12 catalyst at different temperatures (reaction condition: 30 bar, H<sub>2</sub>/feed molar ratio of 10, LHSV 1.5 h<sup>-1</sup> and TOS at 8 h)

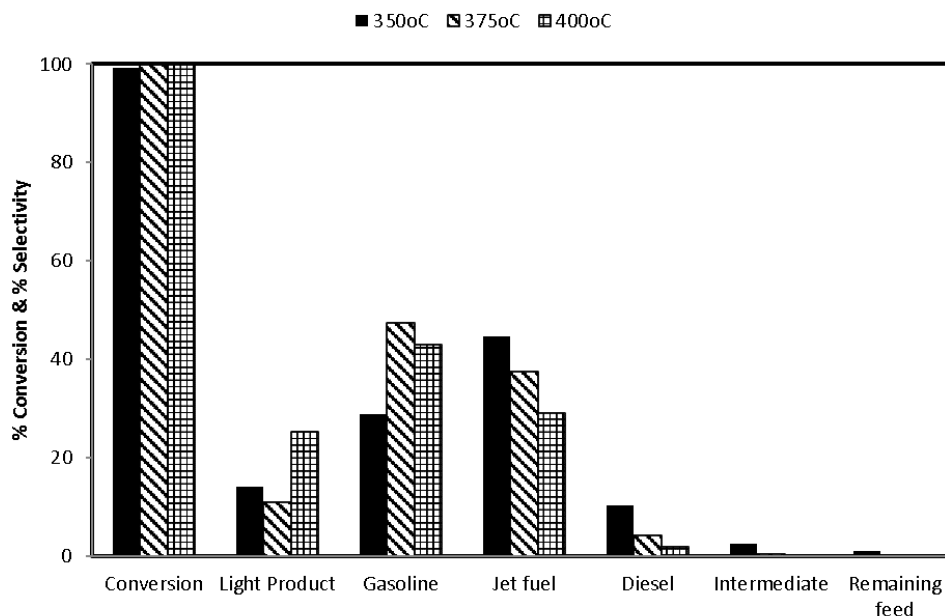


**Figure 4.13** The product distribution over 5 wt.% Co/HZSM-12 catalyst at different temperatures ( Reaction condition: 30 bar, H<sub>2</sub>/feed molar ratio of 10, LHSV 1.5 h<sup>-1</sup> and TOS at 8 h)

#### 4.3.2 Effect of Different Metal Loading (Co, Ni, and Co-Ni)

For investigating the effect of different metal loading to the support HZSM-12 on the product selectivity and the product yield, the conversion of PFAD to bio-jet fuel was held at 350 °C, 30 bar, H<sub>2</sub>/feed molar ratio of 10, and LHSV 1.5 h<sup>-1</sup>. Figure 4.14 clarified that the PFAD conversion over mono-metallic Co/HZSM-12 lead as the highest selectivity to the biojet fuel which is about 44.6% compare to mono-metallic nickel and bimetallic nickel. It was confirm that cobalt has better hydrogenation and dehydrogenation function compared to nickel. In addition, bimetallic Co-Ni lead as the second high selectivity to biojet fuel and follow by nickel which are 32.8% and 30.3%, respectively. Beside has the highest bio-jet selectivity production, cobalt also gave the highest ratio of iso-paraffin to normal paraffin which is good for the property of bio-jet fuel, while the other mono-metallic nickel has slightly high of iso-paraffin/n-paraffin. However, bimetallic Co-Ni was performed oppsitley, it has lower ratio of iso-paraffin/n-paraffin as confirm by Figure 4.16. It



might be because the interaction between Co and Ni in the support as shown in TPD-NH<sub>3</sub> data, the peak shift to lower temperature between the Co and Ni graphs. Moreover, it can be confirmed that metal cobalt has good isomerization reaction function as compared to nickel which is good for bio-jet fuel production. It was also confirmed by TPD-NH<sub>3</sub> result that Co has strong acid site as compared to nickel. Therefore, Co/HZSM-12 has been chosen as the best metal loading to produce bio-jet fuel over support HZSM-12 catalyst.

From the result gained, Co/HZSM-12 with temperature 350 °C was selected as the optimal condition for continuing to the next objective which is the effect of reducing time in order to gain the highest bio-jet fuel product.

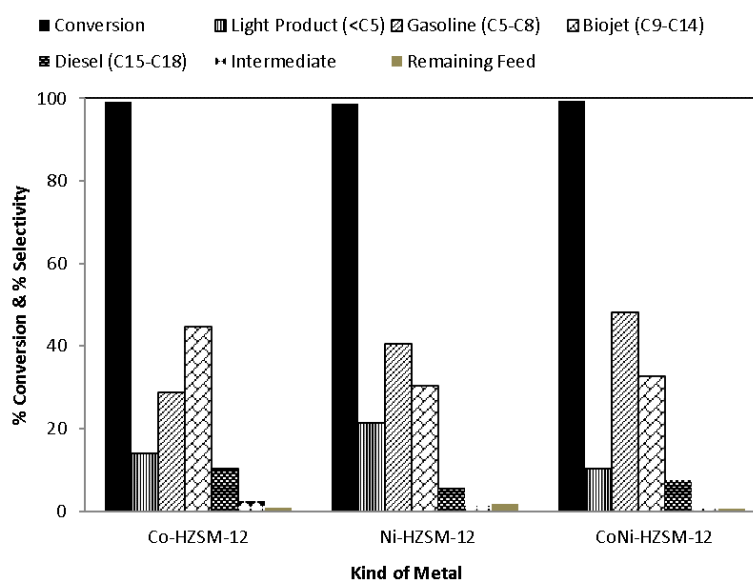


**Figure 4.14** The conversion and selectivity of products over 5 wt.% HZSM-12 catalyst at different metal loading Co, Ni, and Co-Ni ( Reaction condition: 350 °C, 30 bar, H<sub>2</sub>/feed molar ratio of 10, LHSV 1.5 h<sup>-1</sup> and TOS at 8 h)

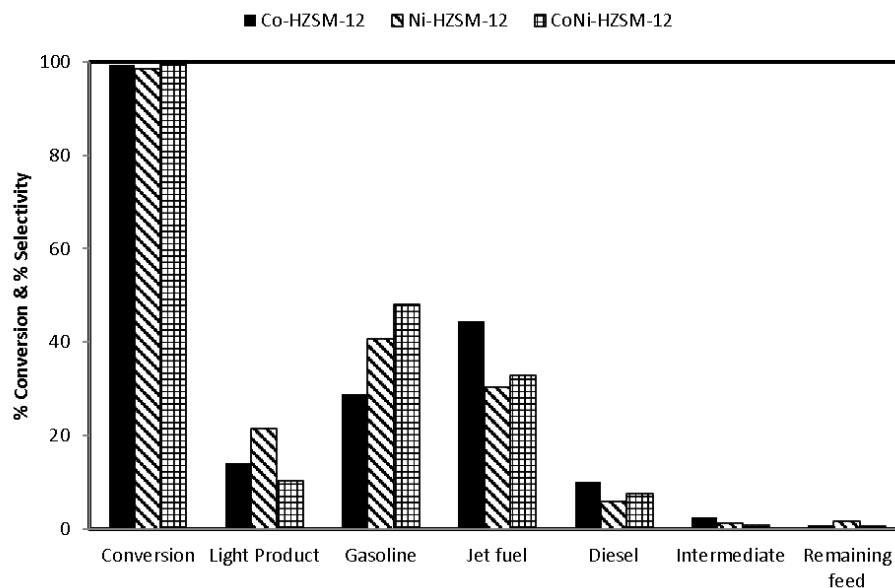


**Figure 4.15** The product distribution over 5 wt.% HZSM-12 catalyst at different metal loading Co, Ni, and Co-Ni ( Reaction condition: 350 °C, 30 bar, H<sub>2</sub>/feed molar ratio of 10, LHSV 1.5 h<sup>-1</sup> and TOS at 8 h)

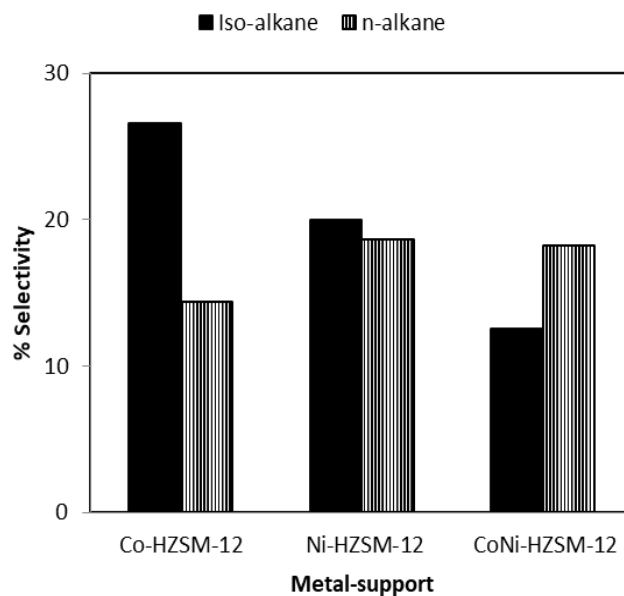


**Figure 4.16** The iso-product/n-product distribution over 5 wt.% HZSM-12 catalyst at different metal loading Co, Ni, and Co-Ni ( Reaction condition: 350 °C, 30 bar, H<sub>2</sub>/feed molar ratio of 10, LHSV 1.5 h<sup>-1</sup> and TOS at 8 h)

#### 4.3.3 Effect of Reaction Pressure

In order to study the effect of reaction pressure on the product selectivity, the conversion of PFAD to bio-jet fuel over 5 wt. % Co/HZSM-12 was conducted at 350 °C, H<sub>2</sub>/feed molar ratio of 10, and LHSV 1.5 h<sup>-1</sup>. Figure 4.17 illustrates that the conversion of PFAD increased with increasing reaction pressure (from 96,9 % to 99,4 %). Moreover, from Figure 4.18 can be observed that the selectivity of light product will decrease with decreasing the reaction pressure, while the selectivity of diesel increase with the depleting pressure and the remaining feed of lower pressure is higher than the higher pressure so it can be lead to the higher selectivity to the bio-jet fuel. In conclusion, the reaction at 20 bar was selected as the optimum reaction condition with bio-jet fuel selectivity about 51.57 %.

From the result obtained, the reaction temperature at 350 °C and 20 bar has been chosen as the optimal reaction temperature for further study the effect of different metal loading (2.5, 5, and 7.5% wt.) because of its good performance in bio-jet fuel selectivity and low selectivity to light product, gasoline, and diesel production.

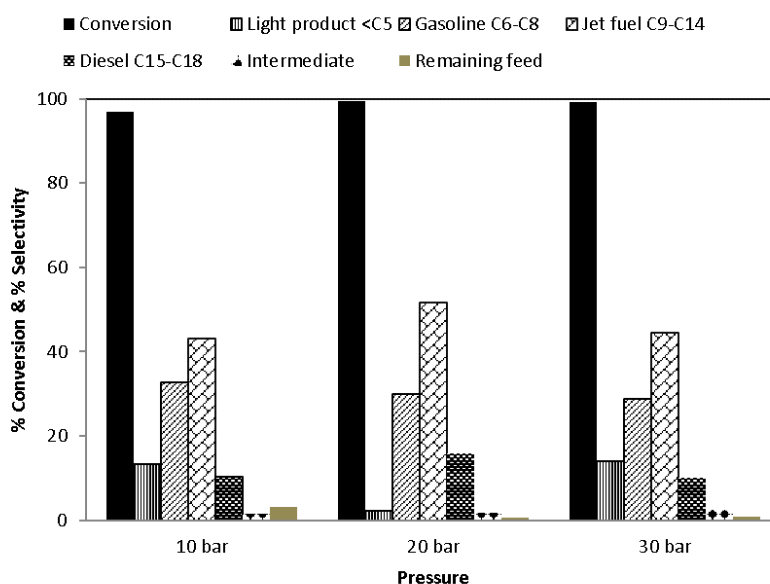


**Figure 4.17** The conversion and selectivity of products over 5 wt.% Co/HZSM-12 catalyst at different reaction pressure (Reaction condition: 350 °C, H<sub>2</sub>/feed molar ratio of 10, LHSV 1.5 h<sup>-1</sup> and TOS at 8 h)

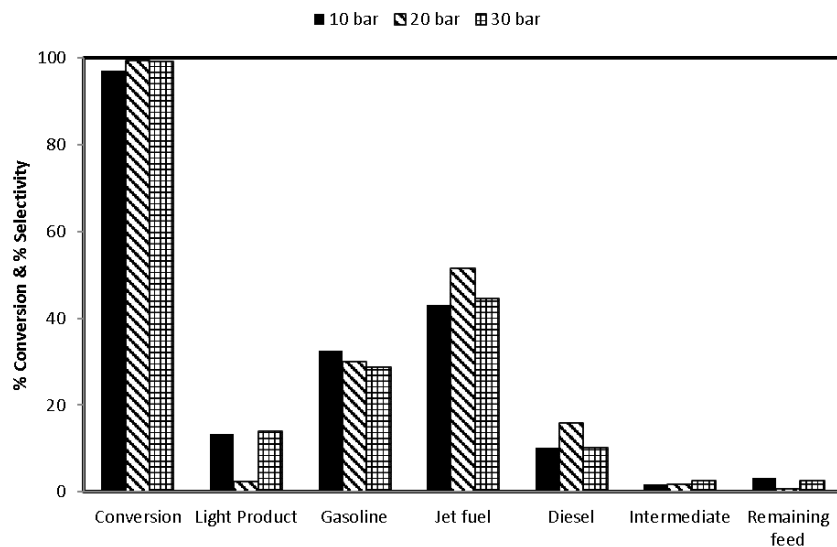


**Figure 4.18** The product distribution over 5 wt.% Co/HZSM-12 catalyst at different reaction pressure ( Reaction condition: 350 °C, 20 bar, H<sub>2</sub>/feed molar ratio of 10, LHSV 1.5 h<sup>-1</sup> and TOS at 8 h).

#### 4.3.4 Effect of Metal (Co) Loading

To investigate the effect of the amount metal (Co) loading to the support HZSM-12 on the product selectivity and the product yield, the conversion of PFAD to bio-jet fuel was held at 350 °C, 20 bar, H<sub>2</sub>/feed molar ratio of 10, and LHSV 1.5 h<sup>-1</sup>. The percent of Co was varied from 2.5 to 7.5 wt.% on support HZSM-12. Figure 4.19 and Figure 4.20 clarified that the PFAD conversion over different amount of metal loading in range 2.5 to 7.5 wt.% has no significant different in terms of conversion. Moreover, 2.5 wt.% gave the lower bio-jet fuel selectivity due to the higher amount of diesel, intermediate, and remaining feed. In addition, the graph also exhibited that the bio-jet fuel selectivity in 5 wt.% and 10 wt.% metal loading almost has the same result which avaragely 51 %. It can be concluded that, the higher metal loading will give more complete dispersion on the support catalyst. However, 5 wt.% Co/HZSM-12 was selected as the optimum metal (Co) loading to produce bio-jet fuel.

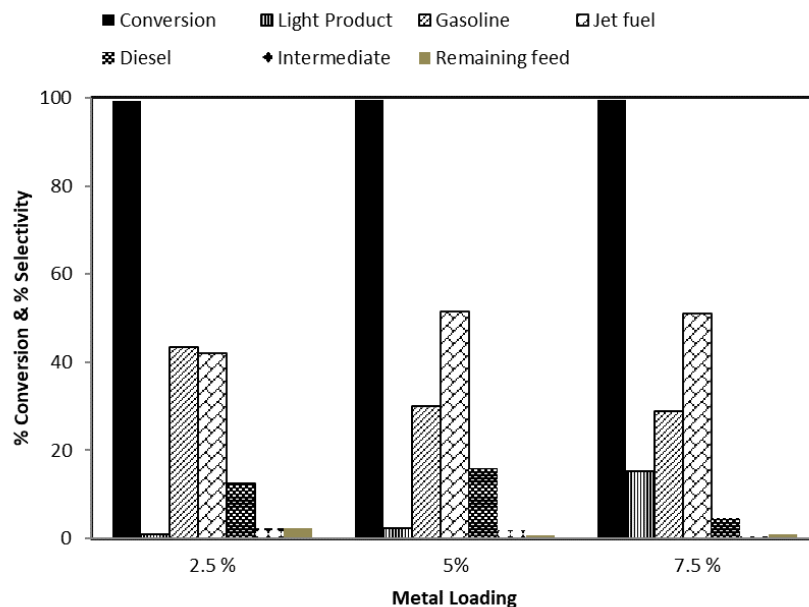


**Figure 4.19** The conversion and selectivity of products over 5 wt.% Co/HZSM-12 catalyst at different amount metal (Co) loading (Reaction condition: 350 °C, 20 bar, H<sub>2</sub>/feed molar ratio of 10, LHSV 1.5 h<sup>-1</sup> and TOS at 8 h)

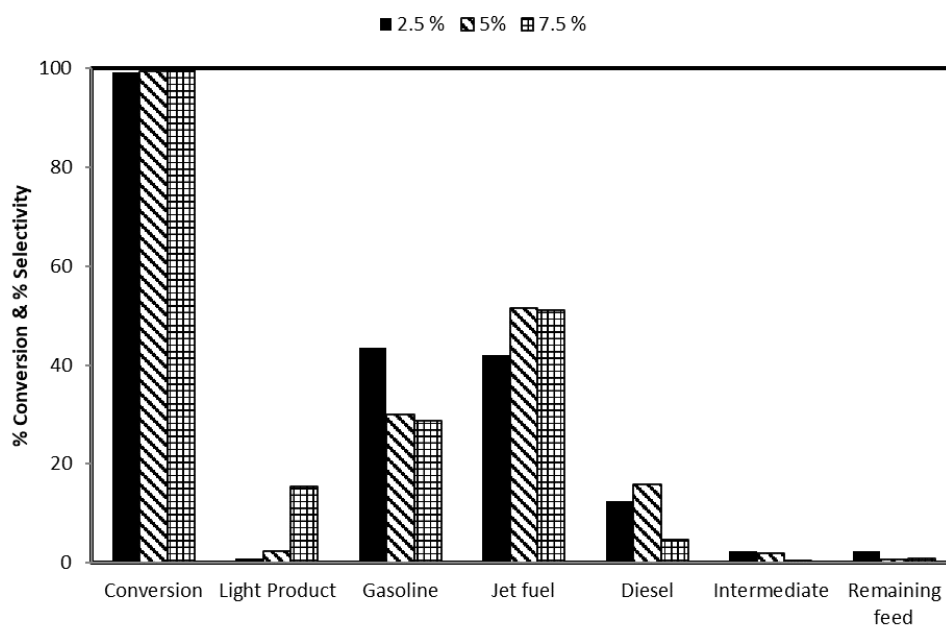
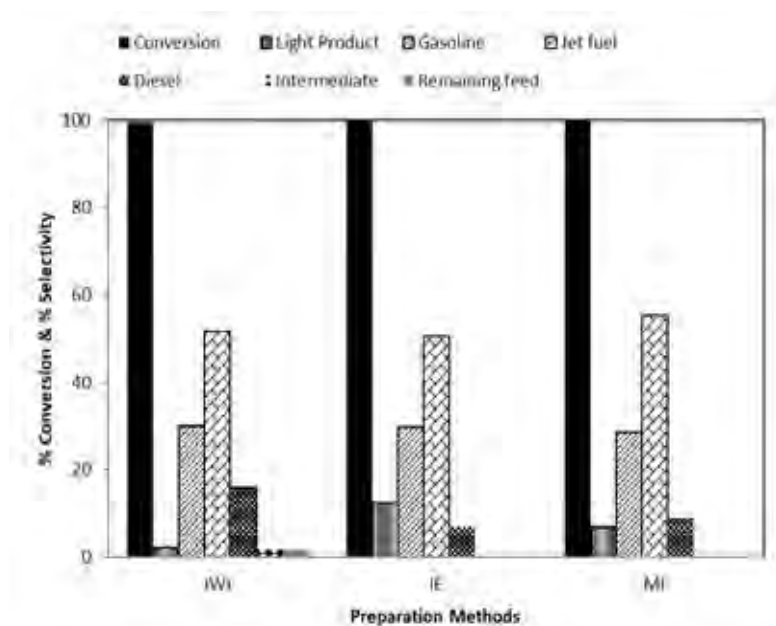


**Figure 4.20** The product distribution over 5 wt.% Co/HZSM-12 catalyst at different amount metal (Co) loading (Reaction condition: 350 °C, 20 bar, H<sub>2</sub>/feed molar ratio of 10, LHSV 1.5 h<sup>-1</sup> and TOS at 8 h)

#### 4.3.5 Effect of Metal Preparation Methods

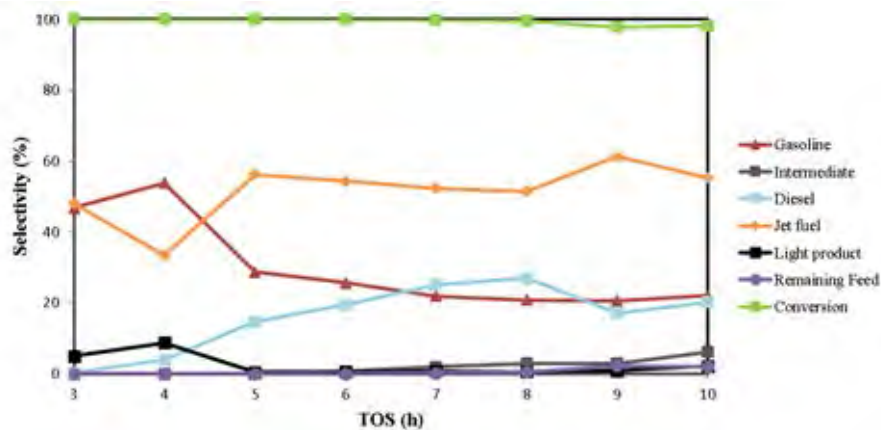
To investigate the effect of metal preparation method on the product selectivity and the product yield, the conversion of PFAD to bio-jet fuel was held at 350 °C, 20 bar, H<sub>2</sub>/feed molar ratio of 10, and LHSV 1.5 h<sup>-1</sup>. The preparation methods which were investigated in this study are incipient wetness impregnation (IWI) with trace amount of water as the solvent, ion exchange (IE) with high amount of water, and melt infiltration (MI) with no water. Figure 4.21 shows that melt infiltration method gives the highest selectivity to bio-jet fuel compared to two other methods. The TEM image explains that melt infiltration method has more complete dispersion. Moreover, the results given by incipient wetness impregnation and ion exchange seem to be similar. The bio-jet fuel selectivity of IWI, IE and MI are 51.57%, 50.49%, and 55.9 % respectively. It can be observed that the more little solution used to load the metal to support the higher dispersion will be gained, which means higher selectivity to bio-jet fuel.

Figure 4.23 shows the colour of calcined Co/HZSM-12 after metal loading of each preparation method. It can be shown that the colour of MI is darker than the other two methods because of complete dispersion of metal to the support which explained the strong interaction or bonding between the metal and the zeolite. Among other methods MI was the free solvent technique which benefits in avoiding metal loss, those all elements of metal were totally integrated with the support which also maybe the reason of the darker color got by MI method.



**Figure 4.21** The conversion and selectivity of products over 5 wt.% Co/HZSM-12 catalyst at different metal preparation methods (Reaction condition: 350 °C, 20 bar, H<sub>2</sub>/feed molar ratio of 10, LHSV 1.5 h<sup>-1</sup> and TOS at 8 h).

(a)



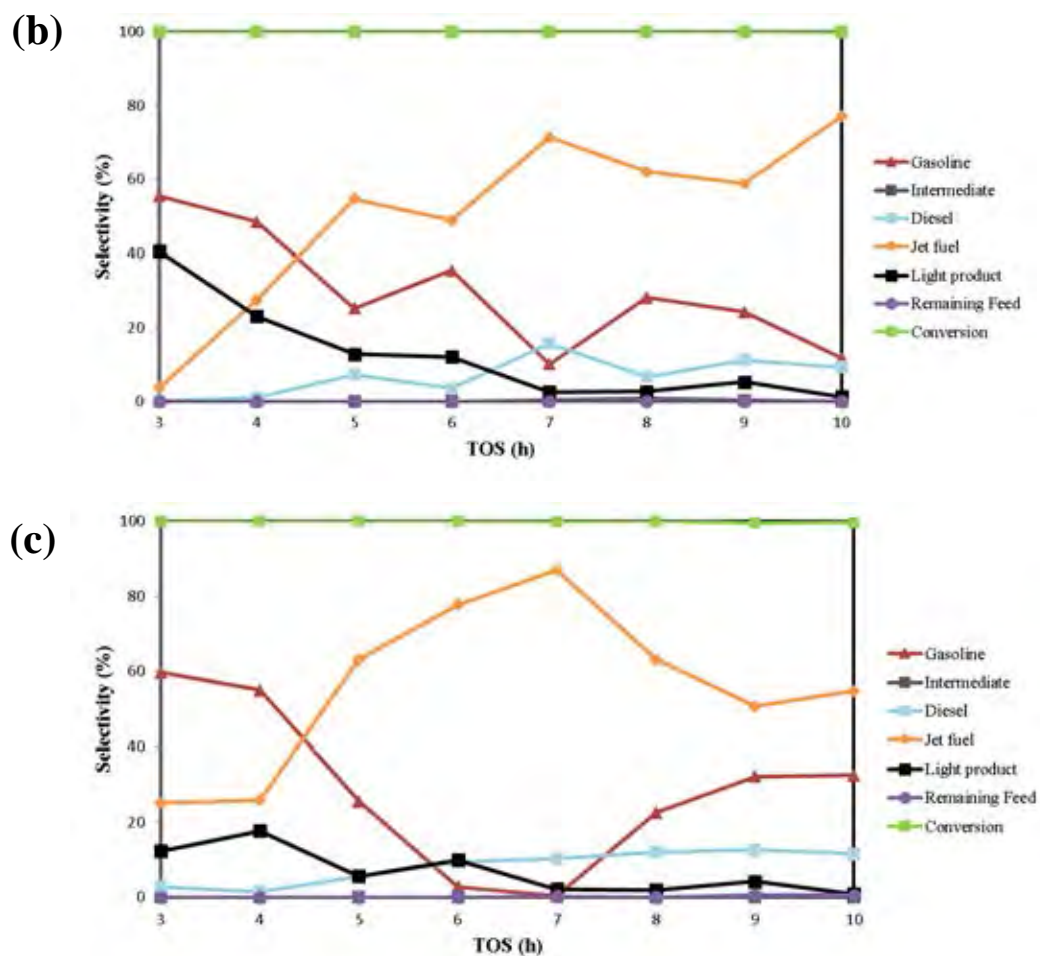


**Figure 4.22** The product distribution over 5 wt.% Co/HZSM-12 catalyst at different different metal preparation methods (a) incipient wetness impregnation (b) ion exchange (c) melt infiltration (Reaction condition: 350 °C, 20 bar, H<sub>2</sub>/feed molar ratio of 10, LHSV 1.5 h<sup>-1</sup> and TOS at 8 h).

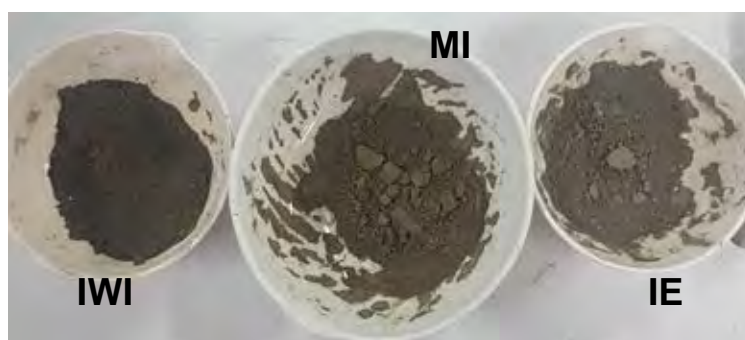
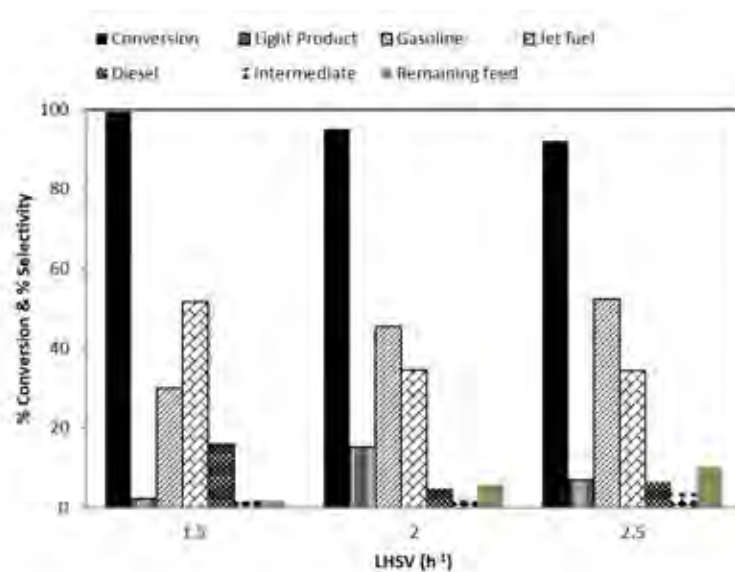


**Figure 4.23** Calcined Co/HZSM-12 metal preparations.

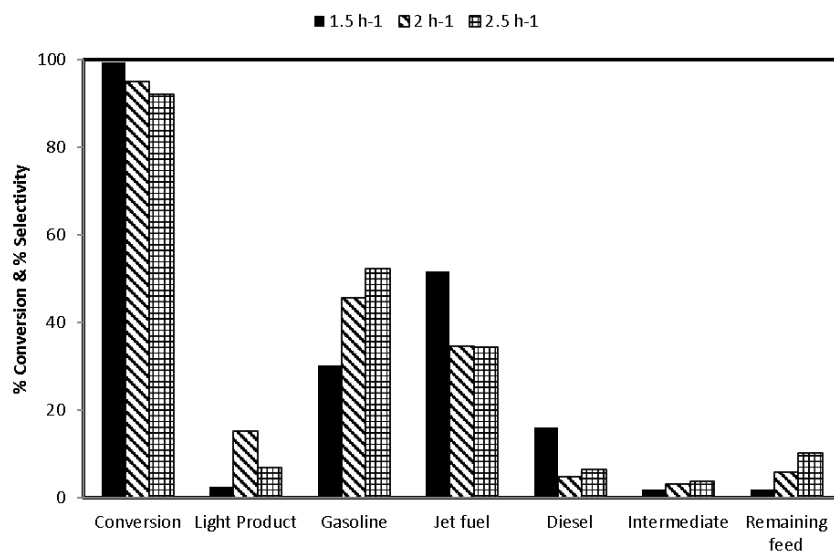


#### 4.3.6 Effect of LHSV

To investigate the effect of LHSV on the product selectivity and the product yield, the conversion of PFAD to bio-jet fuel was held at 350 °C, 20 bar, H<sub>2</sub>/feed molar ratio of 10, and LHSV 1.5 h<sup>-1</sup>. The LHSV value was varied from 1.5-2.5 h<sup>-1</sup>. Figures 4.25 and 4.26 exhibit the conversion and selectivity of product. It can be seen that the selectivity of bio-jet fuel decreased with increasing number of LHSV and higher amount intermediate and remaining feed. It indicates that more LHSV more feed are not converted to hydrocarbon. It also shows that there is some declining in term of conversion with the increasing of LHSV value. The light products seem to be low at lower LHSV number it might be due to the oligomerization of olefins and the other lighter products such as ethylene in high residence time. Consequently, the number of heavier products such as jet-fuel increased.



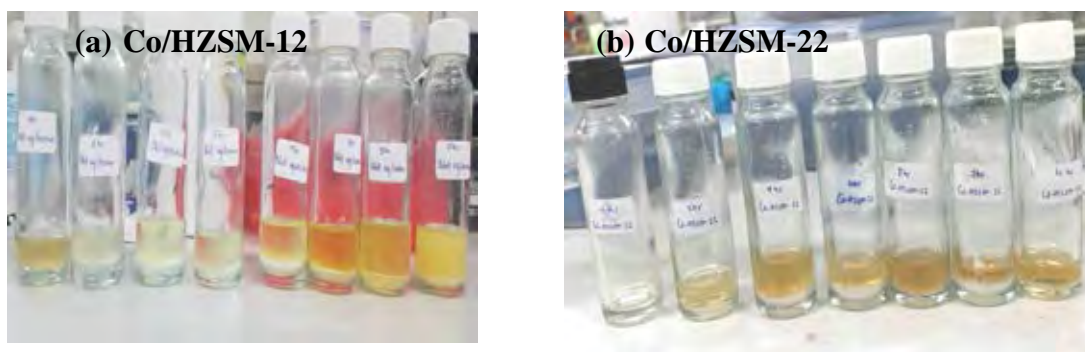
**Figure 4.24** The conversion and selectivity of products over 5 wt.% Co/HZSM-12 catalyst at different LHSV (Reaction condition: 350 °C, 20 bar, H<sub>2</sub>/feed molar ratio of 10, and TOS at 8 h).



**Figure 4.25** The product distribution over 5 wt.% Co/HZSM-12 catalyst at different different LHSV (Reaction condition: 350 °C, 20 bar, H<sub>2</sub>/feed molar ratio of 10, and TOS at 8 h).

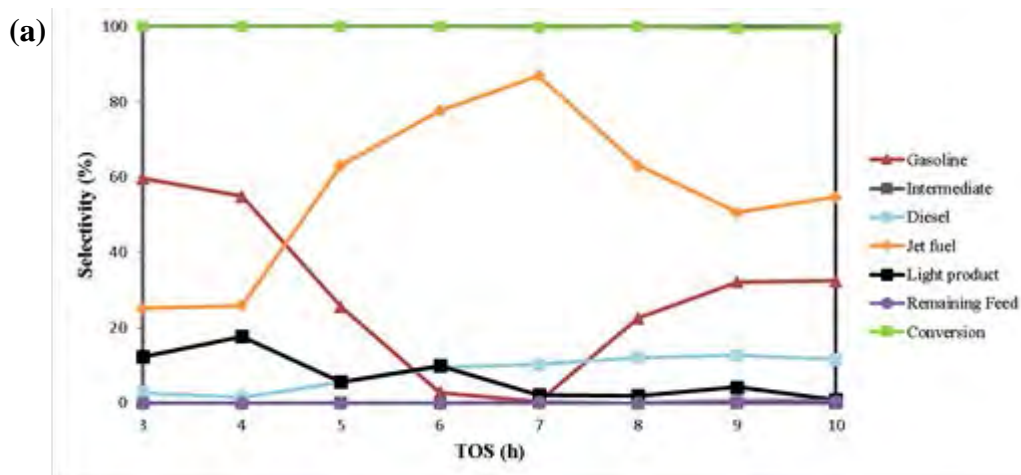
#### 4.3.7 Effect of Supported Catalysts (Co/HZSM-12 and Co/HZSM-22)

To investigate the effect of catalysts support on the product selectivity and the product yield, the conversion of PFAD to bio-jet fuel was held at 350 °C, 20 bar, H<sub>2</sub>/feed molar ratio of 10, and LHSV 1.5 h<sup>-1</sup>. Figure 4.26 (a), (b) exhibit the liquid products obtained over 5 wt.% Co/HZSM-12 and Co/HZSM-22 by melt infiltration method.



**Figure 4.26** Liquid products obtained over (a) 5 wt.% Co/HZSM-12 and (b) 5 wt.% Co/HZSM-22 catalysts by melt infiltration method (Reaction condition: 350 °C, 20 bar, LHSV 1.5 h<sup>-1</sup>, H<sub>2</sub>/feed molar ratio of 10).

The activity of each zeolite Co/HZSM-12 and Co/HZSM-22 can be seen in Figures 4.27 (a) and (b) respectively. From the Figure 4.27 (a) it can be seen that the selectivity of bio-jet fuel tend to be constant and relatively higher from both gasoline and diesel. However, after 8 h the main product decrease slightly, while diesel selectivity increase. Moreover, the selectivity of bio-jet fuel over Co/HZSM-12 is higher than Co/HZSM-22. It can be confirmed by BET result that parent HZSM-22 has lower pore diameter and surface area as compared to parent HZSM-12. Moreover, the crystallinity of parent HZSM-22 still not fully synthesized due to hard method of preparation.



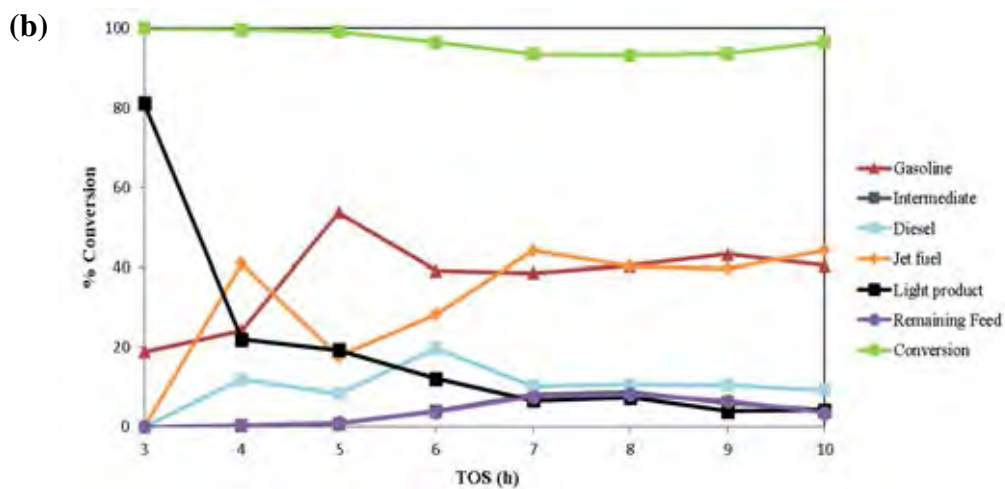


**Figure 4.27** The conversion and selectivity of products that obtain over (a) 5 wt.% Co/HZSM-12 and (b) 5 wt.% Co/HZSM-22 catalysts by melt infiltration method. (Reaction condition: 350 °C, 20 bar, H<sub>2</sub>/feed molar ratio of 10, and TOS at 8 h).

Figure 4.28 explains that Co/HZSM-12 exhibited complete conversion, whereas Co/HZSM-22 only gain 95% conversion, this indicates that incomplete crystallinity on HZSM-22 affect the result of reaction.

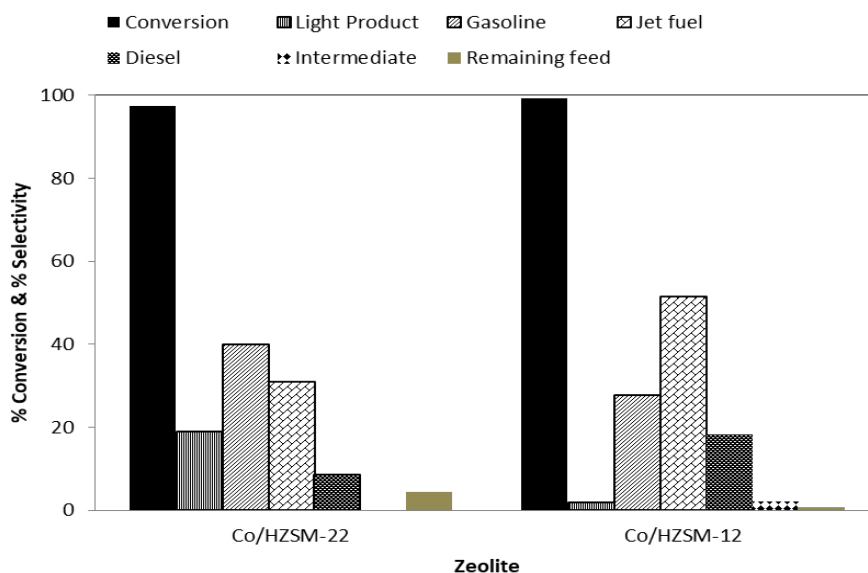


**Figure 4.28** The conversion and selectivity of products over 5 wt.% Co/HZSM-12 and 5 wt.% Co/HZSM-22 (Reaction condition: 350 °C, 20 bar, H<sub>2</sub>/feed molar ratio of 10, and TOS at 8 h)

#### 4.4 Proposed Reaction Pathway

The proposed reaction pathway is shown in Figure 4.29. The pathway of biojet production from palmitic acid as the main component in PFAD was deoxygenation of fatty acid to long chain hydrocarbon in the range of diesel (C<sub>15</sub>–C<sub>18</sub>) then further hydrocracking/ hydroisomerization into bio-jet range (C<sub>9</sub>–C<sub>14</sub>). There are three main reaction pathways deoxygenation to convert fatty acid to long chain hydrocarbon by (i) Hydrodeoxygenation (HDO) pathway which consumed large quantity of H<sub>2</sub> and consequence produced H<sub>2</sub>O, separation of oxygen in fatty acid takes place via C=O bond hydrogenation, C–O bond rupture and further C–C bond cleavage by aldehyde and alcohol as intermediates, (ii) Decarbonylation (DCN) pathway which consumed H<sub>2</sub> for forming aldehyde as an intermediate and producing H<sub>2</sub>O and CO (carbon monoxide) by C–O bond cleavage and C–C bond rupture, respectively, (iii) Decarboxylation (DCX) pathway, occur by elimination –COOH as CO<sub>2</sub> which consumed no H<sub>2</sub> and favor increasing reaction temperature, oxygen in fatty acid is removed in the form of CO<sub>2</sub> (carbon dioxide) by the direct attack at C–C bond (Hermida *et al.*, 2015).



coke deposit as compared to nickel and bimetallic cobalt-nickel on zeolite HZSM-12. Monometallic nickel on HZSM-12 gave the highest coke formation which was 33.49%, then follow by bimetallic CoNi and monometallic Co with the number of coke deposit about 29.76% and 28.63%, respectively under IWI method. The graph also exhibited the number of coke deposit in different zeolite catalysts. According to the result, Co/HZSM-12 gave the lower coke formation as compared to Co/HZSM-22. However, both of those catalyst gave less amount of coke compared to other bifunctional catalysts, it might be due to the lower cracking activity of both zeolite.

**Table 4.4** Percent Coke of Co, Ni, Co-Ni/HZSM-12, Co/HZSM-12 (MI) and Co/HZSM-22 (MI).

Catalysts	Coke (%)
Co/HZSM-12 (MI)	7.83
Co/HZSM-22 (MI)	23.41
Co/HZSM-12 (IWI)	28.63
CoNi/HZSM-12 (IWI)	29.76
Ni/HZSM-12 (IWI)	33.49

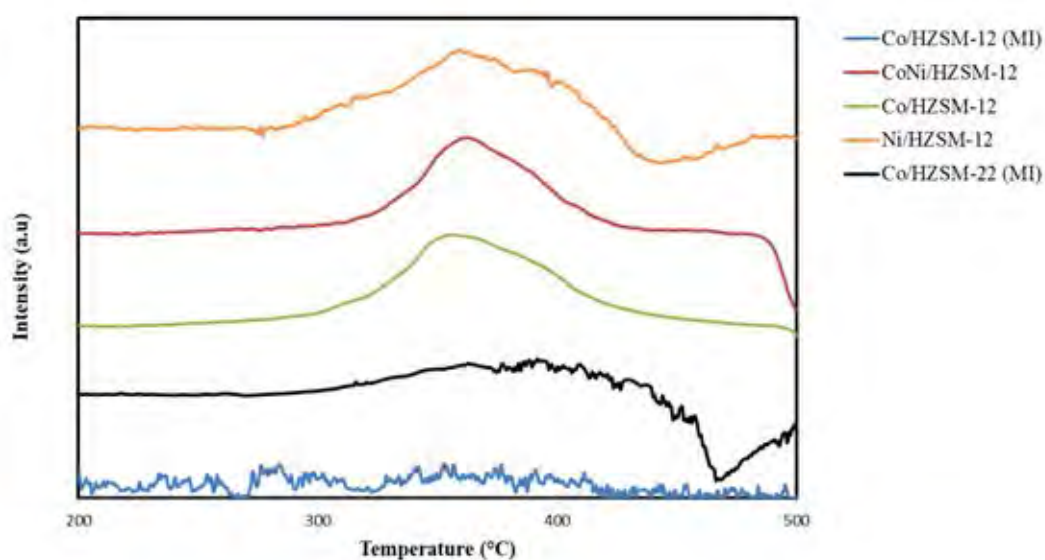


**Figure 4.30** TPO profile of Co/HZSM-12 and Co/HZSM-22.

## CHAPTER V

### CONCLUSSION AND RECOMENDATION

#### 5.1 Conclusions

The synthesis of HZSM-12 with different metal loading (Co, Ni, and CoNi) have been confirmed by XRD, XRF, BET result and TEM image. Different metal preparation methods to HZSM-12 zeolite are also elucidated by those characterization techniques. All metals seem to be well dispersed on support zeolite HZSM-12 corresponded to TEM and BET results. However, melt infiltration method gives the highest dispersion and have some agglomeration on the support. The 5 wt.% Co/HZSM-12 over melt infiltration method gained the highest conversion for about 99.8% and the selectivity to bio-jet fuel about 55.4% under reaction condition 350 °C, 20 bar, LHSV of 1.5 h<sup>-1</sup> and H<sub>2</sub>/feed ratio of 10. The temperature used in this study is in range 350 – 400 °C. The higher temperature applied in the system the higher cracking activity to produce lighter product and gasoline. The optimum temperature to selective bio-jet fuel is 350 °C. The effect of reaction pressure to the conversion of product is slightly increased with the number of pressure, but the appropriate pressure to bio-jet fuel is 20 bar. In addition, Co on support HZSM-12 gave the highest ration of *iso* to normal product as compared to Ni and bimetallic Co-Ni due to the better isomerization reaction of metal cobalt. Furthermore, the amount of metal loading on the support also give different result which 5 wt. % and 7.5 wt.% have no significant different on the bio-jet fuel selectivity, while 2.5 wt. % gain less conversion and less selectivity. Different methods of metal preparation were also studied in this research such as incipient wetness impregnation, ion exchange, and melt infiltration. Among those methods melt infiltration has been chosen as the best method to apply metal on zeolite because it gives highest selectivity and conversion. Moreover, another zeolite which is HZSM-22 was also synthesized to know the effect of zeolite crystal to bio-jet fuel production. Co/HZSM-12 showed higher conversion and selectivity to bio-jet fuel compared to Co/HZSM-22, it might be due to incomplete synthesis of HZSM-22. The



lost of heat and unsteable stirrer could be the reason behind the incomplete synthesis of HZSM-22 by dynamic hydrotrothermal method. The formation of hydrocarbon from fatty acid over bi-functional catalyst happened through an aldehyde and alcohol intermediate and transform to heavier hydrocarbon then subsequently hydro-isomerization and hydrocracking to bio-jet fuel and other lighter products.

## **5.2 Recommendation**

The HZSM-22 with incomplete crystallization also gives high enough selectivity to bio-jet fuel. The problem of the synthesis process is the limitation of the instrument used in this study such as unsteable stirrer and the lost of heat during the treatment because of oven free.

In recommendation, for further study of bio-jet fuel production can be used HZSM-22 with more complete crystallization to gain more jet-fuel product by changing the method of catalyst synthesis using the HZSM-22 seed.

## REFERENCES

- Akinfalabi S. I., Umer R., Robiah Y., Yun H. T. Y. (2017) Synthesis of biodiesel from palm fatty acid distillate using sulfonated palm seed cake catalyst. Journal of Renewable Energy 111, 611-619.
- Antonio C. G, F.I. Gómez C, J.A. de L. F, S. Hernández. (2017) A review on the production processes of renewable jet fuel. Renewable and Sustainable Energy Reviews 79, 709–729
- Bauer F., Karsten F., Marko B., Wolf-Dietrich E., Thomas K., and Roger G. (2014). Hydroisomerization of long-chain paraffins over nano-sized bimetallic Pt-Pd/H-beta catalysts. Catalyst Science Technology 4, 2045-4054.
- Bezemer G.L., Bitter J.H., Kuipers H. P. C.E., Oosterbek H., Holewijn J.E, Xu X., Kapteijn F., Dillen J.V and de Jong K.P (2006) Cobalt Particle Size Effects in the Fischer–Tropsch Reaction Studied with Carbon Nanofiber Supported Catalysts. J. Am. Chem. Soc.128,12 (3956-3964)
- Bonnie T. Y. and Mohtar Y. (2009) Characteristics and properties of fatty acid distillate from palm oil. PIPOC 2009 Int. Palm Oil Congress – Oleo&Spec. Chem. Conf., 309–312.
- Blanc D. L, Clovois F and Marjo V. (2017) Mapping the linkages between oceans and other Sustainable Development Goals: A preliminary exploration. DESA Working Paper. No. 149
- Brouwer, D.H. (2008) A structure refinement strategy for NMR crystallography: an improved crystal structure of silica-ZSM-12 zeolite from <sup>29</sup>Si chemical shift tensors. Journal of Magnetic Resonance 194(1), 136-146.
- Cao, Y., Shi, Y., Liang, J., Wu, Y., Huang, S., Wang, J., Yang, M. and Hu, H. (2017) High iso-alkanes production from palmitic acid over bi-functional Ni/HZSM-22 catalysts. Chemical Engineering Science 158, 188-195.
- Cao, Y., Yanchun S., Yunfei B., Keijing W., Shaojian W., Yulong W., and Shaobin H. (2018) Hydrodeoxygenation and hydroisomerization of palmitic acid over bi-functional Co/H-ZSM-22 catalysts. Fuel Processing Technology 172, 29-35.

- Cheng, J., Li, T., Huang, R., Zhou, J., and Cen, K (2014) Optimizing catalysis conditions to decrease aromatic hydrocarbons and increase alkanes for improving jet biofuel quality. Bioresource Technology 158, 378-382.
- Cho Hyun J., Jin-Kuk K., Faisal A., Yeong K. Y. (2013) Life-cycle greenhouse gas emissions and energy balances of a biodiesel production from palm fatty acid distillate (PFAD). Journal of Applied Energy 111, 479–488.
- Connor', H.A. (1932) Hydrogenolysis of oxygenated organic compounds The Department of Chemistry of Standford University 54, 4678-4690.
- Daramola., Michael O, Elizabeth F. Aransiola and Tunde V. Ojumu (2012).Potential Applications of Zeolite Membranes in Reaction Coupling Separation Processes. Materials 5(11), 2101-2136.
- De Lucas, A., Sánchez, P., Fúnez, A., Ramos, M.J. and Valverde, J.L. (2006) Influence of clay binder on the liquid phase hydroisomerization of n-octane over palladium-containing zeolite catalysts. Journal of Molecular Catalysis A: Chemical 259(1-2), 259-266.
- Den Breejen J.P., Radstake P.B., Bezemer G.L., Bitter J.H., Froseth V., Holmen A and de Jong K. P. (2009) On the Origin of the Cobalt Particle Size Effects in Fischer–Tropsch Catalysis. J. Am. Chem. Soc.131,20 (7197-7203)
- Deane P., Brian O´. G., and Richard O.S (2017) Biofuels for Aviation: Policy Goals and Costs. Europe's Energy Transition. <http://dx.doi.org/10.1016/B978-0-12-809806-6.00012-2>
- De Sousa, F.P., Cardoso, C.C. and Pasa, V.M.D. (2016) Producing hydrocarbons for green diesel and jet fuel formulation from palm kernel fat over Pd/C. Fuel Processing Technology 143; 35-42.
- Elhaj H. F. A., Andrew L. (2014) The worldwide production of bio-jet fuels - The current developments regarding technologies and feedstocks, and innovative new R&D developments. Technical Report DOI: 10.13140/RG.2.1.2898.6400.

- Eller Z Zoltán V and Jenó H. (2016) Advanced production process of jet fuel components from technical grade coconut oil with special hydrocracking. Fuel 182; 713–720.
- Flaming A, Russel M. W. Heidi H and Linda S. (2107) The sustainable development goals: A case study. Marine Policy 86; 94–103
- F.S. Xiao, S. Zheng, J.M. Sun, R.B. Yu, S.L. Qiu, R.R. Xu, Journal of Catalysis 176 (1998) 474–487.
- Galadima, A. and Muraza, O. (2015) Catalytic upgrading of vegetable oils into jet fuels range hydrocarbons using heterogeneous catalysts: A review. Journal of Industrial and Engineering Chemistry 29, 12-23.
- Grebmeier, J. (2012). Shifting Patterns of Life in the Pacific Arctic and Sub-Arctic Seas. Annual Review of Marine Science. 4: 63–78.
- Group ATA (2017) Facts & figures.
- Han H. S, Chul J. K, Cheon H. C, Chae H. S, and Jeongsik H. (2018) Ignition delay time and sooting propensity of a kerosene aviation jet fuel and its derivative blended with a bio-jet fuel. Fuel 232;724-728.
- Hermida, L., Abdullah, A.Z. and Mohamed, A.R. (2015) Deoxygenation of fatty acid to produce diesel-like hydrocarbons: A review of process conditions, reaction kinetics and mechanism. Renewable and Sustainable Energy Reviews 42, 1223-1233.
- Ju, C., Zhou, Y., He, M., Wu, Q. and Fang, Y. (2016) Improvement of selectivity from lipid to jet fuel by rational integration of feedstock properties and catalytic strategy. Renewable Energy 97, 1-7.
- Lee, H.W., Jeon, J.-K., Jeong, K.-E., Kim, C.-U., Jeong, S.-Y., Han, J. and Park, Y.-K. (2013) Hydroisomerization of n-dodecane over Pt/Y zeolites with different acid characteristics. Chemical Engineering Journal 232, 111-117.
- Li, T., Cheng, J., Huang, R., Yang, W., Zhou, J. and Cen, K. (2016) Hydrocracking of palm oil to jet biofuel over different zeolites. International Journal of Hydrogen Energy 41(47), 21883-21887.

- Liu, Y., Yao, L., Xin, H., Wang, G., Li, D. and Hu, C. (2015) The production of diesel-like hydrocarbons from palmitic acid over HZSM-22 supported nickel phosphide catalysts. Applied Catalysis B: Environmental 174-175, 504-514.
- Kapor Nazratul Z. A, Gaanty P. M., Mohd Hasbi A. R., Mashitah M. Y. (2017) Palm fatty acid distillate as a potential source for biodiesel productiona Review. Journal of Cleaner Production 143 1-9.
- Koushki M., Masoomah N., Fatemeh C. (2015) Physico-chemical properties, fatty acid profile and nutrition in palm oil. Journal of Paramedical Sciences (JPS) Vol.6, No.3 ISSN 2008-4978
- Mayasari Fi., Rinaldy D. (2014) Vegetable Oil Based Biodiesel Feedstock Potential in Indonesia. Makassar International Conference on Electrical Engineering and Infonnatics (MICEEI) 978-1-4799-6726-1114/.
- Miao C., Oscar Marin-F., Tao D., Difeng Ga., Yong W., Manuel Garcia-P., Shulin C. (2018) Hydrothermal Catalytic Deoxygenation of Fatty Acid and Bio-oil with in Situ H<sub>2</sub>. ACS Sustainable Chem. Eng. 2018, 6, 4521–4530
- Mupondwa Edmund., Xue Li., Lope Tabil., Kevin Falk., Richard Gugel (2016) Technoeconomic analysis of camelina oil extraction as feedstock for biojet fuel in the Canadian Prairies. Journal of Biomass and Bioenergy 95, 221-234.
- Pattanaik, B.P. and Misra, R.D. (2017) Effect of reaction pathway and operating parameters on the deoxygenation of vegetable oils to produce diesel range hydrocarbon fuels: A review. Renewable and Sustainable Energy Reviews 73, 545-557.
- Ping Bonnie T. Y., Mohtar Y. (2009). Characteristics and Properties of Fatty Acid Distillates from Palm Oil. Oil Palm Bulletin 59 p.2-11.
- Q. Bu *et al.*, "A Review of Catalytic Hydrodeoxygenation of Lignin-Derived Phenols from Biomass Pyrolysis. Bioresource Technology. 124, 470 (2012).
- Qihua Yang., Emiel J.M. H. (2012) CO–PROX reactions on copper cerium oxide catalysts prepared by melt infiltration. Journal of Catalysis Applied Catalysis B: Environmental 123– 124, 424– 432.

- Regnskogfondet, Rainforest Foundation Norway. (2016). Palm Fatty Acid Distillate (PFAD) in biofuels. Zero and Rainforest Foundation Norway Paper.
- Rustan Arild C., Christian A. D. (2005). Fatty Acids: Structures and Properties. doi: 10.1038/npg.els.0003894
- Sajjadi Baharak., Abdul A. A. R., Hamidreza A. (2016) A comprehensive review on properties of edible and non-edible vegetable oil-based biodiesel: Composition, specifications and prediction models. Renewable and Sustainable Energy Reviews 63, 62–92.
- Sankaranarayanan T. M., Antonio B., Cristina O., Inés M., Prabhas J., Juan M. Coronado., David P., Serranoa.P., Pizarro. (2015). Hydrodeoxygenation of anisole as bio-oil model compound oversupported Ni and Co catalysts: Effect of metal and support properties. Catalysis Today 243 (2015): 163–172.
- Santos, R.C.R., Valentini, A., Lima, C.L., Filho, J.M. and Oliveira, A.C. (2011) Modifications of an HY zeolite for n-octane hydroconversion. Applied Catalysis A: General 403(1-2), 65-74.
- Scherzer, J. and Gruia, A.J. (1996) Hydrocracking Science and Technology. New York: Marcel Dekker.
- Snåre, M., Kubičková, I., Mäki-Arvela, P., Eränen, K. and Murzin, D.Y. (2006) Heterogeneous Catalytic Deoxygenation of Stearic Acid for Production of Biodiesel. Industrial & Engineering Chemistry Research. 45, 5708-5715.
- Sousa Fabiana P., Larissa N. S., Daniel B. de R., Luiz Carlos A. de., Vânia M.D. P. (2018) Simultaneous deoxygenation, cracking and isomerization of palm kernel oil and palm olein over beta zeolite to produce biogasoline, green diesel and biojet-fuel. Journal of Fuel 223, 149–156
- S.T. Wong, H.P. Lin, C.Y. Mou, S.T. Wong, H.P. Lin, C.Y. Mou, (2000) Journal of Applied Catalysis A 198, 103–114.
- Thra'n D., and J. Ponitka (2016). Government Policy on Delivering Biofuels for the Aviation Sector. Biofuels for Aviation. <http://dx.doi.org/10.1016/B978-0-12-804568-8.00013-5>.
- Top Ab Gapor Md.(2010). Production and utilization of palm fatty acid distillate (PFAD). Journal of Lipid Technology 22, 1.

- Tran T.T. Nga, Yoshimitsu Uemura, Sujan Chowdhury, Anita Ramli. (2016) Vapor-phase hydrodeoxygenation of guaiacol on Al-MCM-41supported Ni and Co catalysts. Applied Catalysis A: General 512: 93–100
- Varqa Dr. Sathia. (2017). Essential Palm Oil Statistics. [www.palmoilanalytics.com](http://www.palmoilanalytics.com)
- Wang W., Chang-Jun L. And Wei W. (2019). Bifunctional catalysts for the hydroisomerization of *n*-alkane: the effect of metal-acid balance and textural structure. Catalyst Science Technology 9, 4162-4187.
- Wang Wei-Cheng., Ling Tao (2016) Bio-jet fuel conversion technologies. Journal of Renewable and Sustainable Energy Reviews 53, 801–822.
- Wang W-C and Ling T. (2016) Bio-jet fuel conversion technologies. Renewable and Sustainable Energy Reviews. 53, 801–822.
- Weng Y, Qiu S, Ma L, Liu Q, Ding M, Zhang Q, et al. (2015) Jet-fuel range hydrocarbons from biomass-derived sorbitol over Ni-HZSM-5/SBA-5 catalyst. Catalyst. 5:2147
- Yang Z, Kezhen Q., Xuesong Z., Hanwu L., Chunhua X., Yayun Z., Moriko Q., Elmar V. (2018) Process design and economics for the conversion of lignocellulosic biomass into jet fuel range cycloalkanes. Journal of Energy 154 ,289-297.
- Yigezu Z. D., Karuppan M. (2014) Catalytic cracking of vegetable oil with metal oxides for biofuel Production. Journal of Energy Conversion and Management 84, 326–333
- Yang Z, Kezhen Q, Xuesong Z, Hanwu L, Chunhua X, Yayun Z, Moriko Q, and Elmar V. (2018) Process design and economics for the conversion of lignocellulosic biomass into jet fuel range cycloalkanes. Energy 154, 289-297
- Yu W, Feiyang Z, Wenming Y, Kunlin T and Hongpeng X.(2018) Development of an optimization methodology for formulating both jet fuel and diesel fuel surrogates and their associated skeletal oxidation mechanisms. Fuel 231,361–372

## APPENDIX

### APPENDIX A1 Overall Mass Balance of Deoxygenation-hydroprocessing at different in Temperature (350, 375 and 400 °C)

**Table A1** Overall mass balance of deoxygenation-hydroprocessing reaction over 5 wt.% Co/HZSM-12 catalyst at different in temperature. (Reaction condition: 30bar, H<sub>2</sub>/feed molar ratio of 10, LHSV of 1.5 h<sup>-1</sup> and TOS at 8 h)

Temperature (°C)		350°C	375°C	400°C
Selectivity of product (wt. %)	C1	0.037467	0.102223	0.046907
	C2	0.000377	0.002082	0.000451
	C3	0.040858	0.017131	0
	C3	0.040858	0.017131	0
	iso-C4	0.036339	0.084931	0.042453
	C4	0.025572	0.045705	0.019753
	iso-C5	0	0	0
	C5	0.016192	0.005048	0.001839
	iso-C6	0.001951	0.000408	0.000948
	C6	0.003305	0.000776	0.000721
	iso-C7	0	0	0
	C7	0.000543	0.000742	0.000423
	iso-C8	0	0.382917	0.463917
	C8	0.266314	0.039441	0.006906
	iso-C9	0.150856	0.01956	0.078486
	C9	0.000289	0.002737	0.004222
	iso-C10	0.039093	0.001335	0.001143
	n-C10	0.074431	0.000177	0.026333
iso-C11	0.161747	0.000045	0.237437	
n-C11	0.000168	0.003776	0.000112	



Selectivity of product (wt. %)	iso-C12	0.001167	0.002206	0.003378
	n-C12	0.001119	0.054862	0.001202
	iso-C13	0.002752	0.20053	0.007165
	n-C13	0.001112	0.000427	0.000793
	iso-C14	0.009907	0.003359	0.013345
	n-C14	0.003213	0.000256	0.001072
	iso-C15	0.044928	0.009309	0.008921
	n-C15	0.005924	0.000536	0.000721
	iso-C16	0.014254	0.002336	0.007254
	n-C16	0.00272	0.000259	0.000469
	iso-C17	0.008718	0.003368	0.003683
	n-C17	0.001062	0.000192	0.000265
	iso-C18	0.014708	0.001062	0.010421
	n-C18	0.009596	0.000191	0.009101
Intermediate	2.533213	0.138959	0.319365	
	Feed remaining	0.859373	0.039838	0.009104
	Conversion	99.22579	99.97169	99.9983

**APPENDIX A2 Overall Mass Balance of Deoxygenation-hydroprocessing at different in kind of metal (Co, Ni and Co-Ni)**

**Table A2** Overall mass balance of deoxygenation-hydroprocessing reaction over 5 wt.% Co/HZSM-12 catalyst at different in kind of metal (Co, Ni and Co-Ni).

(Reaction condition: 350°C, 30bar, H<sub>2</sub>/feed molar ratio of 10, LHSV of 1.5 h<sup>-1</sup> and TOS at 8 h)

Kind of Metal		Co	Ni	Co-Ni
Selectivity of product (wt. %)	C1	0.037467	0.015451	0.005587
	C2	0.000377	0	0.00559
	C3	0.040858	0	0.003329

Selectivity of product (wt. %)	C3	0.040858	0.003058	0.007221
	iso-C4	0.036339	0.004001	0.004972
	C4	0.025572	0	0
	iso-C5	0	0.000145	0.000172
	C5	0.016192	0.000421	0.000375
	iso-C6	0.001951	7.2E-05	0.000127
	C6	0.003305	0	0
	iso-C7	0	0.000106	0.000127
	C7	0.000543	0.203996	0.05655
	iso-C8	0	0.30777	0.38485
	C8	0.266314	7E-05	0.003171
	iso-C9	0.150856	0.038916	0.004391
	C9	0.000289	0.000677	0.012136
	iso-C10	0.039093	0.046109	0.14001
	n-C10	0.074431	0.186127	0.237113
	iso-C11	0.161747	0.002149	0.000371
	n-C11	0.000168	0.000552	0.002204
	iso-C12	0.001167	0.013333	0.000532
	n-C12	0.001119	0.085532	0.004715
	iso-C13	0.002752	0.003048	0.005553
	n-C13	0.001112	0.012134	0.020838
	iso-C14	0.009907	0.004734	0.001178
	n-C14	0.003213	0.017512	0.031627
	iso-C15	0.044928	0.001081	0.002239
	n-C15	0.005924	0.019246	0.026818
	iso-C16	0.014254	0.001172	0.002301
	n-C16	0.00272	0.006287	0.008345
	iso-C17	0.008718	0.000269	0.000358
	n-C17	0.001062	0.010393	0.014627
	iso-C18	0.014708	0.002928	0.010253

	n-C18	0.009596	0.012711	0.002322
	Intermediate	2.533213	1.225895	0.868518
	Feed remaining	0.859373	1.640754	0.779253
	Conversion	99.22579	98.63548	99.47123

**APPENDIX A3 Overall Mass Balance of Deoxygenation-hydroprocessing at different in reducing time (2, 3, and 4 hr)**

Table A3 Overall mass balance of deoxygenation-hydroprocessing reaction over 5 wt.% Co/HZSM-12 catalyst at different in reducing time (2, 3, and 4 hr). (Reaction condition: 350°C, 30bar, H<sub>2</sub>/feed molar ratio of 10, LHSV of 1.5 h<sup>-1</sup> and TOS at 8 h)

Reducing Time		2 hr	3 hr	4 hr
Selectivity of product (wt. %)	C1	0.037467	0.060195	0.053633
	C2	0.000377	0.008043	0.004261
	C3	0.040858	0.017517	0.028669
	C3	0.040858	0.02527	0.018341
	iso-C4	0.036339	0.01919	0.015823
	C4	0.025572	0.003318	0.014036
	iso-C5	0	0.013354	0.00706
	C5	0.016192	0.000568	0.000664
	iso-C6	0.001951	0.001131	4.68E-05
	C6	0.003305	7.91E-05	5.18E-05
	iso-C7	0	5.93E-05	1.11E-05
	C7	0.000543	8.88E-05	0.245731
	iso-C8	0	0.211935	0.134503
	C8	0.266314	0.0002	5.44E-05
	iso-C9	0.150856	0.01797	0.000279
C9	0.000289	0.277064	0.259991	

Selectivity of product (wt. %)	iso-C10	0.039093	0.012721	0.026851
	n-C10	0.074431	0.099279	0.06585
	iso-C11	0.161747	0.000805	0.000615
	n-C11	0.000168	0.008918	0.015153
	iso-C12	0.001167	0.003482	0.004036
	n-C12	0.001119	0.015097	0.017004
	iso-C13	0.002752	0.004621	0.002907
	n-C13	0.001112	0.016838	0.006988
	iso-C14	0.009907	0.003767	0.005341
	n-C14	0.003213	0.065233	0.012952
	iso-C15	0.044928	0.004171	0.002723
	n-C15	0.005924	0.036292	0.015143
	iso-C16	0.014254	0.009701	0.002196
	n-C16	0.00272	0.017708	0.008261
	iso-C17	0.008718	0.005211	0.003416
	n-C17	0.001062	0.020849	0.014763
	iso-C18	0.014708	0.013123	0.009244
	n-C18	0.009596	0.003628	0.001316
Intermediate	2.533213	0.551263	0.010913	
Feed remaining	0.859373	0.064877	0.007927	
Conversion	99.22579	99.93743	99.99307	

**APPENDIX A4 Overall Mass Balance of Deoxygenation-hydroprocessing at different in pressure (10, 20 and 30 bar)**

Table A4 Overall mass balance of deoxygenation-hydroprocessing reaction over 5 wt.% Co/HZSM-12 catalyst at different in pressure (10, 20 and 30 bar). (Reaction condition: 350°C, H<sub>2</sub>/feed molar ratio of 10, LHSV of 1.5 h<sup>-1</sup> and TOS at 8 h)

Pressure (bar)		10 bar	20 bar	30 bar
Selectivity of product (wt. %)	C1	0.099686	0.015497	0.037467
	C2	0.005345	0.000828	0.000377
	C3	0.012704	0.003475	0.040858
	C3	0.004359	0.001223	0.040858
	iso-C4	0.003658	0.001033	0.036339
	C4	0.002505	0.000629	0.025572
	iso-C5	0.001485	0.000453	0.000000
	C5	0.000769	0.000220	0.016192
	iso-C6	0.001703	0.000018	0.001951
	C6	0.000229	0.000000	0.003305
	iso-C7	0.000085	0.000000	0.000000
	C7	0.319335	0.000017	0.000543
	iso-C8	0.000161	0.299151	0.000000
	C8	0.000151	0.002373	0.266314
	iso-C9	0.000029	0.000597	0.150856
	C9	0.171598	0.021263	0.000289
	iso-C10	0.023396	0.146184	0.039093
	n-C10	0.223149	0.301973	0.074431
	iso-C11	0.000034	0.000196	0.161747
	n-C11	0.001703	0.002621	0.000168
iso-C12	0.000310	0.001213	0.001167	
n-C12	0.003965	0.004185	0.001119	
iso-C13	0.001217	0.001279	0.002752	
n-C13	0.004116	0.029684	0.001112	

Selectivity of product (wt. %)	iso-C14	0.000888	0.004144	0.009907
	n-C14	0.02387	0.062848	0.003213
	iso-C15	0.000918	0.002982	0.044928
	n-C15	0.00853	0.027396	0.005924
	iso-C16	0.001629	0.003511	0.014254
	n-C16	0.007268	0.017088	0.00272
	iso-C17	0.001428	0.003052	0.008718
	n-C17	0.026068	0.026353	0.001062
	iso-C18	0.032651	0.016105	0.014708
	n-C18	0.008133	0.000784	0.009596
	Intermediate	2.533213	1.828013	1.680671
	Feed remaining	0.859373	0.635473	3.133835
	Conversion	99.22579	99.4356	96.9794

**APPENDIX A5 Overall Mass Balance of Deoxygenation-hydroprocessing at different in metal loading (2.5, 5, and 5 %)**

Table A5 Overall mass balance of deoxygenation-hydroprocessing reaction over 5 wt.% Co/HZSM-12 catalyst at different in metal loading (2.5, 5, and 5 %) (Reaction condition: 350°C, 20 bar H<sub>2</sub>/feed molar ratio of 10, LHSV of 1.5 h<sup>-1</sup> and TOS at 8 h)

Metal loading ( wt. %)		2.5 %	5%	7.5%
Selectivity of product (wt. %)	C1	0.002876	0.015497	0.063890
	C2	0.000511	0.000828	0.000606
	C3	0.002184	0.003475	0.059844
	C3	0.001160	0.001223	0.065856
	iso-C4	0.000672	0.001033	0.045351
	C4	0.000801	0.000629	0.000000
	iso-C5	0.000329	0.000453	0.030446
	C5	0.000014	0.000220	0.003109
	iso-C6	0.000556	0.000018	0.005209

Selectivity of product (wt. %)	C6	0.000000	0.000000	0.000000
	iso-C7	0.000045	0.000000	0.000815
	C7	0.221780	0.000017	0.059605
	iso-C8	0.210362	0.299151	0.176215
	C8	0.000013	0.002373	0.000145
	iso-C9	0.000605	0.000597	0.088316
	C9	0.000000	0.021263	0.078578
	iso-C10	0.399283	0.146184	0.127090
	n-C10	0.000600	0.301973	0.136637
	iso-C11	0.001950	0.000196	0.000371
	n-C11	0.000643	0.002621	0.005582
	iso-C12	0.004904	0.001213	0.001752
	n-C12	0.000156	0.004185	0.004354
	iso-C13	0.009416	0.001279	0.001918
	n-C13	0	0.029684	0.001948
	iso-C14	0.003445	0.004144	0.000731
	n-C14	0.003066	0.062848	0.002745
	iso-C15	0.00349	0.002982	0.000309
	n-C15	0.002545	0.027396	0.001427
	iso-C16	0.004764	0.003511	0.000275
	n-C16	0.001501	0.017088	0.006428
	iso-C17	0.004011	0.003052	0.002869
	n-C17	0.022212	0.026353	0.016994
iso-C18	0.082809	0.016105	0.009723	
n-C18	0.011619	0.000784	0.000861	
Intermediate	2.351042	1.828013	0.422298	
Feed remaining	0.887771	0.635473	0.904559	
Conversion	99.22244	99.4356	99.49324	

**APPENDIX A6 Overall Mass Balance of Deoxygenation-hydroprocessing at different in preparation methods (IWI, IE and MI)**

Table A6 Overall mass balance of deoxygenation-hydroprocessing reaction over 5 wt.% Co/HZSM-12 catalyst at different in preparation methods (IWI, IE and MI) (Reaction condition: 350°C, 20 bar H<sub>2</sub>/feed molar ratio of 10, LHSV of 1.5 h<sup>-1</sup> and TOS at 8 h)

Preparation Methods		IWI	IE	MI
Selectivity of product (wt. %)	C1	0.015497	0.067171	0.032794
	C2	0.000828	0.00374	0.002158
	C3	0.003475	0.021156	0.013015
	C3	0.001223	0.018256	0.011068
	iso-C4	0.001033	0.012605	0.007789
	C4	0.000629	0.010431	0.006572
	iso-C5	0.000453	0.004919	0.003182
	C5	0.000220	0.000062	0.000050
	iso-C6	0.000018	0.001172	0.000898
	C6	0.000000	0.000407	0.000281
	iso-C7	0.000000	0.000043	0.112170
	C7	0.000017	0.000000	0.044575
	iso-C8	0.299151	0.281475	0.120557
	C8	0.002373	0.000000	0.106053
	iso-C9	0.000597	0.010771	0.000318
	C9	0.021263	0.199017	0.190306
	iso-C10	0.146184	0.023024	0.026483
	n-C10	0.301973	0.207302	0.180361
iso-C11	0.000196	0.000241	0.000142	
n-C11	0.002621	0.011519	0.007460	
iso-C12	0.001213	0.005348	0.005557	



Selectivity of product (wt. %)	n-C12	0.004185	0.014094	0.016680
	iso-C13	0.001279	0.015414	0.006781
	n-C13	0.029684	0.00965	0.011097
	iso-C14	0.004144	0.00857	0.007774
	n-C14	0.062848	0.011802	0.01944
	iso-C15	0.002982	0.000683	0.000717
	n-C15	0.027396	0.011208	0.02014
	iso-C16	0.003511	0.001489	0.00174
	n-C16	0.017088	0.002263	0.003327
	iso-C17	0.003052	0.001244	0.001432
	n-C17	0.026353	0.019982	0.020367
	iso-C18	0.016105	0.020026	0.015261
	n-C18	0.000784	0.002557	0.001766
	Intermediate	1.828013	0.18046	0.059723
	Feed remaining	0.635473	0.007679	0.178581
	Conversion	99.4356	99.99398	99.86842

**APPENDIX A7 Overall Mass Balance of Deoxygenation-hydroprocessing at different in LHSV (1.5, 2 and 2.5 h<sup>-1</sup>)**

Table A7 Overall mass balance of deoxygenation-hydroprocessing reaction over 5 wt.% Co/HZSM-12 catalyst at different in LHSV (1.5, 2 and 2.5 h<sup>-1</sup>) (Reaction condition: 350°C, 20 bar H<sub>2</sub>/feed molar ratio of 10, LHSV of 1.5 h<sup>-1</sup> and TOS at 8 h)

LHSV (h <sup>-1</sup> )		1.5 h <sup>-1</sup>	2 h <sup>-1</sup>	2.5 h <sup>-1</sup>
	C1	0.015497	0.097225	0.038411
	C2	0.000828	0.007841	0.003472
	C3	0.003475	0.020417	0.016581
	C3	0.001223	0.006949	0.006212
	iso-C4	0.001033	0.005063	0.006217

Selectivity of product (wt. %)	C4	0.000629	0.000696	0.002961
	iso-C5	0.000453	0.002114	0.002268
	C5	0.000220	0.000000	0.000000
	iso-C6	0.000018	0.000103	0.000657
	C6	0.000000	0.000006	0.000000
	iso-C7	0.000000	0.000000	0.000168
	C7	0.000017	0.000000	0.000000
	iso-C8	0.299151	0.301062	0.481070
	C8	0.002373	0.012108	0.000035
	iso-C9	0.000597	0.012873	0.013305
	C9	0.021263	0.139355	0.107172
	iso-C10	0.146184	0.039079	0.052464
	n-C10	0.301973	0.195728	0.158967
	iso-C11	0.000196	0.000331	0.004731
	n-C11	0.002621	0.005852	0.006579
	iso-C12	0.001213	0.00112	0.00351
	n-C12	0.004185	0.006021	0.005888
	iso-C13	0.001279	0.004002	0.007249
n-C13	0.029684	0.008758	0.012996	
iso-C14	0.004144	0.003193	0.00542	
n-C14	0.062848	0.033188	0.020674	
iso-C15	0.002982	0.002437	0.001405	
n-C15	0.027396	0.016838	0.014868	
iso-C16	0.003511	0.001313	0.003033	
n-C16	0.017088	0.009679	0.003322	
iso-C17	0.003052	0.001503	0.002731	
n-C17	0.026353	0.018226	0.014055	
iso-C18	0.016105	0.029658	0	
n-C18	0.000784	0.005008	0	
Intermediate	1.828013	3.07086	3.603617	
Selectivity of product (wt. %)				

	Feed remaining	0.635473	5.793962	10.04612
	Conversion	99.24747	95.02267	92.08227

**APPENDIX A8 Overall Mass Balance of Deoxygenation-hydroprocessing at different in Zeolite (Co/HZSM-12 and Co/HZSM-22)**

Table A7 Overall mass balance of deoxygenation-hydroprocessing reaction over 5 wt.% Co/HZSM-12 catalyst at different in different in Zeolite (Co/HZSM-12 and Co/HZSM-22) (Reaction condition: 350°C, 20 bar H<sub>2</sub>/feed molar ratio of 10, LHSV of 1.5 h<sup>-1</sup> and TOS at 8 h)

LHSV (h <sup>-1</sup> )		Co/HZSM-12	Co/HZSM-22
Selectivity of product (wt. %)	C1	0.03279	0.05476
	C2	0.00216	0.00049
	C3	0.01302	0.04171
	C3	0.01107	0.05872
	iso-C4	0.00779	0.04003
	C4	0.00657	0.00000
	iso-C5	0.00318	0.02756
	C5	0.00005	0.00245
	iso-C6	0.00090	0.00397
	C6	0.00028	0.00000
	iso-C7	0.11217	0.01085
	C7	0.04457	0.00000
	iso-C8	0.12056	0.32830
	C8	0.10605	0.02843
	iso-C9	0.00032	0.05962
	C9	0.19031	0.00000
iso-C10	0.02648	0.00000	
n-C10	0.18036	0.00000	

Selectivity of product (wt. %)	iso-C11	0.00014	0.00985
	n-C11	0.00746	0.06746
	iso-C12	0.00556	0.02979
	n-C12	0.01668	0.11988
	iso-C13	0.00678	0.00124
	n-C13	0.01110	0.00088
	iso-C14	0.00777	0.00205
	n-C14	0.01944	0.00301
	iso-C15	0.00072	0.02786
	n-C15	0.02014	0.00922
	iso-C16	0.00174	0.00899
	n-C16	0.00333	0.00809
	iso-C17	0.00143	0.02591
	n-C17	0.02037	0.01311
	iso-C18	0.01526	0.00456
	n-C18	0.00177	0.01123
Intermediate	0.05972	4.538025008	
	Feed remaining	0.17858	4.427739546
	Conversion	99.86842	96.03714155

## CURRICULUM VITAE

**Name:** Ms. Ariya Eka Alel

**Date of Birth:** January 04, 1995

**Nationality:** Indonesia

**University Education:**

2013–2017 Bachelor Degree of Chemical Engineering, Faculty of Industrial Technology, Islamic University of Indonesia, Yogyakarta, Indonesia

**Proceedings:**

1. Alel, A.E., and Jongpatiwut, S. (2019, May 30) Production of Bio-jet Fuel from Palm Fatty Acid Distillate (PFAD) over Metal supported HZSM-12 Catalyst. Proceedings of The 25<sup>th</sup> PPC Symposium on Petroleum, Petrochemicals, and polymers and The 10<sup>th</sup> Research Symposium on Petroleum and Materials Technology, Bangkok, Thailand.

**Presentations:**

1. Alel, A.E., and Jongpatiwut, S. (2019, November 19-21) The Effect of Zeolite Morphology on the Conversion of Palm Fatty Acid Distillate (PFAD) to Bio-jet Fuel. The 8<sup>th</sup> International Conference on Environment, Chemistry and Biology (ICECB 2019), Paris, France.